Author:
Fusillo, Raffaella

Title:
Understanding the volcanic history of Corbetti caldera (Main Ethiopian Rift)

An integrated study of the stratigraphic reconstruction and the geochemical characterization of the deposits

Understanding the volcanic history of Corbetti caldera (Main Ethiopian Rift). An integrated study of the stratigraphic reconstruction and the geochemical characterization of the deposits

Raffella Fusillo

Supervisors: Prof. J.D. Blundy and Dr. R. Brooker

A dissertation submitted to the University of Bristol in accordance with the requirements for the award of the Degree of Master of Science by Research

School of Earth Sciences

September 25, 2018

Word Count: 32799

To John Prosser

Abstract

Corbetti caldera is a Quaternary volcanic complex in the southern sector of the Main Ethiopian Rift. There is little published work on this volcanic complex and its volcanic history is poorly constrained. However, Corbetti caldera has recently shown to undergo active deformation (Biggs et al.(2011)) and this event encouraged a deeper knowledge of its volcanic behaviour in order to improve the volcanic risk assessment of the area.

This work aims at understanding the volcanic history of Corbetti caldera by the combination of stratigraphic and geochemical investigations. New $^{40}Ar/^{39}Ar$ dating analyses have been also carried out on two of the main eruptions from both the syn and post caldera activity. The stratigraphic reconstruction, based on the Unconformity Bounded Stratigraphic Units method (UBSU, Salvador (1987)) as modified for the volcanic terrains by De Rita et al. (1997), revealed a complex eruptive history characterized by two eruptive epochs and four eruptive units. The concept of lithosome (Giordano et al. (2006), Fusillo et al.(2015)) has been also applied and four lithosomes have been identified (*Corbetti Composite Lithosome,* Urji lithosome, Danshe lithosome and *Chabbi Composite Lithosome*). Corbetti caldera shows a compositional gap, typical of bimodal magmatism as found elsewhere in the Ethiopian Rift (Alutu, Gedemsa, Boseti, Fantale). A petrogenesis of protracted fractional crystallization from alkali-basalt is hypothesized for most of the Quaternary calderas along the rift and the same model might be also applied to Corbetti magmatic system. The sampling and geochemical analyses for the first time of a basaltic deposit from the post-caldera activity of Corbetti, along with the new geochemical analyses of the rhyolites, allowed a comparison with the products of the Quaternary calderas of Alutu, Gedemsa, Boseti, Fantale, for a more comprehensive understanding of Corbetti volcanic history.

References

Biggs, J., Bastow, ID., Keir, D. and Lewi, E., 2011. Pulses of deformation reveal frequently recurring shallow magmatic activity beneath the Main Ethiopian Rift. Geochemistry Geophysics Geosystems 12, ISSN: 1525---2027**'.**

Fusillo, R., Di Traglia, F., Gioncada, A., Pistolesi, M., Wallace, P.J., Rosi, M., 2015. Deciphering post-caldera volcanism: insight into the Vulcanello (Island of Vulcano, Southern Italy) eruptive activity based on geological and petrological constraints. Bulletin of Volcanology 77:76 DOI 10.1007/s00445-015-0963-6.

Giordano, G., De Benedetti, A.A., Diana, A., Diano, G., Gaudioso, F., Marasco, F., Miceli, M., Mollo, S., Cas, R.A.F., Funiciello, R., 2006. The Colli Albani mafic caldera (Roma, Italy): stratigraphy, structure and petrology. Journal of Volcanology and Geothermal Research, 155, 49–80.

Scaillet, B., Macdonald, R., 2003. Experimental constraints on the relationships between peralkaline rhyolites of the Kenya Rift Valley. Journal of Petrology 44, 1867–1894.

Scaillet, B., Macdonald, R., 2006b. Experimental constraints on pre-eruption conditions of pantelleritic magmas: evidence from the Eburru complex, Kenya Rift. Lithos 91, 95–108.

Author's Declaration

I declare that the work in this thesis was carried out in accordance with the regulations of the University of Bristol. This work has not been submitted for any other academic award and it is entirely my own work except where indicated by specific reference in the text. Any views expressed in the dissertation are those of the author.

Acknowledgements

I would like to thank my supervisors, Prof. J.D Blundy and Dr. R. Brooker for giving me the opportunity to study one of the most interesting geodynamic and volcanic area on the earth. I have really learnt a lot from you.

Special thanks go to W. Hutchison for useful scientific discussions and advice for processing of LIDAR imagery, and F. Di Traglia, for reviewing the second chapter, "*The volcanic geology and evolution of the Corbetti Caldera (Main Ethiopian Rift)*" and for providing, as always, fundamental suggestions.

For technical assistance I am indebted to Ben Buse and Stuart Kearns (University of Bristol) for teaching me how to use the EMP and SEM , Iain Mcdonald (University of Cardiff), for ICP-OES and LA-ICP –MS analyses and Andrew Calvert (USGS) for $^{40}Ar/^{39}Ar$ dating analyes.

I will always remember my field assistants Asmamaw Chanie, Fekadu Aduna, Michael Hutchinson, Tulu Bedada, for their incomparable assistance, support in the field and especially for their kindness.

I would like also to thank the 'international' crew of researchers of the department, Pablo Palacios, Mikel Diaz, Luca Ziberna, e Mattia Pistone for their immense availability to help me and for their precious advice.

A big thank to my colleagues-housemates but especially friends, Alia Jasim, Maria Chapela Lara and Sasi Kansubha. Without them this work would not have been possible. Thanks also to the friends of mine, the Italian volcanologists Gianluca Sottili e Andrea Todde for their warm volcanological conversation .

Finally I would like to thank Stefano and my family for their unconditional love and support. I am especially thankful to my sister Romina for endless advice and encouragement.

The friends of ever: Marina, Laura, Beatrice and Salvatore, always present despite the distance.

A thought is also for Peter, Simon, Key, Sharon, Phil, Celia and David. Their company and friendship has been providential, grazie compagni!

This research has been sponsored by European Research Council Advanced Grant "CRITMAG" to J. Blundy**.**

Contents

1 Geological background

1.1 The Main Ethiopian Rift

The Main Ethiopian Rift (MER) is a section of the East African Rift System (EARS-extending from Afar -Red Sea–Gulf in the Aden junction in the north, to Mozambique in the south) which accommodates extension between the Nubian (African) and Somalian plates.
The MER covers the portion of land which extends from Afar to the Turkana depression and Kenya Rift, and is divided into three sectors: northern, central, and southern (Fig. 1.1).
The Main Ethiopian Rift along with the Afar depression, represents the two main physiographic segments of the Ethiopian Rift (Hayward and Ebinger, (1996), Corti (2009), Mazzarini et al.(2013))

The Main Ethiopian Rift is the biggest and most active of the intraplate rifts (Mohr & Zanettin, (1988)), where continental break-up is characterized by intense volcanism. The volcanism started with the emplacement of 600,000 km^2 (Kieffer et al. (2004)) of basaltic plateau from the Oligocene to Miocene, whereas during Pliocene and Quaternary, the volcanism localized along the rift and in the Afar depression, with the development of several volcanic centers (Mohr & Zanettin, (1988)).

The Nubian and Somalian plates are currently drifting apart (McKenzie (1970), Jestin et al. (1994), Chu & Gordon (1998), (1999)) and the formation of the Red Sea and Gulf of Aden basins, has led some authors (Ebinger & Casey, (2001)) to suggest that East African Rift System is at the initial stage of the formation of oceanic crust. This makes the EARS a unique place where is possible to study the development of the volcanism during continental break–up setting prior the formation of an oceanic basin.

1.2 Geodynamic and geological setting of the Main Ethiopian Rift.

The Main Ethiopian Rift represents the northern termination of the East African Rift System and it has been divided into three section (northern, central, and southern) on the basis of the timing and the pattern of the fault systems, of different characteristics of the lithosphere and on the basis of the rift's orientation. (Mohr (1983), Hayward and Ebinger (1996), Bonini et al. (2005), Corti, (2009)) (Fig.1.1). The MER is also considered the best place for studying the progression of the extension of the continental lithosphere and the associated tectonic and volcanism, and how they contribute to the continental rift and break-up.

The differences observed along-axis in fault architecture and lithospheric characteristic in the three sectors of the MER, have been interpreted reflecting a different stage in the development of the rift, from advanced rifting in the Northern MER to a less developed rifting towards the South (Corti et al. (2013)).

The main tectonic features of the Main Ethiopian Rift are the two fault systems, the Silti-Debre Zeyit Fault Zone (SDFZ) or boundary fault system and the Wonji Fault belt (Fig.1.1). The orientation of the boundary faults (SDFZ) is N40^{o} E in the northern part of the rift and 30^{o} E in the central MER (Corti (2008)). The boundary fault system characterizes the major escarpment that divides the rift valley from the Ethiopian and the Somalian plateaus (Fig.1,1). It developed along the rift in different time, between Late Miocene and Early Pliocene, and it has been active until the beginning of Pleistocene (Woldengabriel et al. (1990), Wolfenden et al. (2004)).

The Wonji Fault Belt system developed at the beginning of the Pleistocene about 2 Myr BP, with an orientation of ~ N20^{o} E in the northern part, and ~N12^{o} E in the central part of the MER, that suggests a variation of the direction in the extension during the Quaternary (Boccaletti et al. (1998)). This faults system is characterized by "sigmoidal, overlapping, right-stepping en-echelon fault segments" (Corti (2008)) (Fig. 1.1). These two faults systems reflect the different general orientation of the three MER sectors.

In the northern MER sector, the rift valley orients as the boundary faults (N40^{o}E) whereas it orients between N25°E and N45°E in the central MER, and it is rotated from N 20^{o}-35^{o} E to N5^{o}-20^{o} E in the southern sector (Corti (2009)).

The Wonji Fault Belt system was associated with the development of Quaternary volcanism along the rift and several volcanic centres rose along the Northern, Central and Southern MER (Woldengabriel et al. (1990), Boccaletti et al (1998), Boccaletti et al (1999)) (Fig.1.1). However the volcanism in the Ethiopian rift started in the northern part during Eocene-Late Oligocene, with the emplacement of the Ethiopia–Yemen flood-basalt province (Trap series) in the East African rift triple junction at the Red Sea–Gulf of Aden.

During these eruptions large volumes of basaltic and intercalated silicic products, were emplaced and formed subaerial volcanic deposits of an average thickness of 500–1500 m and maximum thickness of 3000 m (Mohr and Zanettin (1988)). They cover an area estimated to be currently 600000 km^2, and about 750000 km^2 before erosion. These deposits form about 90% of the Ethiopian and Somalia plateaus and 10% of the Yemen part, whereas smaller volumes of this deposits have been identified in the Afar depression (Corti (2009)).

These flood basalts province ranges in composition from tholeiitic to alkaline lava flows, interbedded with silicic lavas and pyroclastic deposits, of predominantly rhyolitic and less abundant trachytic composition (Mohr and Zanettin , 1988). The main eruptions occurred in a short period of time (from 31 to 28 Ma) during Oligocene (Baker et al., (1996), Pik et al., (1998), Ukstins et al., (2002); Coulié et al., (2003)). From Oligocene to upper Miocene (30 Ma to 10 Ma) a second stage of volcanism along the Ethiopian rift was characterized by a series of shield volcanoes developed over the volcanic plateau. This volcanic episode emplaced smaller volumes of products of transitional - alkali basalt and minor of benmoreite - trachyte composition (Piccirillo et al. (1979)).

A third phase of volcanism was from Pliocene to Quaternary and was connected to the main event of the formation of the Main Ethiopian Rift and the Afar depression. In this stage the volcanism was characterized mainly by peralkaline rhyolitic pyroclastic flow deposits and fall-out deposits, and by lesser lava flows. These silicic rocks were mostly emplaced by volcanic center-calderas along the rift and the basaltic products, associated with them, represented subordinate deposits. These basaltic products were mostly aligned along the Wonji Fault Belt and forming cinder cones and lava flows.

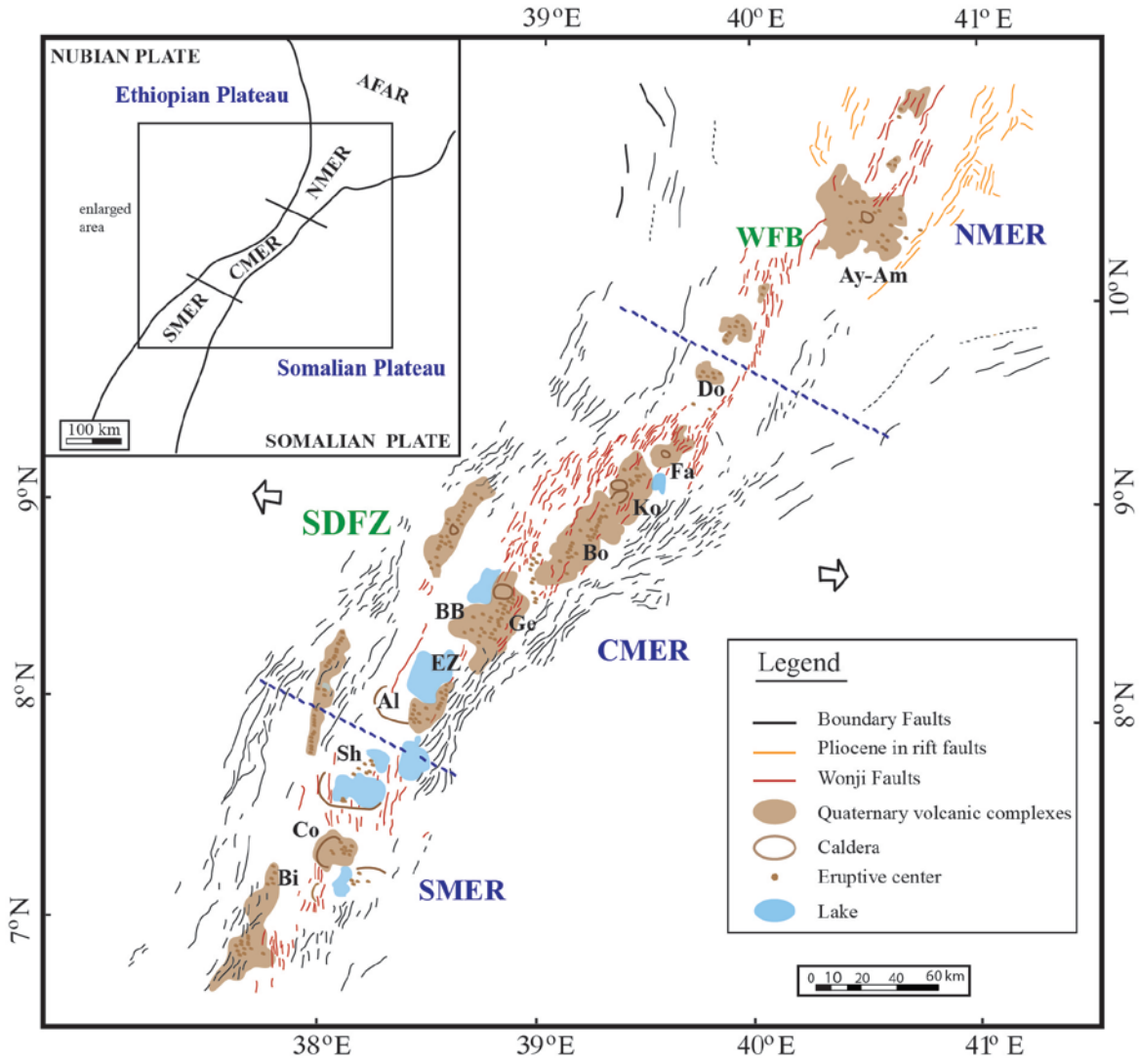

Figure 1.1

Sketch of the Main Ethiopian Rift and the fault patterns and main volcanic centres associated (modified after Keir et al. (2015)). The names of Quaternary volcanic complexes are abbreviated as follow: "Al, Aluto; Ay-Am, Ayelu-Amoissa; BB, Bora-Bericha; Bi, Bilate; Bo, Boseit; Co, Corbetti; Do, Dofen; EZ, East Ziway; Fa, Fantale; Ge, Gedemsa; Ko, Kone and Sh, Shalla". WFB denotes the Wonji Fault Belt system whereas SDFZ denotes the Silti-Debre Zeyit Fault Zone (boundary fault system). The arrows indicate the extension direction (Kogan et al. (2012)).

1.3 Relationship between tectonic and magmatism in the Main Ethiopian Rift

The Ethiopian rift represents a unique place on the earth where is possible to understand how magma intrusion affects the continental break-up. The Ethiopian rift indeed shows the development of the subaerial phase of rifting from a young stage at the southern part, to the beginning of the sea-floor extension stage at the north in Afar (Ebinger and Hayward, (1996); Hayward and Ebinger, (1996); Ebinger and Casey, (2001)). The progressively evolved stage of rifting from the south to the north offers the opportunity to study and to understand the processes characterizing the rifting in the time and the active role of the magma intrusion in the extension process.

The timing of the rifting in the East African Rift System was diachronous. The rifting started in the Gulf of Aden about 35 Ma (d'Acremont et al., (2005)) and took place in the Red Sea about 28 Ma (Wolfenden et al., (2005)), while 25 Ma occurred in northern Kenya (Morley et al., (1992); Hendrie et al., (1994)). Finally rifting developed in the Main Ethiopian Rift about 15–18 Ma (Wolfenden et al., (2004)). Geophysical studies (Rooney et al. (2011)) have shown separated areas of magmatic intrusion in the crust along the MER, and this could implies that the development of the early phase of a mid-ocean ridge is already in act. However, studies on the velocity structure of the uppermost mantle do not show any correlation with the magmatic intrusion in the crust and this implies that the processes of the oceanic basins are not yet occurring beneath the MER (Bastow et al., (2005), (2008)).

It has been seen that the Main Ethiopian Rift is characterized by two important fault systems, the Silti-Debre Zeyit Fault Zone (SDFZ) and the Wonji Fault Belt (WFB) (Fig.1.1). These two different faults system had a different role in the development and evolution of the magmatism during the extensional processes within the MER. Early models regarding the origin and evolution of the rifting in the MER involved melting, and this required that some portions of the asthenosphere were emplaced as diapirs into the lithosphere (Mohr (1987)). More recent studies on the contrary, suggest that the extension of the lithosphere changes from slip along the boundary fault system (SDFZ), to concentrated magma intrusions as dikes and the associated faulting on the rift floor (Ebinger and Casey, (2001); Casey et al., (2006)). These two important faults systems show specific structural and geochemical features.

During Miocene times, striking border faults with an orientation of about NE in the northern MER and N-S orientation in the central and southern MER, have accompanied extensional strain along the Main Ethiopian Rift (Rooney et al. (2011)). Starting from ~ 2 Ma the extension migrated in the present rift valley and covering a zone of about 20 km wide . This occurred with the development of Quaternary-recent strike-slip faults , fissures and aligned volcanic centres having an orientation of about NNE (Ebinger and Casey, (2001)).
Mohr ((1962); (1967b)) for the first time, described this Quaternary- recent volcanic tectonic system as the Wonji Fault Belt (WFB), but it has been described in more recent works (Ebinger and Casey, (2001); Keir et al., (2006a)) also as axial Quaternary magmatic segments. The WFB is considered the initial stage of the continental rift where the extension is mainly caused by the intrusion of magma batches before developing towards the formation of an oceanic basin. (Hayward and Ebinger, (1996); Ebinger and Casey, (2001); Keranen et al., (2004); Daly et al., (2008)). Further studies showed that about 80% of the extension developing in the Main Ethiopian Rift, is at present located within the the Wonji Fault Belt system (Bilham et al., (1999)).

The Silti-Debre Zeyit Fault Zone (SDFZ) is ~ 100 km long and 2-5 km wide (WoldeGabriel et al., (1990)), and, in the southern limit, shows possible overlap with the WFB structure (WoldeGabriel et al., (1990); Rooney, (2010)). Although it has been less considered in the discussion about the volcanism along the rift, the Silti-Debre Zeyit Fault Zone, represents an important area of the Plio-Quaternary magmatism developed along the western margin of the rift depression (WoldeGabriel et al., (1990); Rooney et al., (2005)). Several scoria cones and associated lava flows are present along the Silti-Debre Zeyit Fault Zone, but for the Wonji Fault Belt, the surface manifestation of faults and fractures is not well displayed (Kurz et al., (2007)). In the southern part of SDFZ, where there is possible overlap with the WFB system, magmas show trace elements distribution similar to those that characterize the northern region of the SDFZ system, but in this part there is evidence of numerous surface faults similar to those of the WFB system (Rooney, (2010)).

In the Main Ethiopian Rift , the Plio-Quaternary volcanism that developed along the eastern margin of the rifting, has been interpreted characterized by shallow magmas system and linked to the WFB system, whereas the volcanic activity occurred along the western rift margin has been associated to a deeper magma system and linked to the SDFZ system(Rooney, (2010)) .

Since the Late Miocene, the volcanism in the Main Ethiopian Rift has shown the typical bimodal basaltic-silicic signature of intraplate volcanism (Boccaletti et al.,(1995), Boccaletti et al., (1999), Trua et al., (1999)). The silicic volcanic centers have developed along the rift floor, lying at the intersection between the strike slip faults, with orientation east–west, and the main faulting trend with orientation northeast–southwest in the rift (Korme et al., (2004); Abebe et al., (2007)). The onset of the peralkaline volcanic centers has been associated with the variation of the deformation rate, whereas an increase of the extension rate within the rift has been interpreted to trigger the transition from the rhyolitic domes to the basaltic scoria cones (Mazzarini et al. (2004), Rooney et al. (2011)).

Several hypotheses have been put forward for the origin of the Ethiopian rift mafic magmas (Deniel et al., (1994); Furman et al., (2006)) with three different sources : i) the Afar plume; ii) the local asthenospheric mantle; iii) the continental lithosphere. The origin of the bimodal nature is also controversial. Different hypotheses have also been done so far, and the origin of the bimodal gap has been attributed the following processes: i) partial melting of the crust (Suneson Lucchitta (1983)); ii) immiscibility of different types of magma (Cherlier et al. (2011)): iii) crystallization of particular mineral phases (Grove and Donnelly (1986)); iv) different processes occurring within magma chambers (Brophy (1991), Freundt-Malecha et al. (2001), Lakhssassi et al. (2010)).

The WFB basalts, particularly those from Gedemsa, Fantale–Dofan, Kone–Boseti, and Shalla magmatic segments, show similar pattern regarding some trace elements (positive Ba, Nb and Ta anomalies). Some authors relate these patterns to a magma mixing between silicic and basaltic liquids (Peccerillo et al., (2003); Rooney, (2010)).

In general a more comprehensive understanding of the evolution of the tectonic and the volcanism associated to the development in the Main Ethiopian Rift, is required to improve our conventional models for explaining rift evolution, including the origin of the silicic magmas and the bimodal relationship with the basalts.

1.4 Overview of the volcanic and geochemical features of the principal MER's calderas .

In order to understand the volcanic nature and characteristic of the Corbetti caldera complex, as part of the rift's Quaternary volcanism, is worth to have an overview of the volcanic and geochemical features of some of the main calderas along the rift : Alutu, Boseti, Fantale and the Boina volcanic center.

The geographical position and the geochemical data available of these calderas make them the most suitable for comparison. Corbetti caldera lies close at the limit between the central and southern sectors of the MER, whereas volcanoes as Alutu, Gedemsa, Boseti, Fantale and Boina, lying in the central sector up to the north in Afar region, have been chosen according to the timing of the extensional tectonics of the rift. Indeed it has been seen that the Main Ethiopian Rift is characterized by different magmatic segment linked to the oblique extension started at the end of Pliocene, due to the re-orientation of the stress field, and proceeded up to the Quaternary east-west extension, that produced sinistral oblique rifting and activated the en- echelon Wonji segements (Boccaletti et al. (1999), Corti (2008)).

These volcanic centres have been object of several studies and especially considered for models to explain possible petrogenesis by fractional crystallization plus some crustal assimilation, (Barberi et al.(1975), Lowenstern and Mahood (1991),Boccaletti et al. (1999), Peccirillo et al. (2003), Giordano (2006), Peccirilo et al. (2007),Ronga et al. (2010), Giordano et al. (2013), Hutchison (2015)). They have been all , with the exception of Boina center, interpreted as calderas on the basis of their volcanic structure. Their volcanic history has been characterized by a pre, syn and post caldera activity , where an ignimbrite or PDC deposit is the product emplaced by the caldera forming eruption. In most of them, while the most evolved composition characterized the pre- caldera activity , the basaltic and trachy-basalt deposits are often associated with the newest eruptions of the post-caldera activity and occurred off the main volcanic edifice.

Alutu is a silicic peralkaline volcano, which lies in the southern part of the central sector of the Main Ethiopian Rift (Fig.1.1). Its volcanic history has been interpreted to start at about 500 ka with a volcanism that emplaced deposits of trachytic, trachy-andesite composition.

Two distinct eruptions emplaced big volume of ignimbrite deposits and occurred at 316 ± 19 ka and 306 ± 12 ka. This resulted in the caldera collapse. The postcaldera volcanism, after a period of rest of ~250 ka, has taken place between 55 ± 19 ka and 16 ± 14 ka, and was characterized by both effusive (lava) and explosive (ignimbrites, fall-out) deposits of "highly-

evolved peralkaline rhyolite" composition. The eruptive vents were aligned across the volcanic complex. Undifferentiated basaltic lava samples were found on the uplifted eastern flank of Aluto and interpreted associated with volcanism preceding the Alutu volcanic complex activity. Blocks of basalt were also identified as lithic clasts within PDC deposits, and other mafic – intermediate lithic clasts have been found within the post- caldera deposits. This suggests that primitive-intermediate products underlie the Aluto complex (Hutchison et al. (2016)

Gedemsa volcano is located in the central part of the central sector of the Main Ethiopian rift, to about NE of Alutu volcano (Fig.1.1). The pre-caldera activity emplaced lava domes ,lava flows and fallout deposits, whereas ignimbrites mostly characterized the deposits of the the syn-caldera activity. From field evidences it has been interpreted that the caldera-forming eruption was not characterized by a single big eruption but , as also observed in Alutu , was related to "several moderate-volume pyroclastic eruptions, which took place in different sectors of the volcano (Cioni et al., (2001))".

The post-caldera activity occurred mostly within the caldera depression with several small coalescing cones and emplaced mainly obsidian domes and flows and pyroclastic fall-out deposits. As also observed at Alutu, the more evolved products from the post-caldera activity show inclusions of mafic-intermediate magma. The juivenile clasts of the syn-caldera deposits (ignimbrites) also show mingling processes between mafic and silicic magmas, although are less numerous than in the post-caldera.

The most recent activity in the area of Gedemsa, developed along the Wonji Fault Belt system on the eastern part of the volcano, but this activity has been interpreted not from Gedemsa volcano but from the newest volcanism developed as basaltic centres along the Wonji Fault Belt system as also observed in other parts along the rift.

The Wonji Basalts at Gedemsa volcano area, are represented by two little eruptive centres located one within the caldera and the other at the foot of the northeastern flank of the volcano. Also the products (lava and scoriae) from the late basaltic eruption occurred within the caldera, although not related to the Gedemsa volcano, show marks of magma mingling. The majority of the Gedemsa products are rhyolites and trachytes, and the less abundant mafic products are transitional basalts. The composition of the inclusions in the post-caldera products, ranges from basalt to benmoreite . Ages of 0.32 ± 0.02 Ma are given (K/Ar method) for the pre-caldera volcanism, and 0.26 ± 0.02 Ma for the post-caldera volcanism (Peccirillo et al. (2003)) .

The **Boseti Volcanic Complex** lies in the northern part of the central sector of MER, to NE of Gedemsa volcano (Fig.1.1). It is composed of the aggregation of "two main volcanic edifices, Gudda and Bariccia". According to previous works (Paola (1972), Brotzu et al. (1974), (1980)) the magmatic activity occurred in three main phases: i) the pre-caldera activity, that formed the "main volcanic edifice" (old Gudda), ii) the caldera forming eruption and iii), the post-caldera activity, which formed the Gudda and Bariccia centeres.

The pre-caldera activity occurred during Pleistocene and was characterized by the emplacement of both basaltic lava flows, spatters and cinder cones and peralkaline rhyolitic lava flows. After the caldera forming eruption with consequent collapse of the old Gudda, the resurgent volcanism was characterized by the new Gudda edifice (Pleistocene-Holocene), that emplaced lava flows of pantelleritic composition, interposed with pantelleritic and comenditic pumiceous deposits and lava flows, and the newest Bariccia volcano . This second eruptive center was characterized by two volcanic episodes. The first episode emplaced the early products of trachytic composition and the late pyroclastics products of of trachytic and rhyolitic composition. The second event emplaced lava flows and pyroclastic deposits of pantelleritic composition (Ronga et al. (2010)).

Fantale is a strato-volcano located in the more northern part of the central sector of the Main Ethiopian Rift, close to the limit with the northern sector of the MER (Fig.1.1). It is characterized by a "summit caldera". The pre-caldera activity was characterized by lava flows and fall-out deposit of trachytic and rhyolitic composition. The main deposit is a welded ignimbrite connected with the caldera forming eruption dated by Williams et al. (2004) at 168ka. Gibson (1970) identifies five units within the welded ignimbrite, where the first units erupted have a pantelleritic composition, whereas the last emplaced have a trachytic composition, suggestsing a zoned magma chamber. The post- caldera rocks include glassy trachyte lava flows and glassy pantelleritic lava flows.

Only two episodes of basaltic volcanism characterized the newest activity of Fantale volcano, emplacing products on the western flank of the main edifice. The eruptive centres of this newest basaltic volcanism, are aligned along the direction of the Wonji Fault Belt system. The most recent basaltic eruption have been dated by historical publication, at 1810 AD. Fantale volcano is currently in a fumarolic phase. (Giordano (2006)).

Since at **Boina – centre** has been tested (Barberi et al. (1975)) that the transitional basalt-pantellerite sequence, characterizing the Boina deposits, was determined by fractional crystallization, this volcanic centre can be chosen as paragon to compare the geochemistry of the other volcanic centres selected, and of Corbetti caldera.The Boina centre is located in the Dabbahu region in the Central -Western Afar rift, and is delimited by the Alayta volcano in the north, and basaltic lava fields in the south. Boina is a shield volcano formed on the fissural basaltic lava fields, and having the last silicic products covering the top of the volcanic structure. The early products were emplaced by fissures with an NNW orientation and that has been interpretd as the prolongation of the Alayta volcano. The succession of the deposits is characterized by basaltic lavas, emplaced by the early fissure activity, lava flows of intermediate composition, that form the shield volcano structure, and the final more evolved products. The more evolved products were erupted as obsidian flows, crystalline domes and less abundant pyroclastics. The basalts therefore, in Boina centre , on the contrary of the most of the other volcanic centres along the rift, are the only product from initial fissure activity, whereas the intermediate and rhyolites rocks were emplaced in the developed phase of the central volcano.

1.5 Previous studies on Corbetti Caldera area

1.5.1 Introduction

The Corbetti Caldera complex lies in the southern part of the Lakes Region, between Shalla and Awasa lakes in the southern sector of the Main Ethiopian Rift.
Corbetti volcano is the expression of Quaternary volcanism associated with the development of the Wonji Fault Belt (WFB) segments. The WFB is the second fault system in the area to develop after the Boundary Fault system in the past 2 Myr (Corti (2008)) and is interpreted to be linked to a phase where magma plays a fundamental role in the rift during the advanced stage of the continental rifting (Kendall et al. 2005, Bastow et al. (2010)). This results in the development of caldera structures, cinder cones and eruptive fissures aligned along the axial direction of the rift valley.

After the caldera forming eruption, the volcanic activity at the Corbetti complex resumed with eruptions from three new vents within the caldera: Uri, Danshe and Chabbi. While the activity of other calderas (Fantale, Kone, Boseti, Gedemsa) along the main axis of the rift is well studied (Gibson et al.(1970), Cioni et al.(2001), Ayalew et al.(2003), Williams et al.(2004), Orsi et al.(2007), Rampey et al.(2010)), the volcanic history of Corbetti Caldera is much less well constrained and few modern studies have been carried out. The first studies on the Corbetti Caldera area took place in the 1960s and early 1970s of the last century (Mohr (1966), Macdonald et al. (1969), Di Paola (1971), Woldegabriel et al.(1991)) when the concepts of eruptive and volcanoclastic units, as well as classification of the tephra and pyroclastic density current deposits were just beginning to develop (Sparks and Walker (1973), Spark (1976), Wright and Walker (1977), Fisher (1979), Wilson and Walker (1982), Druitt and Sparks (1982), Walker (1983), Fisher and Schmincke (1984), Walker (1985), Valentine and Fisher (1986)).

More recently, fumarolic and hydrothermal activity in the area has also prompted geothermal investigations for a potential geothermal energy development (“ The Geological Survey of Ethiopia and its activities” - First International Conference on Geothermal Energy in the East African Rift Region (ARGeoC1), Addis Ababa, Ethiopia (2006); “Geology and Surface Alteration of the Corbetti Caldera Area” - Geothermal Institute, University of Auckland, (1984), E.F. Loyd, Technical Report - United Nations (1973))

Apart from this cursory interest, Corbetti is remained a volcano of little interest, along with many of the other centres in this part of the rift, that were considered quiescent with no historic activity. However, this situation has recently changed as it was realized that Corbetti and neighbouring Alutu, Bora, and Haledebi, have been undergoing extremely active deformation in the last twenty years. In particular at Corbetti, ground-deformations recorded by space-borne InSAR data, revealed that subsidence affected the caldera floor in the late '90s (1997-2000) followed by an inflation that started since 2009, coherent with a source of deformation ~5 km deep (Biggs et al. (2011)).

In the absence of a detailed knowledge of the eruptive history, an assessment of volcanic hazard should be primary based on the stratigraphy and investigation of the past activity in order to reduce the level of uncertainty related to the volcanic hazard elements (i.e. pyroclastic flows, lava flows, tephra fallout, volcano type, eruption frequency, etc, Aspinall et al. (2011)). The aim of this work is to provide a stratigraphic reconstruction of Corbetti's activity along with a new geological map and geochemical characterization of the deposit, in order to temporally constrain the volcanic evolution of Corbetti complex and to improve the understanding of its eruptive history.

1.5.2 Previous studies on Corbetti Caldera

In this section I review the previous studies on the Corbetti Caldera area, which were the result of investigations between the end of the sixties and the beginning of the eighties. The last study is of Raprich et al. in 2105. This forms the basis for a good comparison with our study and further development of the understanding of Corbetti volcanic complex.

The first studies of the geology of the volcanic complex were by Mohr (1966) and Di Paola (1971), with Macdonald et al. (1969) adding geochemical data from one of the most recent deposit of Corbetti Caldera. Both the United Nations (in 1973) and the Geothermal Institute of the University of Auckland (in 1984) assessed Corbetti complex for potential geothermal energy development.

In addition to these early investigations, the first publication of chronological data of Corbetti Caldera deposit was by Woldegabriel et al. (1991). This dated one of the most recent obsidian flow from Chabbi volcano with the K/Ar methods, that resulted to be emaplaced 0.02± 0.01 m.y.B.P.

The last work regarding the Corbetti volcanic system is from Rapprich et al. (2015). In this paper the authors studied one explosive eruption and obsidian lava deposits from the early and last post caldera activity. They also presented a geological map of the area, isotopic analyses ($^{87}Sr/^{86}Sr$) of the products from the explosive eruption investigated and dating of deposits from Corbetti post-caldera activity, with radiocarbon dating.

Mohr (1966), investigated the deposits from Chabbi volcano, of the post-caldera vent of the Corbetti caldera complex. He describes Chabbi as a composite volcano that emitted "obsidian lavas and pumice-ash flows". He identified seven eruptive centres ("the Main Vent , the East Vent, the Hot Cone, the West Vent, the North Vent, the North – East Vent I and the North East Vent II") which have been active at different periods during its volcanic history, although the author does not provide a temporal sequence of the activity.

The Main Vent is described as a dome formed on older pyroclastic beds "over which extensive obsidian lava flows have flowed in very recent times". These obsidian lava flows are reported as the youngest and most voluminous deposits emplaced by Chabbi.

Mohr described the activity of the rest vents (the East Vent, the Hot Cone, the West Vent, the North Vent, the North-East Vents I and II) as being characterized by the emplacement of earlier pyroclastics deposits followed by lava flows which occurred in several phases for each vent. Mohr hypothesized that the North Vent had the most extensive volcanic deposits although he did not carry out any survey in the north sector of Chabbi.

Macdonald and Gibson (1969) provided a seminal study on the geochemistry of Corbetti caldera. In this work they carried out the first chemical composition analyses of the obsidian flows from the newest eruptive center of Chabbi. The analyses suggested a transitional composition between comendites and pantellerites for the Chabbi's obsidian flows. However, the authors classified the Chabbi lavas as pantellerites on the basis of the 12.5 % normative mafic constituents, using "the arbitrary division between these groups established by Lacroix (1927) and adopted by Noble (1968)".

Gibson and Macdonald noted for the first time two particular features of Chabbi obsidian flows : i) the obsidian flows appear to be completely lacking phenocrysts ; ii) the composition of Chabbi products, probably erupted over several thousand of years, remained constant.

They suggested for the aphyric texure of Chabbi products that crystallization was "inhibited by high viscosity, itself a function of a relatively anhydrous nature".

To explain the constant composition of the magma that fed all the volcanic activity of Chabbi , they hypothesized a complete fusion of a peralkaline granite. They suggest this as a probable process to generate homogeneous rhyolite magma assuming that it was superheated and remained so up to the eruption.

They also hypothesized a liquid immiscibility relationship between basalt and rhyolite at temperature above the rhyolite liquidus. The silicic liquidus would have separated from the basalt and brought to the surface in a superheated condition that would have inhibited the crystallization. However Gibson and Macdonald state that the lack of basalt samples from Chabbi deposits makes this last hypothesis questionable.

In conclusion Macdonald and Gibson propose a combination of superheating followed by supercooling due to the dryness, to explain the lack of crystals in Chabbi products. Regarding the peculiarity of Chabbi magma composition, they stated that whether the composition could have been produced by a recurrent process involving a "eutectic" composition (fractional crystallization or partial fusion of basic material), or whether the Chabbi lavas could have been derived from a single magma batch, this is not known. What is interesting is that Macdonald and Gibson stated that Chabbi appears to be , for the nature of its products, a 'unique volcano'.

Di Paola (1971), provided the first description of the volcanology and geology of the Corbetti Caldera volcanic complex. He identified for the first time the caldera structure and the subsequent volcanic activity. He describes several fissures eruptions that characterized the activity before the volcano-tectonic caldera collapse, after which further activity resumed with the eruptions of the "two recent peralkaline volcanoes, Urji and Chabbi". He reports a coarse and unwelded ignimbritic deposit covered "by a typical ignimbritic formation" as the most ancient products of the area. Di Paola describes this deposit having in the lower part a "welded with the typical fiamme structure", whereas in the upper part the ignimbrite remains un-welded and rich in pumices. He points out how it was not possible to clearly identify any center of eruption for this ignimbritic deposit.

Another important feature in the Corbetti area, is formed by several layers of un-welded pumices which reach the maximum thickness (> 200 m) on the west part of Corbetti Caldera. Di Paola claimed it was not possible to establish any relationship between the ignimbritic deposit and the pumice layers. The last activity of Corbetti Caldera was characterized by several pumice flows and air-fall deposits associated with obsidian flows from Urji and Chabbi vents .

Di Paola recognized several NNE-SSWsteps faults that affected the older volcanic deposits of the area but that pre-dates the products of the most recent vents. He interpreted theses faults along with the massive amount of pyroclastic deposits of the volcano complex, as the product of a big eruption that induced a regional collapse which formed the Corbetti Caldera. The ignimbrite formation and pumice layers outcrop on the north and west rim, whereas the south rim is cut into rhyolitic lava deposit.

Following the caldera forming eruption, the resumed activity was associated with the Urji and Chabbi vents. Di Paola describes Urji as a pyroclastic volcano and suggested its birth as the most important event of the post-caldera activity of the Corbetti complex. In Di Paola's reconstruction of Corbetti volcanic history, the activity of Chabbi was contemporary with the Urji vent. Di Paola describes Chabbi deposits as mostly formed by pyroclastics and interprets the massive obsidian flows on the western and southwestern side of Chabbi, as a final localized activity of the volcano. The author suggests that the entire volcanic activity in the Corbatti Caldera area, including Urji and Chabbi, represented a highly explosive manifestation of silicic magma with a very high volatile content. Only at the end, Corbetti activity was characterized by a degassed magma which was erupted as obsidian flows.

The author also presented chemical analyses of a pumices sample collected on the northern slope of Chabbi and reported that "the alkali-olivine basalts products are clearly subordinate to the silicic rocks in the Corbetti caldera area".

Di Paola considered Corbetti Caldera as being dormant with the many thermal manifestations and steam fumaroles (with a minor quantity of H_2S) characterizing the current activity.

Altaye (1984) provides the most detailed description of the stratigraphy and petrography, along with the first geological map of Corbetti Caldera (Fig. 1.2), in unpublished work as report for a diploma in Energy Geothermal Technology , "Geology and Surface Alteration of the Corbetti Caldera Area", University of Auckland (1984).

The main target of Altaye's work was to reconstruct the past and the present history of a dynamic hydrothermal system, based on the geology of the area, with particular emphasis on the surface alteration and the development of clay minerals. This report work also identifies for the first time another volcanic center named Danshe, in addition to Urji and Chabbi, as the expression of the post-caldera activity.

In terms of Corbetti stratigraphy, Altaye (1984) maintains the division of deposits between 'Caldera and Pre-Caldera Rocks' and 'Volcanic rocks post-caldera succession'.

He identifies five units in both the 'Caldera and Pre-caldera Rocks' sequence (Qawi, Qwb, Qr1, Qp1, Qqwp) and the 'Volcanic rocks- post caldera' sequence (Qr2, Qcp, Qlib, Qb, Qr3). He points out how the proposed sequence is open to alternative interpretation because of the lack of any age determinations. Altaye further reports, that the age assumed by Di Paola (1971) for the 'Volcanic rocks post-caldera' covered a few thousand years, while the period for the 'Caldera and Pre-caldera Rocks' was of a few hundred thousand years.

The 'Caldera and Pre- Caldera Rocks' succession starts with the **Qawi** –unit, characterized by ignimbrites deposits outcropping on the western and northern caldera rim. This is followed by the **Qwb** –unit, a basaltic deposit, although this deposit does not outcrop in the study area but the author was able to observe from the core sample of a drilled well**.** The following unit, **Qr1**-, includes peralkaline rhyolitic lava domes and southern caldera rim rocks. It is overlaid by the **Qp1**- unit, a 'pumiceous ignimbrite' deposit found in deep gorges of Chabbi and interpreted as the product of the caldera forming eruption. The last unit of the 'Caldera and Pre-Caldera Rock' succession is the **Qqwp** –unit, formed of 'layered pumice pyroclastics', which outcrops on the southern, northern and western slope of the caldera rim.

The sequence of the 'Volcanic rocks post-caldera' starts with the **Qr2** –unit, characterized by 'obsidian lava covered by pumices'. The author interprets the deposit of pumices as possibly produced by vents aligned east-west and north-south direction. The following unit is the **Qcp** – unit, which is made up by 'recent pumice falls and flows' and it is identified in different places in the Corbetti area. The author describes it as emplaced from 'a number of centers'. The succession continues with the **Qlib** –unit described as hyaloclastites resulting from explosive activity of basic magma occurring in shallow water. However, **Qlib** does not outcrop inside the Corbetti Caldera. The following unit is the **Qb** –unit, is characterized by 'basaltic lava flows and scoria cones'. One of the main features of this unit its associatied with features of hydrothermal activity. **Qb** outcrops mainly outside Caldera with a single outcrop on the North-western caldera rim in the form of a dyke.

Altaye (1984) interprets this unit as the products of volcanism associated with the 'Corbetti-Shalla–sector' of the Wonji fault belt. The "Volcanic rocks post-caldera" sequence closes with the **Qr3**-unit, a 'recent obsidian lava flows' deposits interpreted as originating from Chabbi volcano and representing the last activity of the Corbetti Caldera. Altaye (1984) also provides a short description of the products of Urji, Danshe, Chabbi vents which represent the post- caldera activity. He describes Chabbi as mainly characterized by 'recent obsidian lavas and partly by pumices falls and flows erupted from several centers'.

He restates the idea of Di Paola (1971) that Chabbi was recently active probably as a result of the opening of secondary NW-SE faults system. Urji vent is described as made up of pumices, ash and obsidian covered by 'pumice falls and flows', while Danshe vent is described as 'totally pyroclastic'.

The author also presented in his work the chemical analyses of two samples collected from the caldera wall, presumably deposits from the syn-caldera activity and one sample from the deeply gullied valley of Chabbi volcano. One of the main aims of Altaye's work was to investigate any change in the chemistry between the syn- and post-caldera activity and also to try to discover any significant fractionation trends within the Corbetti caldera products, as they appear to be chemically and mineralogically uniform.

Based on the Al_2O_3 vs FeO^T classification diagram proposed by Macdonald (1974) , Altaye classified all the analysed Corbetti samples as peralkaline, rhyolite, pantellerites.

In general Altaye (1984) suggested a crystal fractionation of akali-basalt as the dominant petrogenetic process that generated the Corbetti caldera products, although he did not collect any basalt sample.

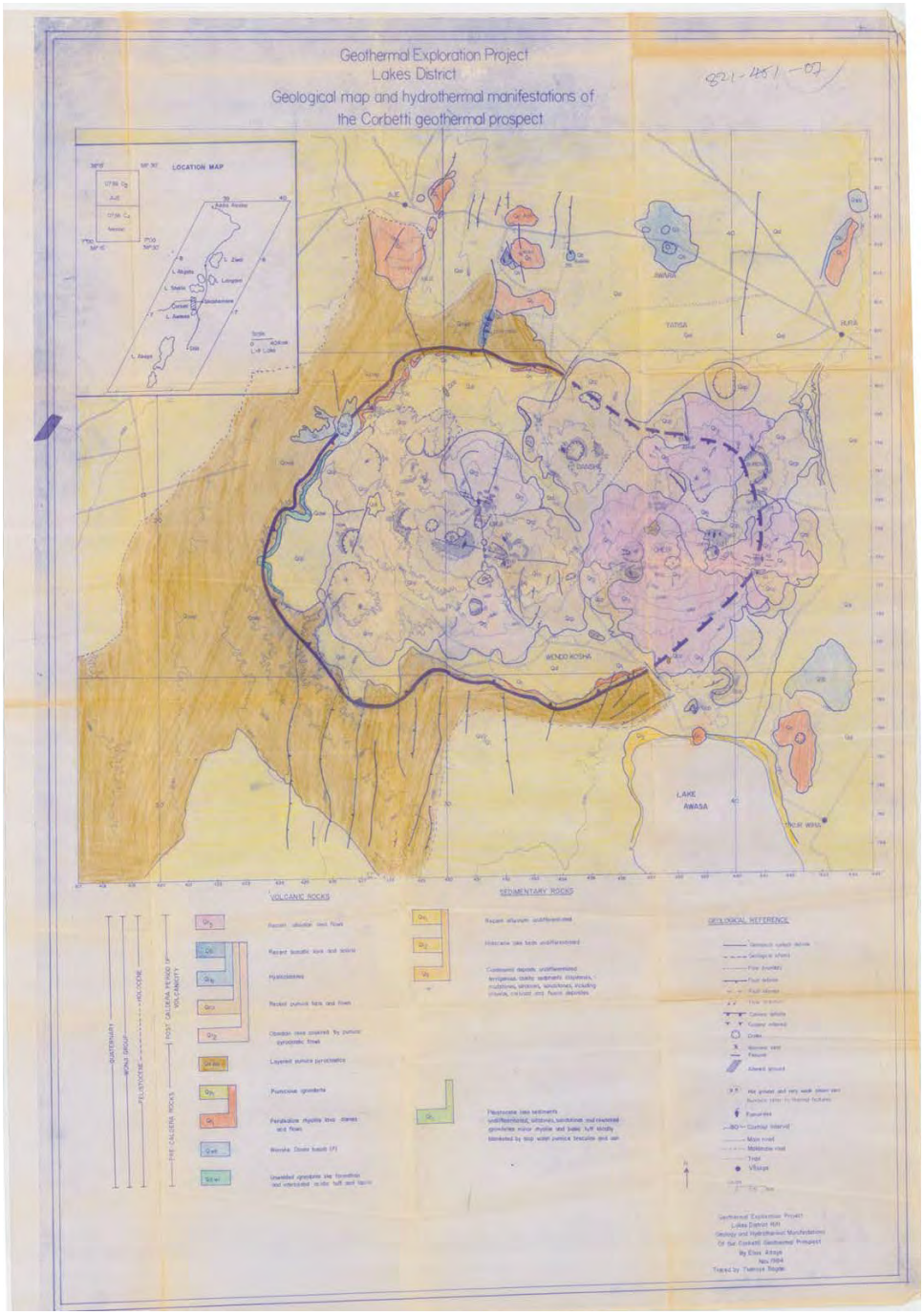

Figure 1.2

The first geological map of Corbetti Caldera by Altaye (1984).

Rapprich et al. (2015) focused their study on one explosive eruption from the post-caldera activity of the vent Wendo Konshe, which corresponds to the Urji vent as indentified in Di Paola (1971) and Altaye (1984). They described the activity of Wendo Konshe (Urji) as following the early post - caldera activity of the vent Artu, which corresponds to the vent identified for the first time by Altaye (1984) as Danshe. They also analysed some of the obsidian lava flows (COX, CO2, CO3, CO6) emitted from Chabbi volcano.

On the basis of their reconstruction the last explosive eruption from Wendo Konshe (Urji) produced a "widespread pumice lapilli deposit, the 'Wendo Konshe younger pumice", likely associated with "a small obsidian lava flow within the Wendo Konshe crater". This deposit overlies the 'Wendo Konshe older pumice'. In a site close to the Wendo Konshe source crater, Rapprich et al. (2015) identified a paleosoil between the younger and the older pumice deposit, whereas a 3m thick of "bedded to laminated phreatomagmatic lapilli tuff of uncertain origin underlie the 'Wendo Knoshe older pumice".

The authors also report that the previous eruptions of Wendo Konshe emplaced thick accumulation of "pumice with monotonous appearance and that therefore the history and evolution of the Wendo Konshe vent is difficult to reconstruct." On the basis of Rapprich et al. (2015) reconstruction, the 'Wendo younger pumice ' would have covered earlier obsidian lava flows (COX, CO2) emplaced by Chabbi and they would have been covered by the following obsidian lava flows **(**CO3, CO4, CO5, CO6) emplaced during the last activity of Chabbi. They also dated another paleosoil between the Wendo Konshe pumice and a yellowish tuff related to the Fike volcano, with radiocarbon dating ^{14}C, and resulting in age of 396 ± 38 years B.C.

Regarding the geochemistry of Corbetti products, Rapprich et al. (2015) investigated both the major and trace elements content. They classified the rocks as peralkaline rhyolite on a TAS diagram and found a shift from comendite to pantellerite composition during the evolution of the post-caldera activity, when plotted on Al_2O_3 vs FeOt diagram. Rapprich et al. (2015), in keeping with previous works (Macdonald and Gibson (1969), Di Paola(1972), Altaye (1984)) did not sample and analyzed any basaltic rocks linked to the Corbetti caldera activity. As a consequence, the authors state that "it was not possible to numerically model the origin of Corbetti volcanic system magmas, because the necessary parental basic end-member was missing, likewise the intermediate members". Therefore they applied to the Corbetti Caldera products, the geochemical model that Peccirillo et al.2003 applied to the Gedemsa volcano in order to explain the petrogenesis of the high volumes of felsic rocks.

The model was also applied to explain the volcanism of other quaternary calderas along the rift (Peccirillo et al. (2007)).

Rapprich et al. (2015) also presented a geological map of the area (Fig.1.3) made by fieldwork in addition to remote sensing techniques using "stereoscopic aerial photos combined with satellite multispectral image Landsat". They also attempted an estimation of the total volume of the Wendo Konshe pyroclastic deposits that resulted to be of 2.3km^3 which is equivalent to 0.4 km^3 of dense rock equivalent (DRE).

Whilst these seminal studies greatly advanced our understanding of this volcanic complex, the methods and terminology used, are for most of them a little dated. In this work I will use new field data along with the UBSU metodolgy (chapter 2) to reconstruct a stratigraphic sequence of Corbetti deposits which allows a better understanding of the Corbetti volcanic evolution. These new field data and the method applied, also allowed production of a new geological map of the Corbetti volcanic complex (chapter 2)

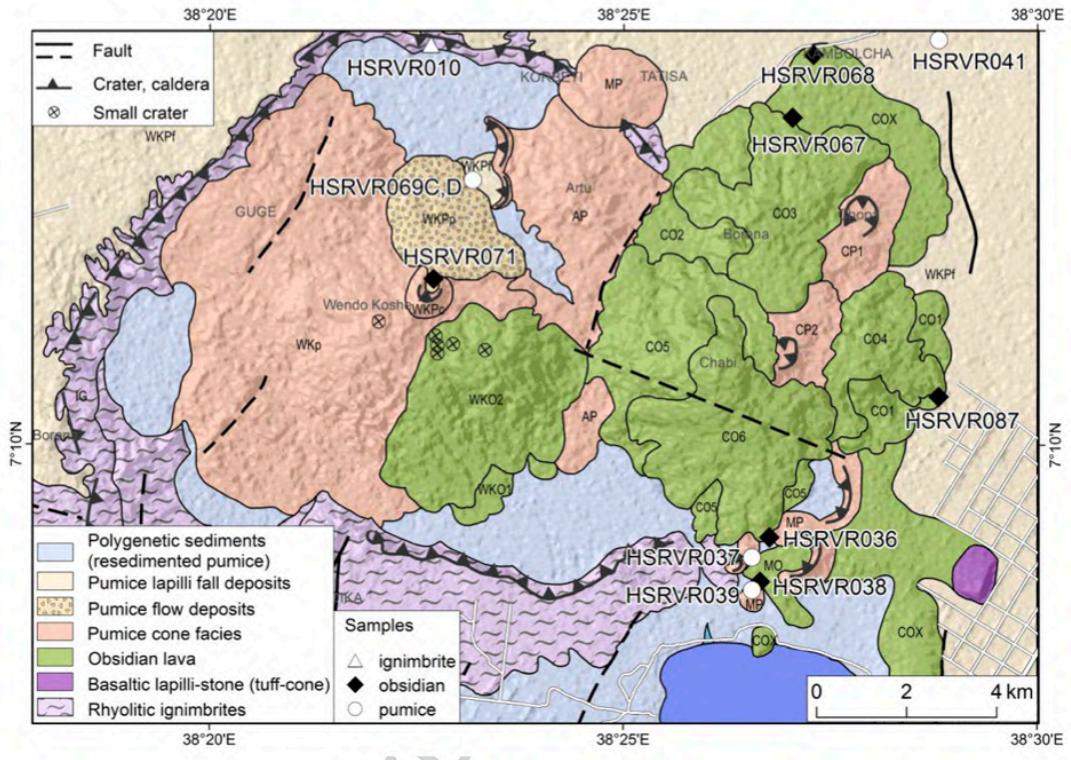

Fig. 1.3
Geological map of Corbetti caldera by Rapprich et al. (2015).

1.6 Thesis overview

1.6.1 Aims of this study

The aim of this research is a more thorough knowledge and understanding of the volcanic history of the Corbetti caldera in the southern sector of the main Ethiopian Rift.

This investigation was carried out concurrently with the cooperation between University of Bristol, University of Oxford , Addis Abeba University and the Ethiopian Mapping Agency , and is related to the ARSF 2012 FLYING SEASON project –"Understanding volcanic hazards in the Main Ethiopian Rift: Alutu and Corbetti" ,

Corebtti caldera, as well as other volcanic centers (Haledebi, Bora, Alutu) in the southern sector of the Main Ethiopian Rift, has shown active deformation recently (from 1997 to 2010) as it has been identified by InSAR investigations (Biggs et al, (2011)), and also shows intense fumarolic activity. This rekindled scientific interest toward this poorly understood volcanic area.

Corbetti volcano is essentially an 'unknown volcano' regarding the uncertainty and risk related to the volcanic hazard elements (i.e. pyroclastic flow hazard, lava flow hazard, volcano type, eruption frequency, etc), but it lies in the highest level of risk, as reported in "GFDRR, Volcano Risk Study; Volcano Hazard and Exposure in GFDRR priority countries and Risk mitigation Measure", (Spinall et al. (2011)). There are currently only few studies available in the literature, and the fact that Corbetti volcano also lies close to densely populated area, Awasa and Shashemene cities, makes this volcanic complex potentially dangerous .

A better understanding of the Corbetti's past volcanic history and behavior, will help to reduce the uncertainty level, and better constrain the volcanic hazard of the area.

New $^{40}Ar/^{39}Ar$ dates has been also determined on the syn-caldera deposits and on products from the newest activity of the post-caldera eruptive epoch. This thesis reports the results for the adopted multidisciplinary approach involving fieldwork and mapping, geochemistry and geochronology , in order to improve our knowledge and understanding of the volcanic activity of Corbetti caldera and to better constrain the assessment of the volcanic hazard of the area.

1.6.2 Thesis Structure

Thesis structure as follows:

Chapter 2, *The volcanic geology and evolution of the Corbetti Caldera (Main Ethiopian Rift),* aims to revise the previously accepted evolution of Corbetti volcanic history through the stratigraphic reconstruction of the past eruptive events. The stratigraphic reconstruction is carried out by using the Unconformity Bounded Stratigraphic Units method (UBSU, Salvador (1987)), modified for the volcanic terrains by De Rita et al. (1997), along with the concept of lithosome, which discriminates deposits related to the same eruptive centre (Giordano et al. (2006), Fusillo et al. (2015)). This chapter also includes a new geological map of the entire caldera and the geological map of one of the post-caldera volcanic center (Chabbi), based on the stratigraphic reconstruction and using both ASTER imagery and high-resolution LIDAR imagery. New $^{40}Ar/^{39}Ar$ dating analyses from products of the syn and post –caldera eruptive epoch of Corbetti caldera (Main Ethiopian Rift), are also presented in relationship with the new stratigraphic reconstruction.

Chapter 3, *The geochemical characterization of Corbetti caldera products (Main Ethiopian Rift)*, focuses on whole rocks' major and trace element composition of the deposits from both pre-syn caldera eruptive epoch and post- caldera eruptive epoch. Particular attention has been put on two considerations: i) observing if the geochemical characterization of the deposits confirmed the stratigraphic reconstruction presented in the chapter 2; ii) observing if there were any similarity in the geochemical characterization between Corbetti deposits and those from other Quaternary calderas along the rift (Alutu, Gedemsa, Boseti, Fantale). These considerations have been used to progress our understanding of the petrogenesis of Corbetti rocks, the magmatic evolution and the consequent volcanic activity of Corbetti caldera.

Chapter 4, *Conclusions : The volcanic history of Corbetti caldera (Main Ethiopian Rift),* summarizes the main results from the stratigraphic, geochemical investigations and the dating analyses .In this section are also presented which further investigations would be necessary to further constrain our understanding of this volcanic complex.

References

Abebe, B., Acocella, V., Korme, T., Ayalew, D., 2007. Quaternary faulting and volcanism in the main Ethiopian Rift. Journal of African Earth Sciences 48 (2–3), 115–124.

Baker, J., Snee, L., Menzies, M., 1996. A brief Oligocene period of flood volcanism in Yemen. Earth and Planetary Science Letters 138, 39–55.

- Barberi, F., Ferrara, G., Santacroce, R., Treuil, M. & Varet, J. 1975. A transitional basalt-pantellerite sequence of fractional crystallisation, the Boina centre (Afar Rift, Ethiopia). Journal of Petrology 16, 22-56.

Bastow, I.D., Stuart, G.W., Kendall, J.M., Ebinger, C.J., 2005. Upper-mantle seismic structure in a region of incipient continental breakup: northern Ethiopian rift. Geophysical Journal International 162 (2), 479–493.

Bastow, I.D., Nyblade, A.A., Stuart, G.W., Rooney, T.O., Benoit, M.H., 2008. Rifting at the edge of the African low velocity anomaly. Geochemistry Geophysics Geosystems Q12022. doi:10.1029/2008GC002107.

Biggs, J, ID Bastow, D Keir and E Lewi 2011. Pulses of deformation reveal frequently recurring shallow magmatic activity beneath the Main Ethiopian Rift. Geochem Geophys Geosystems 12, Q0AB10.

Bilham, R., Bendick, R., Larson, K., Mohr, P., Braun, J., Tesfaye, S., Asfaw, L., 1999. Secular and tidal strain across the main Ethiopian rift. Geophysical Research Letters 26(18), 2789–2792.

Boccaletti, M., Getaneh, A., Mazzuoli, R., Tortorici, L., Trua, T., 1995. Chemical variations in a bimodal magma system; the Plio-Quaternary volcanism in the Dera Nazret area(Main Ethiopian Rift, Ethiopia). Africa Geoscience Review 2 (1), 37–60

Boccaletti, M., Bonini, M., Mazzuoli, R., and Abebe, B., 1998, Quaternary oblique extensional tectonics in the Ethiopian Rift (Horn of Africa): Tectonophysics, v. 287, p. 97–116.

Boccaletti, M., Bonini, M., Mazzuoli, R. & Trua, T. 1999. Plio-Quaternary volcanotectonic activity in the northern sector of the Main Ethiopian Rift: Relationships with oblique rifting. *J. Afr. Earth Sci.* 29,679–698

Bonini, M., G. Corti, F. Innocenti, P. Manetti, F. Mazzarini, T. Abebe, and Z. Pecskay (2005), Evolution of the Main Ethiopian Rift in the frame of Afar and Kenya rifts propagation, Tectonics, 24, TC1007, doi:10.1029/ 2004TC001680.

Brophy, J. G. Composition gaps, critical crystallinity, and fractional crystallisation in orogenic (calc-alkaline) magmatic systems. 1991.Contrib. Mineral. Petrol. 109, 173–182

Casey, M., Ebinger, C., Keir, D., Gloaguen, R., Mohamed, F., 2006. Strain accomadation in transitional rifts: extension by magma intrusion and faulting in Ethiopian rift magmatic segments. In: Yirgu, G., Ebinger, C., Maguire, P. (Eds.), The Afar Volcanic Province within the East African RRift System. Special Publication of the Geological Society, London, pp. 143–164.

Charlier, B. et al. 2011.Large-scale silicate liquid immiscibility during differentiation of tholeiitic basalt to granite and the origin of the Daly gap. Geology 39, 907–910 .

Corti, G., 2008, Control of rift obliquity on the evolution and segmentation of the main Ethiopian rift. Nature Geoscience, v. 1, p. 258–262, doi: 10.1038/ngeo160.

Corti, G. (2009), Continental rift evolution: From rift initiation to incipient break- up in the Main Ethiopian Rift, East Africa, Earth Sci. Rev., 96, 1–53, doi:10.1016/j.earscirev.2009.06.005.

Corti, G., Philippon, M., Sani, F. D., Keir , Kidane, T. (2013). Re-orientation of the extension direction and pure extensional faulting at oblique rift margins: Comparison between the Main Ethiopian Rift and laboratory experiments. Terra Nova, doi:10.1111/ter.12049.

Coulié, E., Quidelleur, X., Gillot, P.Y., Coutillot, V., Lefevre, J.C., Chiessa, S., 2003. Comparative K–Ar and Ar/Ar dating of Ethiopian and Yemenite Oligocene volcanism:

implication for timing and duration of the Ethiopian traps. Earth and Planetary Science Letters 206, 477–492.

Chu, D. and Gordon, R. G. (1998). Current plate motions across the Red Sea. Geophysical Journal International 135, 313-328.

Chu, D. and Gordon, R. G. (1999). Evidence for motion between Nubia and Somalia along the Soutwest Indian ridge. Nature 398, 64-67.

D'Acremont, E., Leroy, S., Beslier, M.-O., Bellahsen, N., Fournier, M., Robin, C., Maia, M., and Gente, P., 2005, Structure and evolution of the eastern Gulf of Aden conjugate margins from seismic reflection data: Geophysical Journal International, v. 160, p. 869–890.

Daly, E., Keir, D., Ebinger, C.J., Stuart, G.W., Bastow, I.D., Ayele, A., 2008. Crustal tomographic imaging of a transitional continental rift: the Ethiopian rift. Geophysical Journal International 172 (3), 1033–1048.

Deniel, C., Vidal, P., Coulon, C., Vellutini, P.J., 1994. Temporal evolution of mantle sources during continental rifting — the volcanism of Djibouti (Afar). Journal of Geophysical Research-Solid Earth 99 (B2), 2853–2869.

Ebinger, C.J., Hayward, N.J., 1996. Soft plates and hot spots: views from afar. Journal of Geophysical Research-Solid Earth 101 (B10), 21859–21876.

Ebinger, C. J. and Casey M. (2001). Continental break-up in magmatic provinces: an Ethiopian example. Geology 29, 527-530.

Freundt-Malecha, B., Schmincke, H. U. & Freundt, A. 2001.Plutonic rocks of intermediate composition on Gran Canaria: The missing link of the bimodal volcanic rock suite. Contrib. Mineral. Petrol. 141, 430–445 .

Furman, T., Bryce, J.G., Rooney, T., Hanan, B.B., Yirgu, G., Ayalew, D., 2006. Heads and tails: 30 million years of the Afar plume. In: Yirgu, G., Ebinger, C., Maguire, P. (Eds.), The

Afar Volcanic Province within the East African Rift System. Special Publication of the Geological Society, London, pp. 95–120.

Fusillo, R., Di Traglia, F., Gioncada, A., Pistolesi, M., Wallace, P.J., Rosi, M., 2015. Deciphering post-caldera volcanism: insight into the Vulcanello (Island of Vulcano, Southern Italy) eruptive activity based on geological and petrological constraints. Bulletin of Volcanology 77:76 DOI 10.1007/s00445-015-0963-6

Giordano, G., De Benedetti, A.A., Diana, A., Diano, G., Gaudioso, F., Marasco, F., Miceli, M., Mollo, S., Cas, R.A.F., Funiciello, R., 2006. The Colli Albani mafic caldera (Roma, Italy): stratigraphy, structure and petrology. Journal of Volcanology and Geothermal Research, 155, 49–80

Grove, T. L. & Donnelly-Nolan, J. M. 1986. The evolution of young silicic lavas at Medicine Lake Volcano, California: Implications for the origin of compositional gaps in calc-alkaline series lavas. Contrib. Mineral. Petrol. 92, 281–302

Hayward, N. J., and C. J. Ebinger (1996), Variations in the along-axis segmentation of the Afar Rift system, Tectonics, 15, 244–257, doi:10.1029/95TC02292.

Hendrie, D.B., Kusznir, N.J., Morley, C.K., and Ebinger, C.J., 1994, Cenozoic extension in northern Kenya: a quantitative model of rift basin development in the Turkana region: Tectonophysics, v. 236, p. 409–438.

- Hutchison, W., Pyle,D., M., Mather, T., A., Yirgu, G., Biggs,J., Cohen, B., E., Barford, D., N., Lewi, E. 2016. The eruptive history and magmatic evolution of Aluto volcano: new insights into silicic peralkaline volcanism in the Ethiopian rift. Journal of Volcanology and Geothermal Research, doi: 10.1016/j.jvolgeores.2016.09.010

Jestin, F., Huchon, P., and Gaulier, J.M. (1994). The Somalia plate and the East African Rift System: Present-day kinematics. Geophysical Journal International 116, 637–654.

Keir, D., Bastow, I.D., Corti, G., Mazzarini, F., and Rooney, T.O., 2015, The origin of along-rift variations in faulting and magmatism in the Ethiopian Rift: Tectonics, v. 34, p. 464–477, doi: 10.1002/2014TC003698.

Keranen, K., Klemper, S.L., Gloaguen, R., Grp, E.W., 2004. Three-dimensional seismic imaging of a protoridge axis in the Main Ethiopian rift. Geology 32 (11), 949–952.

Kieffer , B., Ardnt, N., Lapierre, H., Bastien, F., Bosch, D., Pecher, A., Yirgu, G., Ayalew, D., Weis, D., Jerram, D., Keller, F. and Meugniot, C. (2004). Flood and shield basalts form Ethiopia: magmas from the African Superswell. Journal of Petrology vol. 45, 4, 793-834

Kogan, L., S. Fisseha, R. Bendick, R. Reilinger, S. McClusky, R. King, and T. Solomon (2012), Lithospheric strength and strain localization in continental extension from observations of the East African Rift, J. Geophys. Res., 117, B03402.

Korme, T., Acocella, V., Abebe, B., 2004. The role of pre-existing structures in the origin, propagation and architecture of faults in the main Ethiopian rift. GondwanaResearch 7 (2), 467–479.

Kurz, T., Gloaguen, R., Ebinger, C., Casey, M., Abebe, B., 2007. Deformation distribution and type in the Main Ethiopian Rift (MER): a remote sensing study. Journal of African Earth Sciences 48 (2–3), 100–114.

Lakhssassi, M., Guy, B., Touboul, E. & Cottin, J-Y 2010. Bimodal distribution of the solid products in a magmatic chamber: Modelling by fractional crystallization and coupling of the chemical exchanges with the differential melt/solid transport. C. R. Geosci. 342, 701–709 .

Mazzarini, F., Corti, G., Manetti, P., Innocenti, F., 2004. Strain rate and bimodal volcanism in the continental rift: Debre Zeyt volcanic field, northern MER, Ethiopia. Journal of African Earth Sciences 39 (3–5), 415–420.

Mazzarini, F., T. Rooney, and I. Isola (2013), The intimate relationship between strain and magmatism: A numerical treatment of clustered monogenetic fields in the Main Ethiopian Rift, Tectonics, 32, 49–64, doi:10.1029/2012TC003146.

McKenzie, D. P., Davies, D. and Molnar, P. (1970). Plate tectonics of the Red Sea and East Africa. Nature 226, 243-248.

Mohr, P.A., 1962. The Ethiopian rift system. Bulletin of the Geophysical Observatory 3 (1), 33–62.

Mohr, P.A., 1967b. Major volcano-tectonic lineament in the Ethiopian rift system. Nature 213 (5077), 664–665.

Mohr, P. (1983), Volcanotectonic aspects of the Ethiopian Rift evolution, Bull. Cent. Rech. Explor, Prod. Elf Aquitaine., 7, 175–189.

Mohr, P., 1987. Structural style of continental rifting in Ethiopia: reverse decollements. EOS Trans. AGU September 1, 721–730.

Mohr., P. A. and Zanettin, B. (1988). The Ethiopian flood basalt province. In: MacDougall, J.,D. (ed) Continental Flood Basalts. Dordrecht: Kluwer Academic, pp. 63-110.

Morley, C.K., Wescott, W.A., Stone, D.M., Harper, R.M., Wigger, S.T., and Karanja, F.M., 1992, Tectonic evolution of the northern Kenyan Rift: Journal of the Geological Society, v. 149, p. 333– 348.

Piccirillo, E. M., Justin-Visentin, E., Zattenin, B., Jioron, J. K., Treuil, M. (1979). Geodynamic evolution from plateau to rift : major and trace elements geochemistry of the central eastern Ethiopian plateau volcanics. Neus Fahrbuch Fur Geologie und Palaontologie 258, 139-179.

Peccerillo, A., Barberio, M.R., Yirgu, G., Ayalew, D., Barbieri, M., Wu, T.W., 2003. Relationships between mafic and peralkaline silicic magmatism in continental rift settings: a petrological, geochemical and isotopic study of the Gedemsa volcano, central Ethiopian rift. Journal of Petrology 44 (11), 2003–2032.

Pik, R., Deniel, C., Coulon, C., Yirgu, G., Hofmann, C., Ayalew, D., 1998. The Northwest Ethiopian plateau flood basalts: classification and spatial distribution of magma types. Journal of Volcanology and Geothermal Research 81, 91–111.

- Ronga, F., Lustrino, M., Marzoli, A., Melluso, L., 2010. Petrogenesis of a basalt–comendite–pantellerite rock suite: the Boseti Volcanic Complex (Main Ethiopian Rift). Mineralo- gy and Petrology 98, 227–243.

Rooney, T., Furman, T., Yirgu, G., Ayalew, D., 2005. Structure of the Ethiopian lithosphere: xenolith evidence in the Main Ethiopian Rift. Geochimica et Cosmochimica Acta 69 (15), 3889–3910.

Rooney, T.O., 2010. Geochemical evidence of lithospheric thinning in the southern Main Ethiopian Rift. Lithos 117, 33–48. doi:10.1016/j.lithos.2010.02.002.

Rooney, T., O., Bastow, I. D., Keir, D. (2011), Insights into extensional processes during magma assisted rifting: Evidence from aligned scoria cones and maars. J. Volcanol. Geotherm. Res., 201, 83–96.

Salvador, A., 1987. Unconformity bounded stratigraphic units. Geol. Soc. Amer. Bull. 98, 232–237.

Scaillet, B., Macdonald, R., 2001. Phase relations of peralkaline silicic magmas and petrogenetic implications. Journal of Petrology 42, 825–845.

Scaillet, B., Macdonald, R., 2003. Experimental constraints on the relationships between peralkaline rhyolites of the Kenya Rift Valley. Journal of Petrology 44, 1867–1894.

Scaillet, B., Macdonald, R., 2006b. Experimental constraints on pre-eruption conditions of pantelleritic magmas: evidence from the Eburru complex, Kenya Rift. Lithos 91, 95–108.

Suneson, N. H. & Lucchitta, I. 1983 .Origin of bimodal volcanism, southern Basin and Range province, west-central Arizona. Geol. Soc. Am. Bull. 94, 1005–1019

Ukstins, I.A., Renne, P.R., Wolfenden, E., Baker, J., Ayalew, D., Menzies, M., 2002. Matching conjugate volcanic rifted margins: $^{40}Ar/^{39}Ar$ chrono-stratigraphy of pre- and syn-rift bimodal flood volcanism in Ethiopia and Yemen. Earth and Planetary Sciences Letters 198, 289–306.

Trua, T., Deniel, C., Mazzuoli, R., 1999. Crustal control in the genesis of Plio-Quaternary bimodal magmatism of the Main Ethiopian Rift (MER); geochemical and isotopic (Sr, Nd, Pb) evidence. Chemical Geology 155 (3–4), 201–231.

WoldeGabriel, G., Aronson, J.L., and Walter, R.C., 1990, Geology, geochronology, and rift basin development in the central sector of the Main Ethiopia Rift: Geological Society of

America Bulletin, v. 102, p. 439–458, doi: 10.1130/0016-7606(1990)102<0439.

Wolfenden, E., Ebinger, C., Yirgu, G., Deino, A. & Ayale, D. 2004. Evolution of the northern Main Ethiopian rift: Birth of a triple junction. Earth Planet. Sci. Lett. 224, 213–228

Wolfenden, E., Ebinger, C., Yirgu, G., Renne, P.R., and Kelley, S.P., 2005, Evolution of a volcanic rifted margin: Southern Red Sea, Ethiopia: Geological Society of America Bulletin, v. 117, p. 846, doi: 10.1130/B25516.1.

2 The volcanic geology and evolution of the Corbetti Caldera (Main Ethiopian Rift)

2.1 Introduction

Corbetti Caldera is a Quaternary volcanic complex in the southern sector of the Main Ethiopian Rift. Its stratigraphy and eruptive history as well as the geochemistry, are poorly constrained and there is only limited published work on this complex (Mohr 1966, Di Paola 1971, McDonald 1969, Wodelgabriel et al.1991, Rapprich et al.2015).

The aim of this chapter is to revise the evolution of Corbetti volcanic history through the stratigraphic reconstruction of the past eruptive events. New $^{40}Ar/^{39}Ar$ dating from syn- and post caldera deposits, is also presented.

The stratigraphic survey has been carried out using the Unconformity Bounded Stratigraphic Units method (UBSU, Salvador 1987), modified for the volcanic terrains by De Rita et al. (1997). Eruptive, primary deposits, and reworked volcaniclastic units have been identified on the basis of erosive unconformity surfaces, lithological features and geometric organization of the deposits. The concept of lithosome was also applied, discriminating deposits related to the same eruptive centre (Giordano et al.2006, Fusillo et al. 2015). The stratigraphic reconstruction is also supported by a detailed morphological analysis of the Corbetti caldera products using high-processing (1-2m pixel) of new LiDAR-derived digital elevation model.

The entire stratigraphic sequence of Corbetti Caldera has been divided in four lithosomes, comprising the pre- and syn-caldera products (*Corbetti composite Lithosome, CCL*) and post-caldera volcanoes (*Urji, UR, Danshe, DA and Chabbi composite lithosomes, CH*), separated by an unconformity surface of the higher rank (S1), corresponding to the caldera collapse faults system. The volcanic activity of Corbetti Caldera is characterized by monogenetic eruptive centres that emplaced pyroclastic deposits followed by obsidian flows, showing a change in volcanic eruption style from explosive to effusive activity. The combination of UBSU method and the morphological analysis based on LIDAR-derived topography, allowed temporal constraints on the volcanic evolution of Corbetti Caldera and provides a new geological map of the area.

2.2 Data Collection

2.2.1 Stratigraphy and geological mapping

Fieldwork was carried out during two different expeditions in May and November 2012. The area was initially studied on Google Earth before the field work campaign, with the aim of identifying possible rock outcrops and as well as means of access. A detailed stratigraphic log of the volcanic succession was measured and described at each site of the investigation.

The fieldwork based on the use of Unconformity Bounded Stratigraphic Units method (UBSU, Chang 1975, Salvador, 1987, 1994), aimed to identify the main stratigraphic unconformities which led to the identification of the main volcanic eruption that characterized the Corbetti volcanic history. The UBSU methodology has been often adopted for mapping the Italian volcanoes (Coltelli et al. 1994, Calvari et al. 1995, Maneti et al. 1995, Rossi et al. 1996, De Rita et al. 1997, Calanchi et al. 1999, Tranne et al. 2002a, Tranne et al. 2002b, Lucchi et al. 2003, De Astis et al. 2006, Di Traglia et al., 2013, Fusillo et al.2015), and I have applied this methodology to volcanic terrains as proposed by de Rita et al. (1997).

This methodology uses the Eruptive Unit (Fisher and Schmincke, 1984) as the basic lithostratigraphic unit within the framework of the UBSU (Fig.2.1). The eruptive units represent the deposits of one eruption identified by breaks of time long enough to cause erosion or deposition of reworked material or paleosol formation in the studied area, and are bounded at their top by second-order unconformities (Fig.2.1).

On the basis of the amplitude and the extent of the erosion surfaces, the unconformities identified in the studied area, were hierarchically categorized. The unconformties were useful in the reconstruction of the time gap related to each unconformity. An unconformity that extends over a wide zone and is related to a large time gap, will be of higher rank than an unconformity that extend over a small area (De Rita et al., 1997, Di Traglia et al., 2013).

First order unconformities are distributed throughout the whole volcanic area and they could be characterized by large areal erosion, locally by decimeter thick paleo-soil, or to be coincident with volcanotectonic features (i.e. caldera collapse; de Rita et al., 1997). Unconformities of second order correspond possibly to paleo-gullies network.

<table>
<tr><td rowspan="11">Eruptive epoch</td><td rowspan="2">Lithosome</td><td>Eruptive unit</td><td></td></tr>
<tr><td>Eruptive unit</td><td></td></tr>
<tr><td colspan="3">S2 unconformity</td></tr>
<tr><td rowspan="2">Lithosome</td><td>Eruptive unit</td><td rowspan="2"></td></tr>
<tr><td>Eruptive unit</td></tr>
<tr><td colspan="3">S2 unconformity</td></tr>
<tr><td rowspan="4">Lithosome</td><td>Eruptive unit</td><td></td></tr>
<tr><td>Eruptive unit</td><td></td></tr>
<tr><td colspan="2">S2 unconfomity</td></tr>
<tr><td>Eruptive unit</td><td></td></tr>
<tr><td colspan="4">S1 unconformity</td></tr>
<tr><td rowspan="3">Eruptive epoch</td><td rowspan="3">Lithosome</td><td>Eruptive unit</td><td></td></tr>
<tr><td colspan="2">S2 unconformity</td></tr>
<tr><td>Eruptive unit</td><td></td></tr>
</table>

Fig.2.1 Recapitulatory Scheme of unconformity bounded stratigraphic units (UBSU method)

The stratigraphic correlation is based on beds (i.e. tephra layers, lava units, post-eruptive deposits) which cover a wide area and these are used as " the datum planes to correlate the stratigraphic sections" (de Rita et al., 1997). Following de Rita et al. (1997), in order to have a stratigraphic correlation, the eruptive units must show "a geometry and a facies association consistent with the paleo-topography and with the emplacement mechanism".

However, since the environmental condition of the studied area did not always allow identification of good stratigraphic sections /outcrops for the identification of the unconformities, the stratigraphic reconstruction has been also carried out by the morphological study of the deposits. In this regard, observations of the morphologies of Corbetti deposits have been carried out by Google Earth images. The concept of Lithosome and composite

Lithosome has been also used (Giordano et al. 2006, Fusillo et al. 2015). Giordano et al. 2006 report the Lithosome as “a morpho-stratigraphic term that in volcanic terrains encloses the concept of ‘volcanic edificie’ (Salvador, 1994) defined by a recognizable morphology that relates to a defined eruptive centre and to a define eruptive style”. Giordano et al. 2006 also adopted the concept of ‘composite Lithosome’ for those lithosomes that “include products from several individual edifices that are genetically, geographically and morphologically related, rather than from one main edifice”. The concept of Lithosome also was very useful for the geological mapping of the Corbetti caldera. Indeed the concept of Lithosome and composite Lithosome allowed the grouping on the map of those deposits emplaced from the same volcanic center and representing eruptive units that due to the scale of the mapping would have not been mapped and allowed a clear identification of the volcanic edifices, and especially of deposits that were from different individual centers but genetically and morphologically linked to the same main edifice.

A stratigraphic successions in volcanic areas, includes both juvenile eruptive products generated by volcanism and the volcaniclastic deposits formed by the reworking of the primary deposits due to the weathering and erosion. The eruptive units comprise the products of explosive (tephra units) and/or effusive activity (lava units), together with the products of reworking that occurred during the eruption (syn-eruptive deposits) and the products of the reworking during landscape response to the volcanic perturbation (post-eruptive units; Manville, 2002; Manville et al., 2009a; Manville et al., 2009b). A tephra unit could be subsequently subdivided into "eruptive phases" and "eruptive pulses" (sensu Fisher and Schmincke, 1984; de Rita et al., 1997), while different "lava flows" could be identified within a single "Lava unit" (Cimarelli et al., 2013).

Primary and reworked volcaniclastic and epiclastic deposits have been classified on the basis of their lithological characteristics, identification of componentry of clasts and matrix, geometry and presence of sedimentary structures, following the nomenclature proposed by White and Houghton (2006). Key points are: (i) all primary volcaniclastic rocks have primary volcaniclastic names (ash, lapilli, bombs or blocks); (ii) all deposits which do not involve temporary storage of material are primary; (iii) deposits no directly related to eruptions are epiclastic; and (iv) volcaniclastic is no longer used for all deposits with a volcanic component, irrespective of origin, but instead replaces pyroclastic in its broadest sense of particles and deposits formed by volcanic eruptions.

Pyroclastics are thus interpretative deposits types applied as a second step after the rock has been given its basic descriptive grains-size name, rather than particle types (Manville et al., 2009a). Epiclastic deposits are from particles released by the erosion and weathering of volcanic rocks and receive a sedimentary name with (syn- and post-eruptive) or without (inter-eruptive) a volcanic modifier.

Considering the lack of previous detailed stratigraphic studies of Corbetti Caldera deposits, based on any reliable scientific method, UBSU and Lithosome / composite Lithosome concept resulted the most suitable tool in order to provide a reconstruction of Corbetti stratigraphy. Indeed the identification of unconformities, that mark temporally volcanic events, allowed the reconstruction of the Corbetti eruptive history. On the contrary in the previous works often the authors were not able to identify the eruptive centres, to establish relationship between the different deposits and to relate the deposits to a specific vent (section 2.4 –Discussion-).

In the case of Corbetti, since the stratigraphic reconstruction involves deposits from different volcanic centers that were active in the area at different times, the rank of an unconformity, which is related to a temporal gap between two different volcanic activity unit (i.e. eruptive epoch, eruptive period, eruption, eruptive phases, Fisher and Schimcke (1984),), is indicated by a number and the same lower rank of unconformity can be identify within the deposits of different eruptive centres.

The part of geological survey in the east sector of Corbetti Caldera, *Chabbi Composite Lithosome*, was carried out by the combination of field work and the application of LIDAR imagery (digital elevation modem and ortho-photos) acquired with the cooperation of the NERC Airborne Research Science Facility project “Understanding volcanic hazards in the Main Ethiopian Rift: Alutu and Corbetti”. The field work allowed direct observations and stratigraphic log description of some of the deposits of Chabbi Composite Lithosome , whereas LIDAR imagery allowed indirect observations and morphological analyses of those deposits that were not possible to study because of the lack of means of access. The LiDAR imagery also provided a high resolution (2m pixel) digital elevation model that was used as basis for the geological mapping of the *Chabbi Composite Lithosome* (Fig.2.5). The geological survey was also guided by the previous work of Mohr (1966).

2.2.2 $^{40}Ar/^{39}Ar$ dating analyses

In order to complete our knowledge and understanding of Corbetti caldera's volcanic history, $^{40}Ar/^{39}Ar$ dating analyses were carried out on the products from the syn and post caldera activity. These data were also used ad part an article that is published in Nature Communications: Hutchison et al.2016 : *"A pulse of rift volcanism in Ethiopia at the dawn of modern humans"*., with authors as follows: William Hutchison*[1], Raffaella Fusillo[2], David M. Pyle[1], Tamsin A. Mather[1], Jon Blundy[2], Juliet Biggs[2], Gezahegn Yirgu[3], Benjamin E. Cohen 4, Richard Brooker[2], Dan N. Barfod[4] and Andrew T. Calvert[5] (*1*-Department of Earth Sciences, University of Oxford, South Parks Road, Oxford OX1 3AN; *2*- UK 2. School of Earth Sciences, University of Bristol, Wills Memorial Building, Queens Road, Bristol BS8 1RJ, UK; *3*.-School of Earth Sciences, University of Addis Ababa, P.O. Box 1176, Addis Ababa, Ethiopia; *4*-NERC Argon Isotope Facility, Scottish Universities Environmental Research Centre, Rankine Avenue, East Kilbride, Scotland G75 0QF, UK;*5*-U.S. Geological Survey, 345 Middlefield Road, MS-937, Menlo Park, California 94025, USA).

The samples preparation was carried out at the USGS of Menlo Park (California, USA) under the supervision of Andrew T. Calvert. Andrew T. Calvert also performed the $^{40}Ar/^{39}Ar$ geochronology analyses. The samples preparation, procedures and instrument parameters used, are as reported in Hutchison et al.2016.The main steps of the procedures and parametres are summarized as follows.

$^{40}Ar/^{39}Ar$ geochronology was carried out using sanidine crystals that were picked up from crushed rock samples after sieving, by heavy liquid, and magnetic techniques. Samples were carefully handpicked under a binocular microscope.

Sanidine crystals from Corbetti samples, after have been separated (25 mg) and wrapped up in Al foil, were inserted in cylindrical quartz vial along with fluence monitors of known age. An K-glass and fluorite were also added in order to measure the interfering isotopes of K and Ca. In order to protect the sanidine crystals from thermal neutrons, the quartz vial were enclosed by 0.5 mm thick of Cd foil during the irradiation. The Corbetti samples were irradiated for a time of on hour, during which the reactor vessel was turned without interruption in order to prevent lateral neutron flux gradients. The vessel was also shaken in order to reduce vertical gradients.

The constants of the reactor of these irradiation, were not distinguishable from those of the latest irradiations, and from weighted mean of constants acquired in the last five years, that had $^{40}Ar/^{39}Ar_K$ = 0.0010±0.0004 , $^{39}Ar/^{37}Ar_{Ca}$ = 0.00071±0.00005 and $^{36}Ar/^{37}Ar_{Ca}$ = 0.000281±0.000006.

As fluence monitor was used a TCR-2 sanidine of an age of 27.87 Ma from Taylor Creek Rhyolite 56. The irradiation was carried out at the TRIGA reactor by the Central Thimble of the USGS in Denver (Colorado, USA). The results were redetermined in reference to Fish Canyon sanidine (28.294 Ma), using $R_{TCs/FCs}$ = 1.00881±0.00046, determined in Menlo Park. As reported in Muffler et al. 2011, TRC-2 has also been used as secondary standard, and it was calibrated in contrast to the primary intralaboratory standard, SB-3 that showed an age of 162.9±0.9 Ma (Lanphere and Dalrymple, 2000). An interrupted laser system of CO_2, and a mass spectrometer as described by Dalrymple (1989), were used to analyse Fluence monitors and unknowns. The differentiation of the mass spectrometry and of the system blanks, are to be considered regarding the precision and accurancy of $^{40}Ar/^{39}Ar$ age analyses of samples from Pleistocene, due to their low radiogenic yields. For this reason, analyses of the splits of atmospheric Ar, contained in a tank linked to the extraction line for these samples, D_{1amu} = 1.010795 ± 0.000169, was carried out to monitor the differentiation of the mass spectrometry and system blanks. System blanks, that contain mass spectrometer backgrounds, were $1.5x10^{-18}$ mol of m/z 36, $9x10^{-17}$ mol of m/z 37, $3x10^{-18}$ mol of m/z 39 and $1.5x10^{-16}$ mol of m/z 40, where m/z is mass/charge ratio. Two SAES ST-172 getters were used at 4 and 0 A., in order to purify gas continually (Ferguson et al. 2013). From the single crystal fusion data, the apparent age were determined by using the atmospheric ratios and by plotting as probability density functions (Deino and Potts, 1992).

2.3 Data

2.3.1 Stratigraphy

The application of the UBSU method on the Corbetti Caldera deposits indicates two orders of unconformity surfaces, marking different volcanic events during the eruptive history of Corbetti Caldera. These unconformities were identified in the 15 analyzed sections as shown in the stratigraphic logs (Fig.2.4, 2.5) and can be recognized in the studied area (Corbetti caldera rim and Corbetti caldera interior).

The first- and second-order unconformities are defined in this work as the boundary between eruptive epoch and eruptive unit respectively, on the basis of the method proposed by the De Rita et al (1998). The first-order unconformity (S1), corresponding to the faults system of caldera collapse on the caldera wall and to paleosol in the caldera plain (Fig. 2.2 (a),(b),(c), 2.3 (b)), defines the boundary between the products of the most recent eruptive epoch (post caldera activity) and the product of the older epoch (pre- and syn-caldera activity). The second-order unconformity, corresponding to an erosional surface/reworked material or paleosoil, defines two different eruptions within the same lithosome (Fig. 2.2 (c), 2.3 (a))

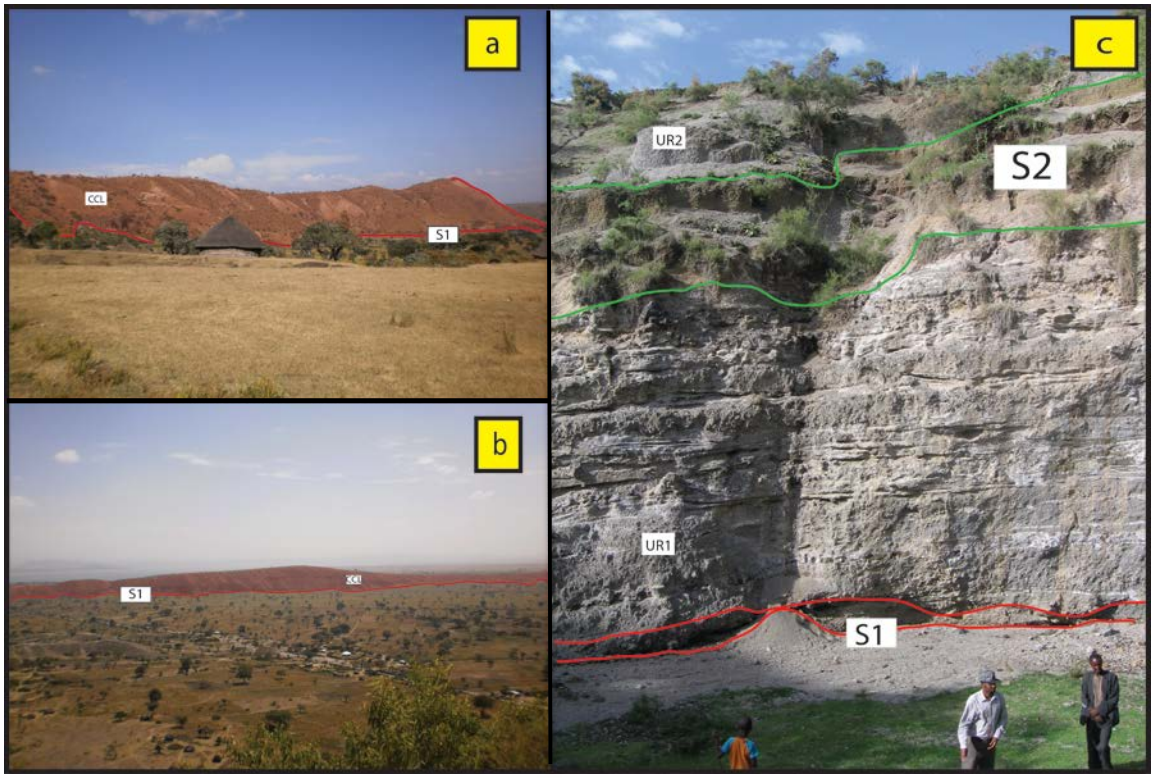

Fig.2.2 (a)-(b): Recognized unconformity of first order (S1), along the caldera wall in the northern and southern sector of caldera respectively ; **(c):** Recognized unconformities of first order (S1) as paleosol in caldera plain and of second order (S2) as paleosol within Urji lithosome (UR)

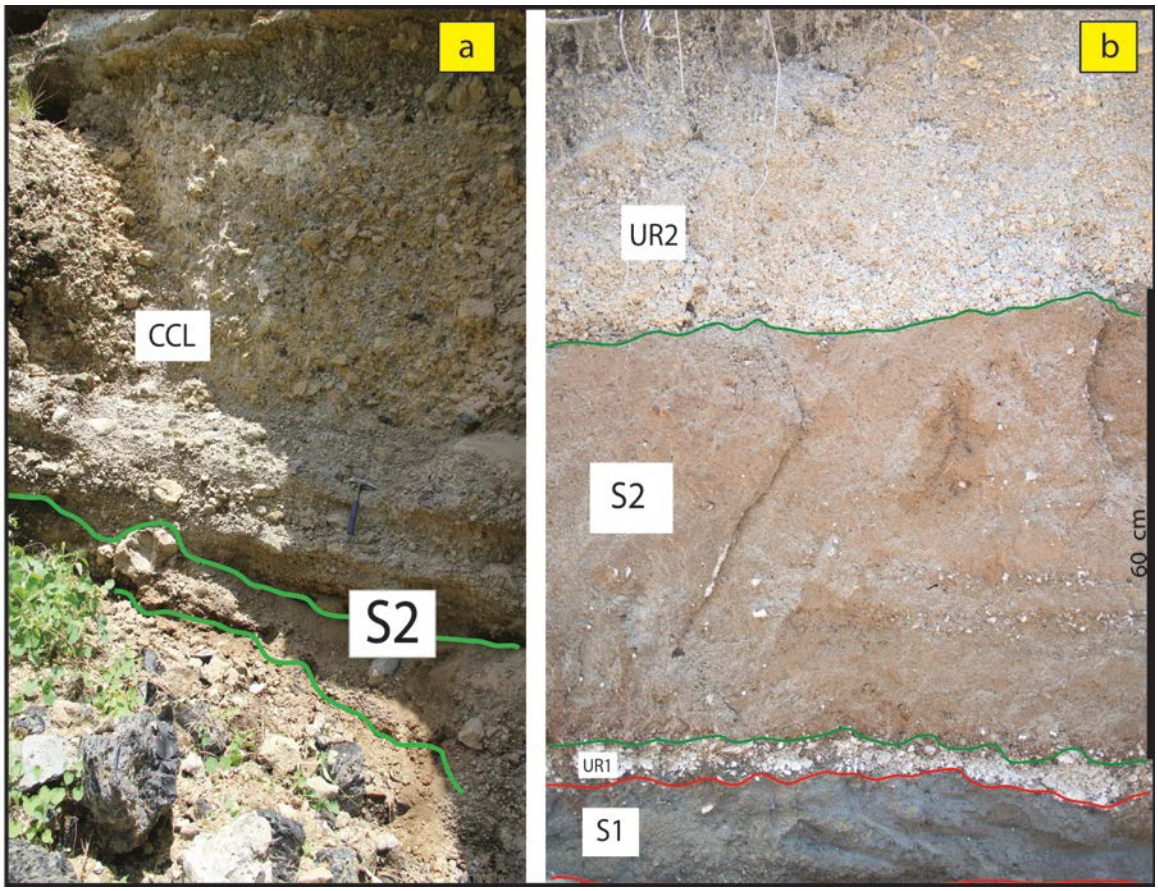

Fig. 2.3 (a) : Recognized unconformity of second order (S2) as reworked material within Corbetti composite lithosome (CCL), stop 3-4, southern sector of caldera**.**
(b) : Recognized unconformities of first order (S1) as paleosol in the caldera plain and of second order (S2) as paleosol within Urji lithososme (UR) .

2.3.2 Lithosomes and Stratigraphic Units

Given the hierarchy of the unconformities it was possible to divide the Corbetti Caldera products into 'pre and syn caldera deposits' and 'post caldera deposits' separated by a first order unconformity (S1). On the basis of the lithosome and Composite lithosome concepts (Giordano et al. 2006), it was possible to identify two composite lithosomes, the *Corbetti Composite Lithosome (CCL)* and the *Chabbi Composite Lithosome (CH)*, as well as two lithosomes, *Urji (UR)* and *Danshe (DA)*

The pre and syn caldera deposits were then gathered into the *Corbetti Composite Lithosome (CCL)* . Within the *CCL* two eruptive units, COR1 Eruptive Unit (COR1 EU), related to 'pre - caldera deposits', and COR2 Eruptive Unit (COR2 EU) related to the 'syn-caldera deposits', were identified, separated by a second order uncoformity (S2). The post caldera deposits were clustered in three different lithosomes, *Urji lithosome*, *Danshe lithosome* and the composite *Chabbi Composite Lithosome*. Within the *Urji lithosome* a second order unconformity (S2) corresponding to a paleosol, indentifies two eruptive units UR 1 and UR2, whereas *Danshe lithososme* is characterized by a pyroclastic sequence that might correspond to an eruptive unit. Any clear unconformity surface has been recognized marking the beginning of the *Chabbi Composity Lithosome* activity.

However on the basis of the location and fresh morphology of Chabbi deposits, it can be stated that *Chabbi Composite Lithosome* was the last manifestation of post-caldera volcanism. *Chabbi Composite Lithosome* is composed by seven different lithosomes made up by the deposits of seven different eruptive vents (CH1, CH2, CH3, CH4, CH5, CH6, CH7) (Fig. 2.5)

Geological map of Corbetti caldera Southern sector of Main Ethiopian Rift (Ethiopia)

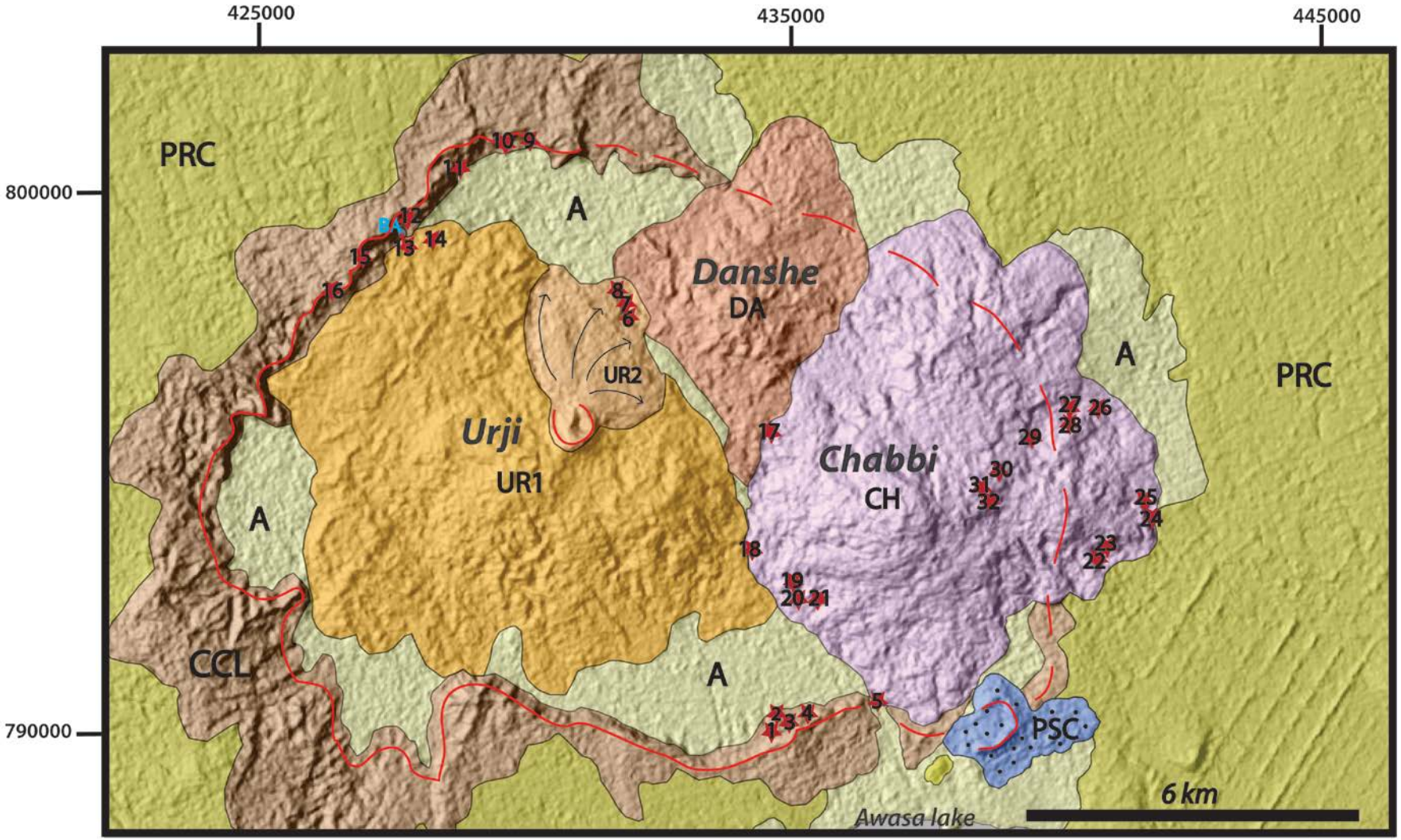

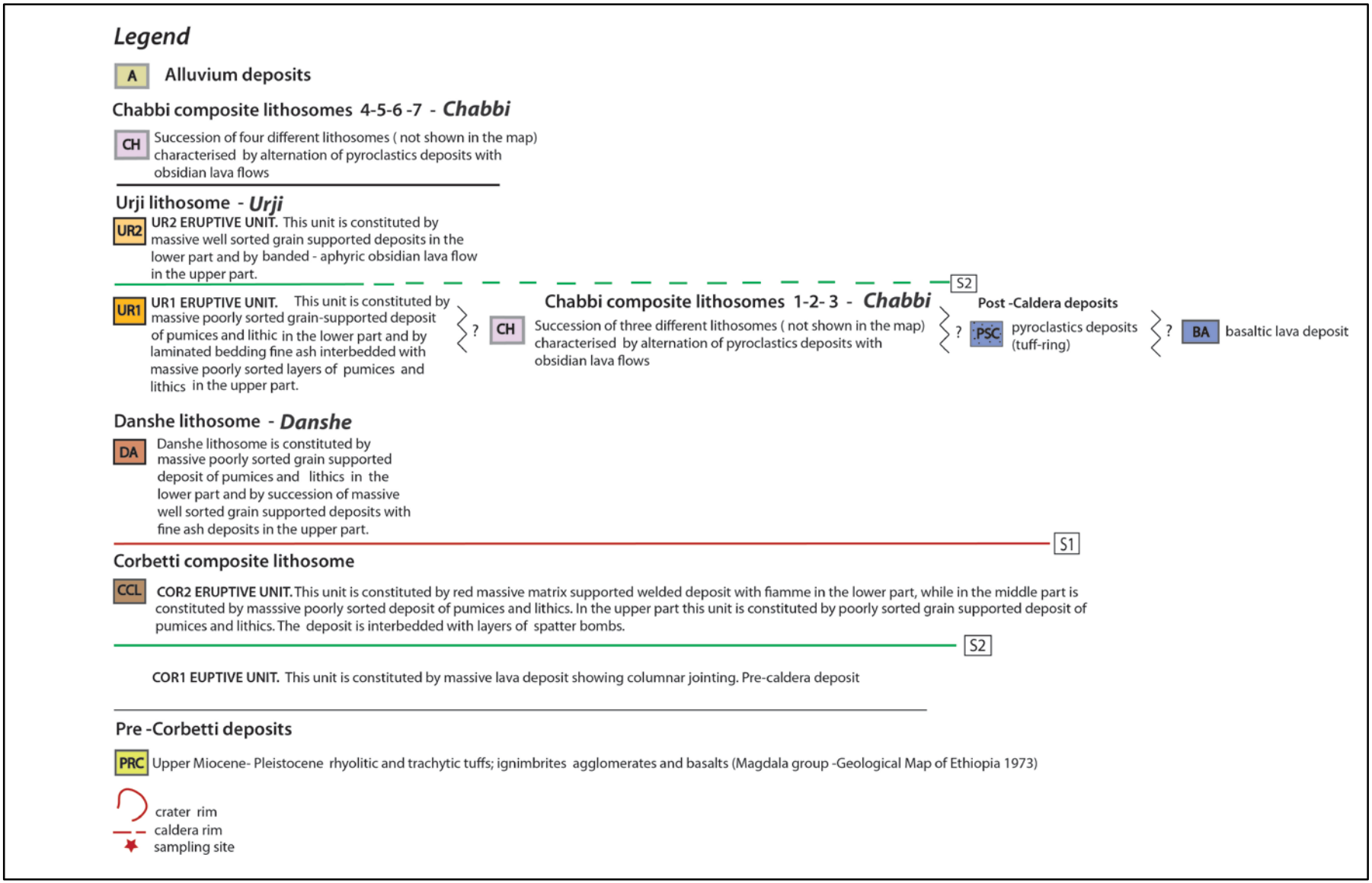

Fig. 2.4 Geological map of Corbetti Caldera. NASA ASTER image - ASTGTM.002:2088835862. Geographic coordinates refer to the UTM 37 system.

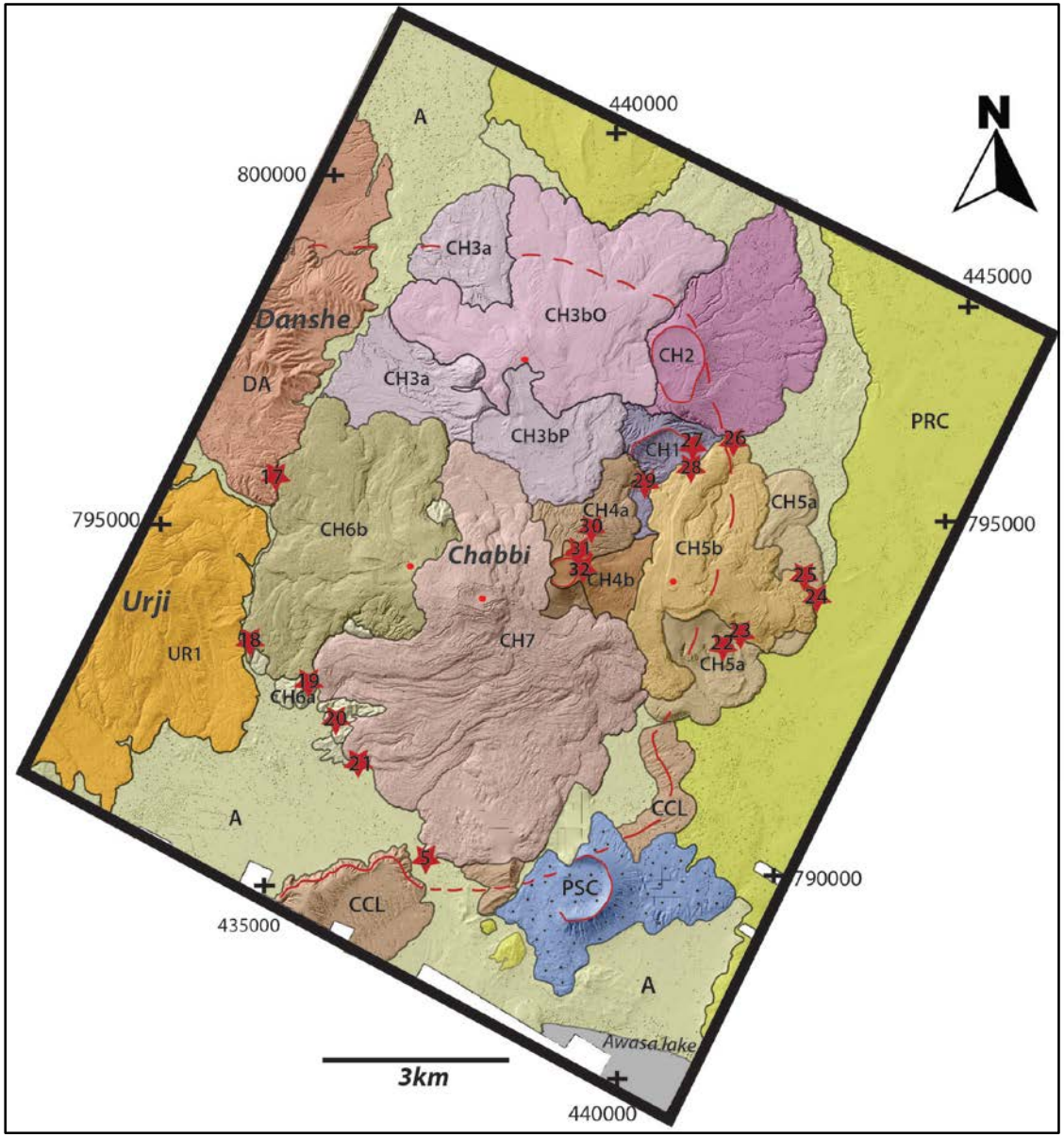

Geological map of Chabbi volcano in Corbetti caldera, Southern sector of Main Ethiopian Rift (Ethiopia)

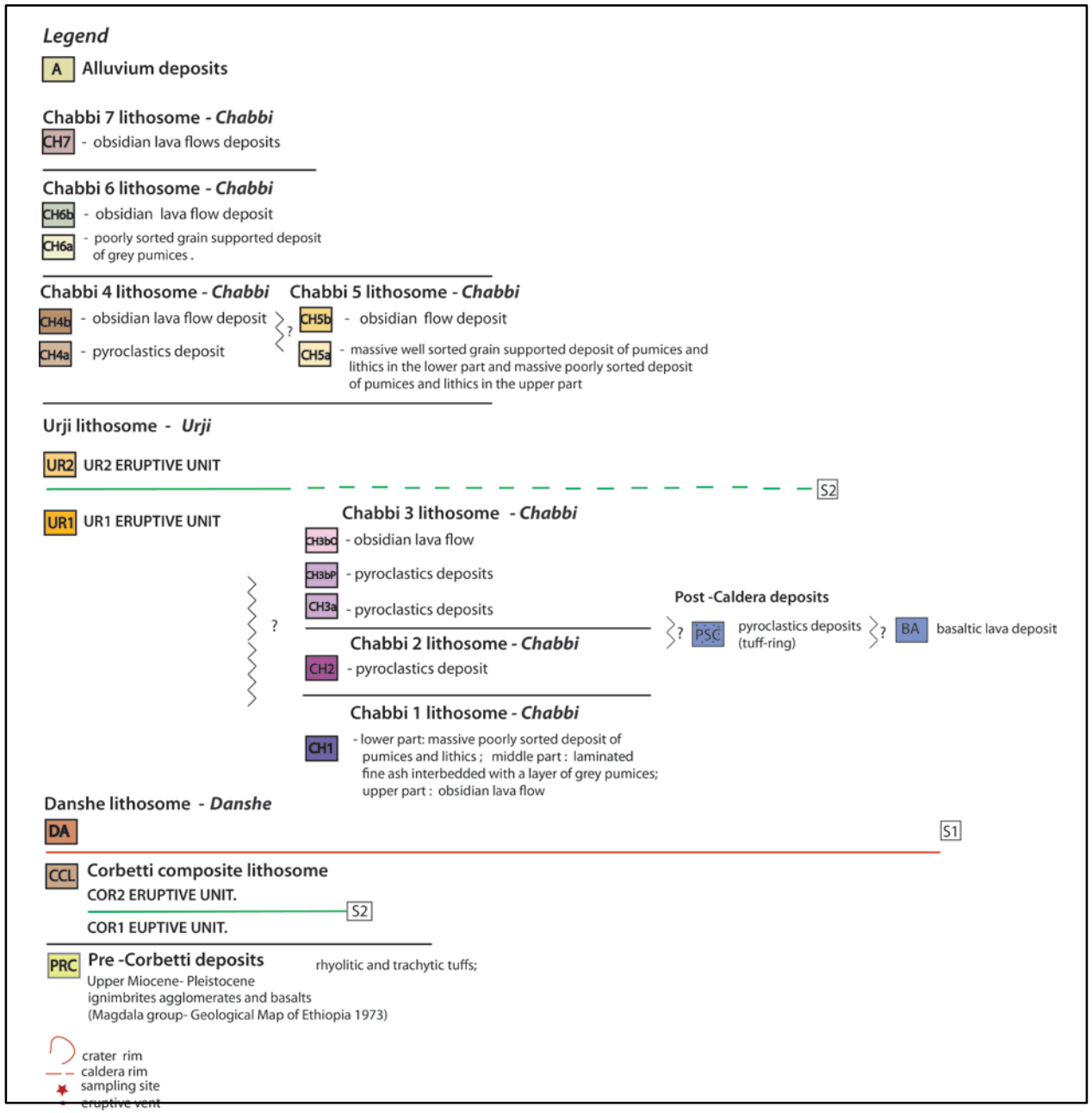

Fig. 2.5 Geological map of *Chabbi Composite Lithosome* (Corbetti Caldera). ARSF LiDAR image . Geographic coordinates refer to the UTM 37 system.

Pre and syn caldera deposits :

Corbetti Composite Lithosome

CCL outcrops at the continuous and steep ridge along the northern, southern and western caldera rim (outcrops n. 1,2, 3, 4, 9, 10, 11, 15,16 Fig.2.4, 2.6 (a))In the lower part it is characterized by the pre-caldera deposits (COR1- eruptive unit) and in the middle-upper part by the syn-caldera deposits (COR2–eruptive unit) (Fig.2.6 (b)).

The COR1 and COR2 eruptive units are separated by a second order unconformity (S2), here represented by a layer of reddish reworked material of 150 cm thickness (Fig.2.3 (a)). The pre-caldera deposit unit (COR1), is composed by a massive lava deposit showing a columnar jointing (Fig.2.7 (a)). The average thickness of the deposit is about 30 m, while the maximum thickness visible on the northern caldera rim, is about 50 m.

The *CCL* stratigraphic sequence then continues with the syn-caldera deposit unit (COR2). This eruptive unit is characterized by a pyroclastic deposit of measured minimum thickness of 10 m. This deposit shows three different facies. In the lower part, the COR2 EU is characterized by a red, massive, matrix supported welded deposit, with the typical fiamme structure and abundant quartz and sanidine phenocrists (Fig.2.7(b)). In the middle part the deposit changes in a facies of massive poorly sorted deposit, with abundant centimeter-size (~ 80%) brown-red lithics and a low percentage of pumice (~20%), ranging in size from fine lapilli to bombs . Both these facies (minimum measured thickness 3.5 m) outcrop on the northwestern caldera rim (outcrops n. 15,16 ,Fig. 2.4, 2.6 (a)). In the upper part, the syn-caldera eruptive unit is characterized by a poorly sorted, grain-supported deposit 3.5 m thick (Fig.2.7 (c)), outcropping on the southern and northern caldera rim (outcrops n.1,2.3.4, 9,10,11, Fig. 2.4, 2.6 (a)). It comprises abundant pumice (~85%), a low percentage of red lithics (~ 10%) and a very small amount of obsidian clasts (~5%). The pumice clasts contain rare olivine, clinopyroxene and sanidine phenocrysts. In the upper part is characterized by a thin layer (~50 cm) of fine ash. The clasts size of the deposit ranges from fine ash to bomb. This facies is interbedded with a layer (estimated thickness ~ 3 m) of large (> 10 m) spatter bombs (Fig.2.7 (c), (d),) outcropping on the southern, northern and western caldera rim (outcrops n.1, 2, 3.4 ,9 , 10,11 ,15 ,Fig. 2.4, 2.6(a))

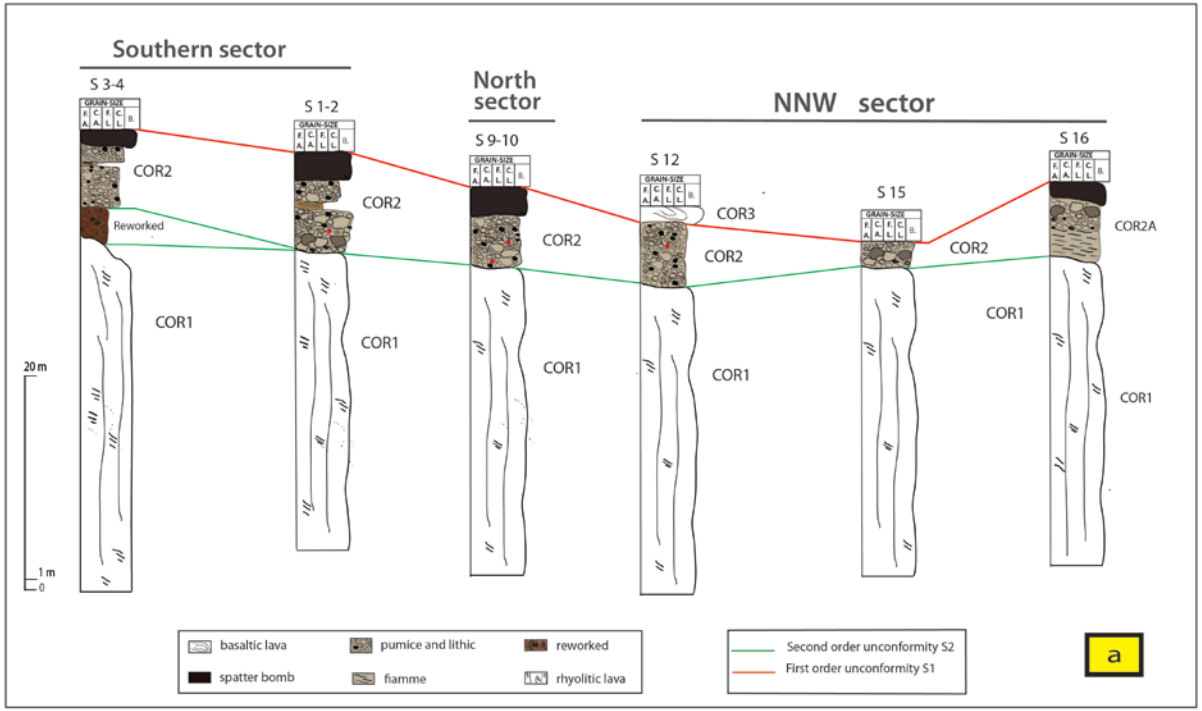

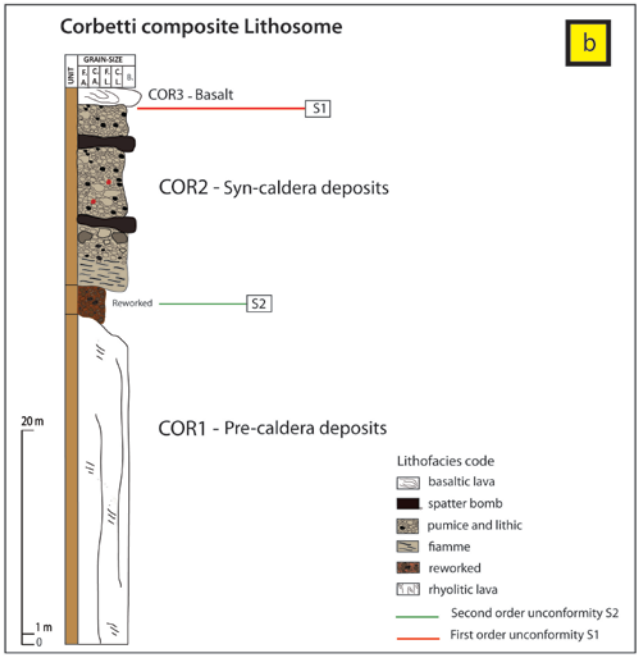

Fig. 2.6 a): stratigraphic logs of the deposits succession within the *Corbetti Composite Lithosome* at the the sampling site (S) along the southern, north and NNW sector of caldera. The unconformities recognized S1 (first order) and S2 (second order) that allowed the stratigraphic correlation , are highlighted. **b):** representative log of the deposits succession within the *Corbetti*

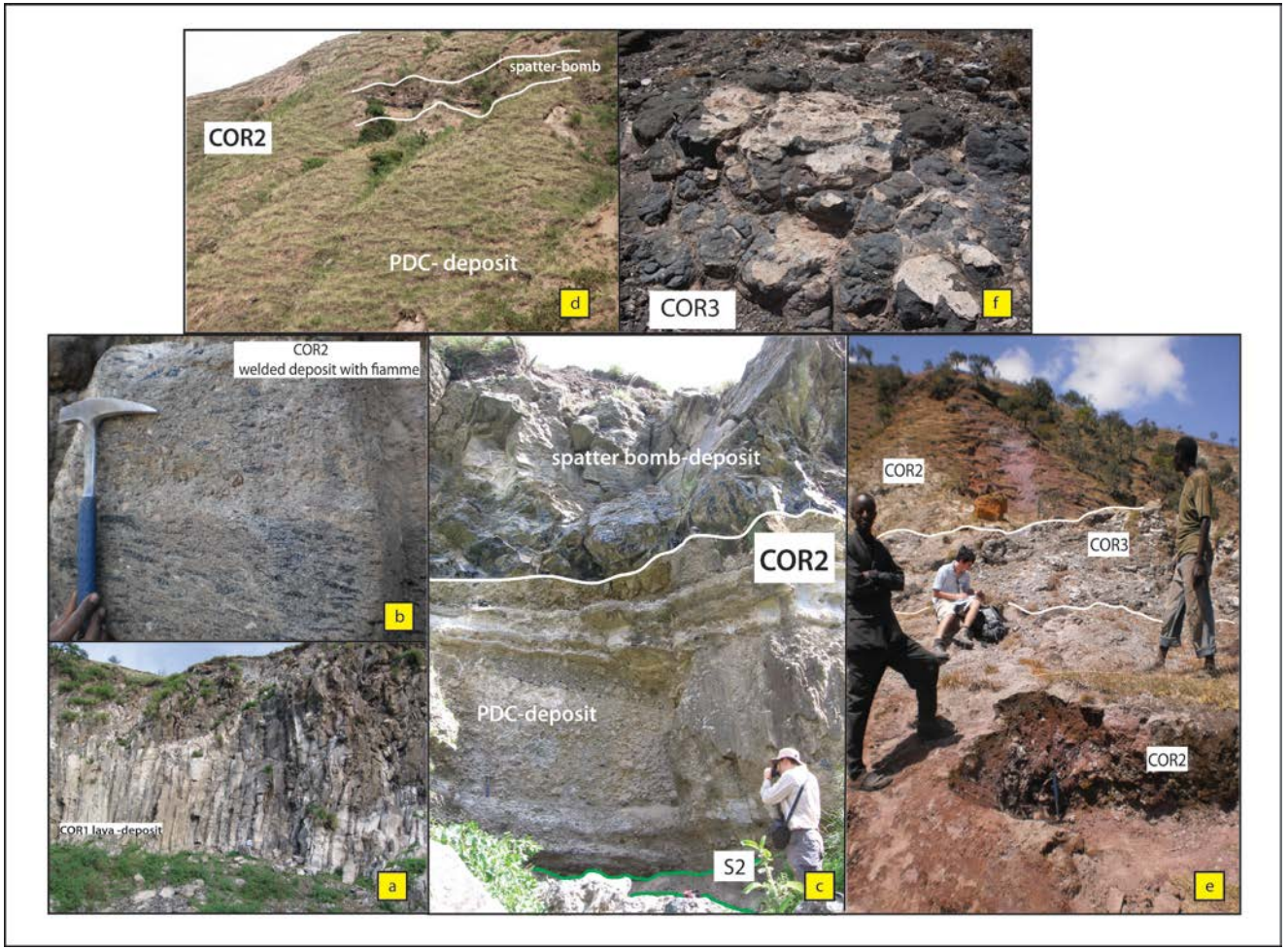

Fig.2.7 *Corbetti Composite Lithosome* deposits: **a)-** COR1 eruptive unit (lava deposit, southern sector of caldera sampling site n. 1,2,3,4); **b)-** COR2 eruptive unit ,fiamme facies, NNW sector of caldera, sampling site n. 16; **c) – d)** COR 2 eruptive unit, PDC and spatter bomb deposit, southern sector, sampling site n.1,2,3,4; **e) -f)** –COR3 eruptive unit, NNW sector of caldera, sampling site n.12.

The *CCL* also includes a lava deposit (COR3 eruptive unit, Fig.2.7 (e), (f)) outcropping on the northwestern caldera rim (outcrop n. 12 ,Fig.2.4). Although the deposit is strongly altered because of the fumarolic activity occurring along the outcrop, it was possible to identify pseudo- pillow shape.

This lava deposit covers the eruptive unit COR2 on the northwestern caldera rim, where there is a fumarole.

Post caldera deposits :

Urji Lithosome

Urji lithosome deposits outcrop in the north-central and NNW sector of the caldera (Fig. 2.4 sampling site n.6,7,8,13,Fig. 2.10) and are separated from the *CCL* by an S1 unconformity, corresponding to a ~1m thick paleosol in the caldera plain (Fig. 2.8, 2.9 (d), 2.10). *Urji lithosome* comprises two eruptive units, UR1 and UR2, separated by a 2 m thick paleo-soil (S2 unconformity) (Fig.2.8).

The Urji eruptive unit, UR1 (Fig. 2.8,2.9 (a), (d)), is characterized at the bottom by a massive, poorly sorted, grain-supported deposit that in the lower part shows abundant lithics (~70%) and a lower percentage of pumices (30%), whereas in the middle part it is characterized by abundant pumice (85%) and lower percentage of lithics (~35%). The pumice has rare clinopyroxene and sanidine phenocrysts. All the clasts range from lapilli to block size.

In the upper part, the eruptive unit UR1, is characterized by an alternation of laminated fine ash and massive and poorly sorted layers of heterogeneous clasts (lithics, pumices) ranging from coarse lapilli to bomb size (Fig.2.8, 2.9 (a), (c)). The thickness maximum of the deposit is 13 m at the outcrop n. 6 (Fig.2.8, 2.9 (a),close to the eruptive vent .The UR2 is a banded obsidian/lava flow deposit of 10 m estimated thickness overlain by a massive, grain-supported deposit (Fig.2.8, 2.9 (a), (b), (d)). The juvenile clasts are grey pomice (~90%) and obsidian fragments (~10%), the grain size ranges from fine lapilli to coarse lapilli . The maximum thicknesses measured at outcrop n. 6 -8 (Fig. 2.9), close to the vent are 300 and 150 cm respectively, while at the site 13 the maximum thickness is 110 cm.

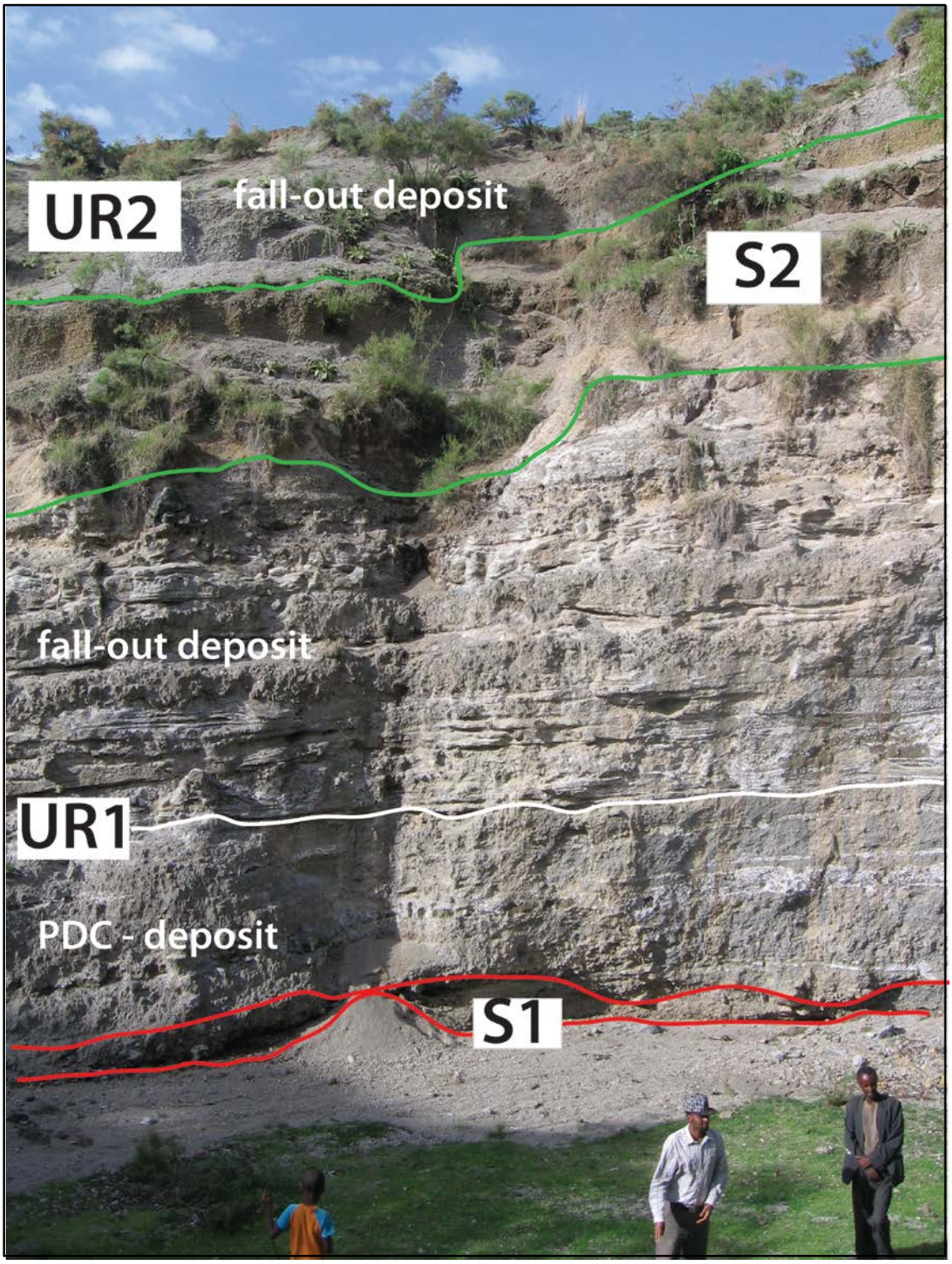

Fig. 2.8`: ***Urji lithosome*-**UR1 eruptive unit (PDC deposits in the lower part and laminated fine ash deposit in the upper part) separated from UR2 eruptive unit (fall-out deposit-facies) by a second order unconformity S2 as paleosol. Sampling site n. 6 within the caldera.

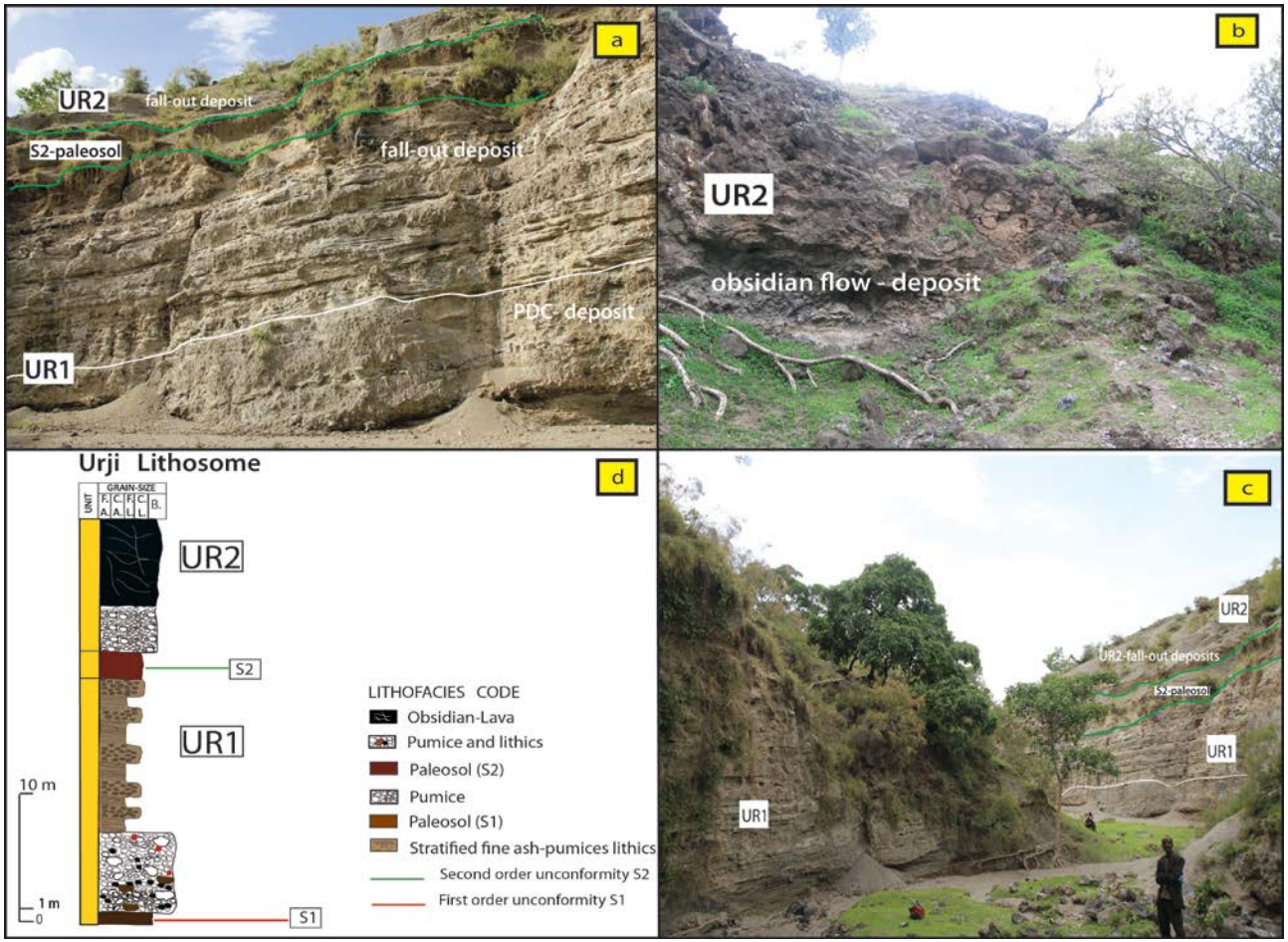

Fig. 2.9`: *Urji Lithosome*- **a)** UR1 eruptive unit (PDC deposits in the lower part and laminated fine ash deposit in the upper part) separated from UR2 eruptive unit (fall-out deposit-facies) by a second order unconformity S2 as paleosol. Sampling site n. 6 within the caldera.; **b)** Obsidian –flow facies within UR2 eruptive unit. Sampling site n.7 within caldera; **c)** Laminated fine ash facies within UR1 eruptive unit separated from UR2 eruptive unit (fall-out facies) by a second order unconformity S2 as paleosol. Sampling site n.8 within caldera; **d)** representative log of the deposits succession within the *Urji Lithosom**e.***

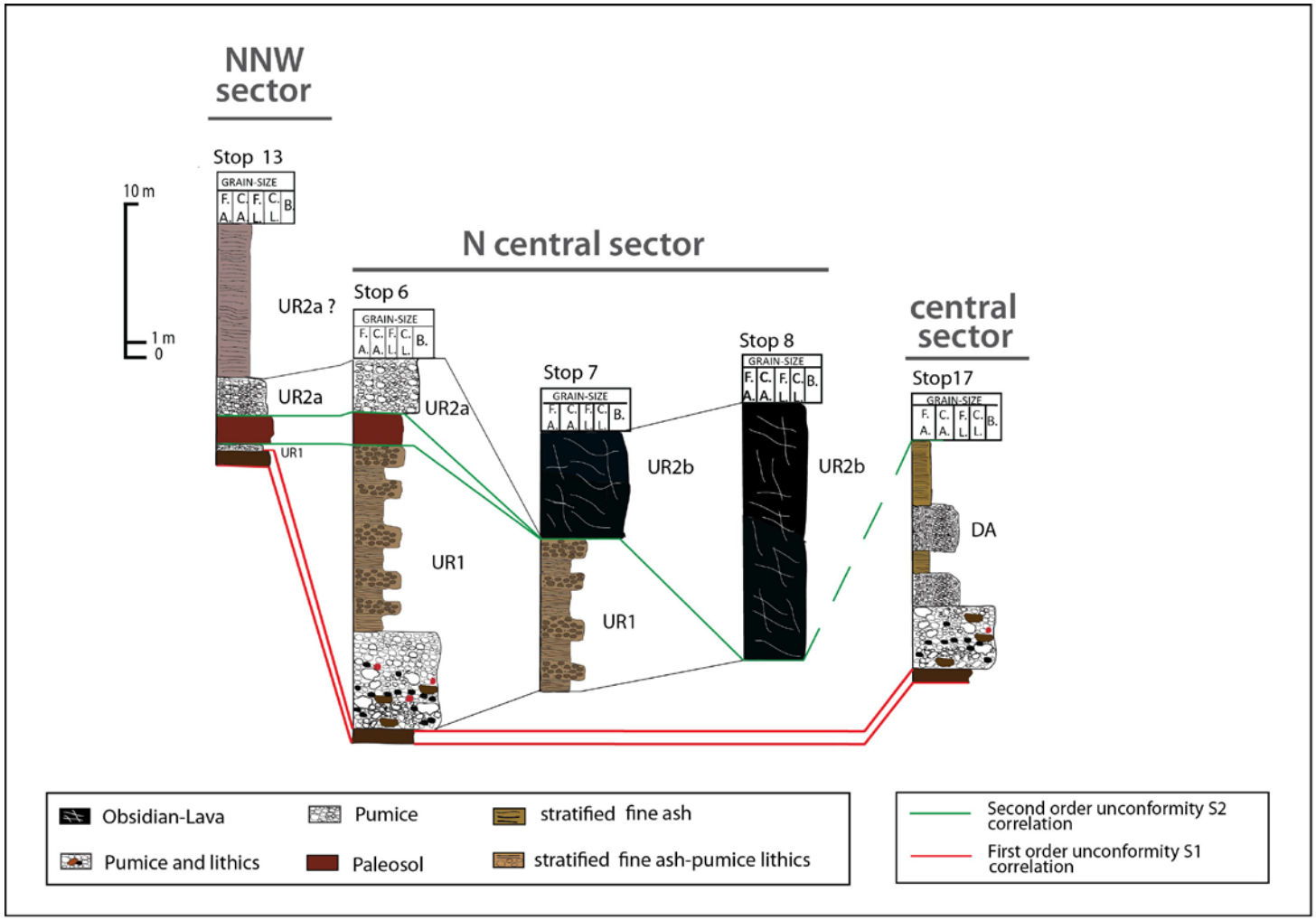

Fig. 2.10: stratigraphic logs of the deposits succession within the *Urji and Danshe lithosomes* at the the sampling site along the NNW, N central and central sector of caldera. The unconformities recognized S1 (first order) and S2 (second order) that allowed the stratigraphic correlation , are highlighted.

Danshe Lithosome

The *Danshe lithosome* is found in the central sector of Corbetti Caldera (outcrops n.17, Fig. 2.4, 2.11) and is separated from the *CCL* by S1 unconformity, corresponding to a ~1m thick deposit of reworked material in the caldera plain (Fig. 2.10, 2.12 (a)).

Danshe lithosome is characterized by a sequence of pyroclastics deposits characterized by three diefferent facies (Fig.2.12 (a), (b)).

The lower part of the Danshe lithosome , DA, (Fig.2.12 (a)) is a massive, poorly sorted, grain-supported deposit. The clasts are mainly (~90%) grey pumice with a low percentage (~10%) of lithics. Maximum measured thickness is 2 m at the outcrop n.17 close to the vent. The middle-upper part of the Danshe products is characterized by an alternation of two facies of fine ash and lapilli deposits (Fig.2.12 (b)).

The lapilli facies is a massive, well sorted , grain - supported deposit. The clasts range from fine to coarse lapilli and they are mainly (~90 %) grey pumices with a low percentage (~10%) of obsidian clasts. Maximun measured thickness is 2 m at the outcrop n. 17 close to the vent. The two fine ash facies show an alternation of massive structure with a laminated bedding. The first level has an estimated thickness of ~ 1m, whereas the second level has an estimated thickness of ~ 2.5 m at outcrop n.17 close to the vent.

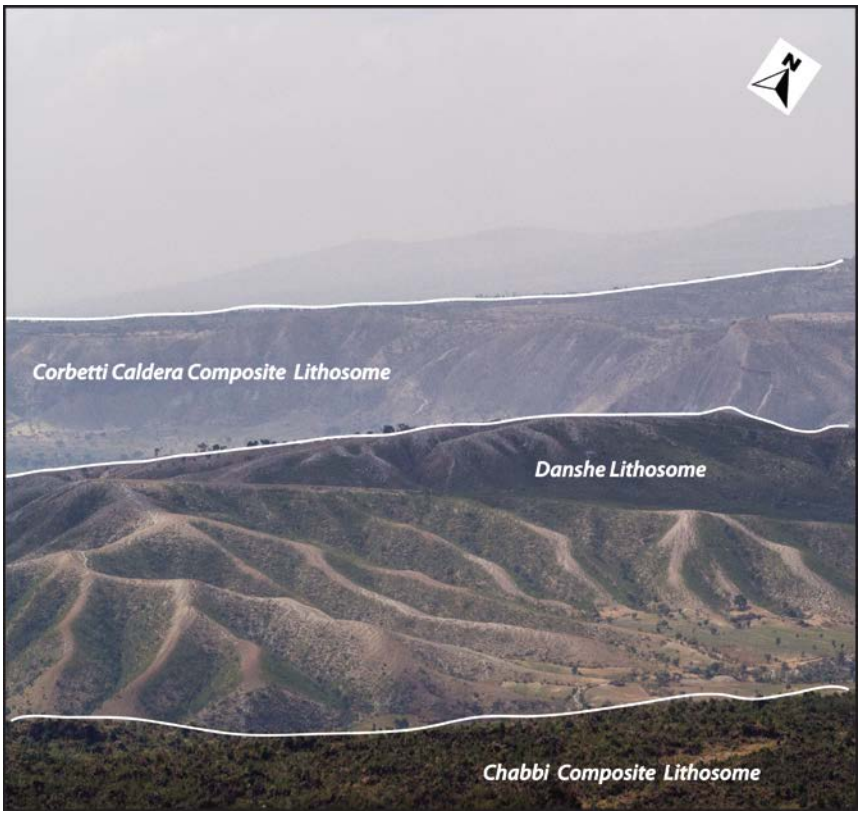

Fig. 2.11 *Danshe Lithosome* deposits within the central sector of Corbetti caldera

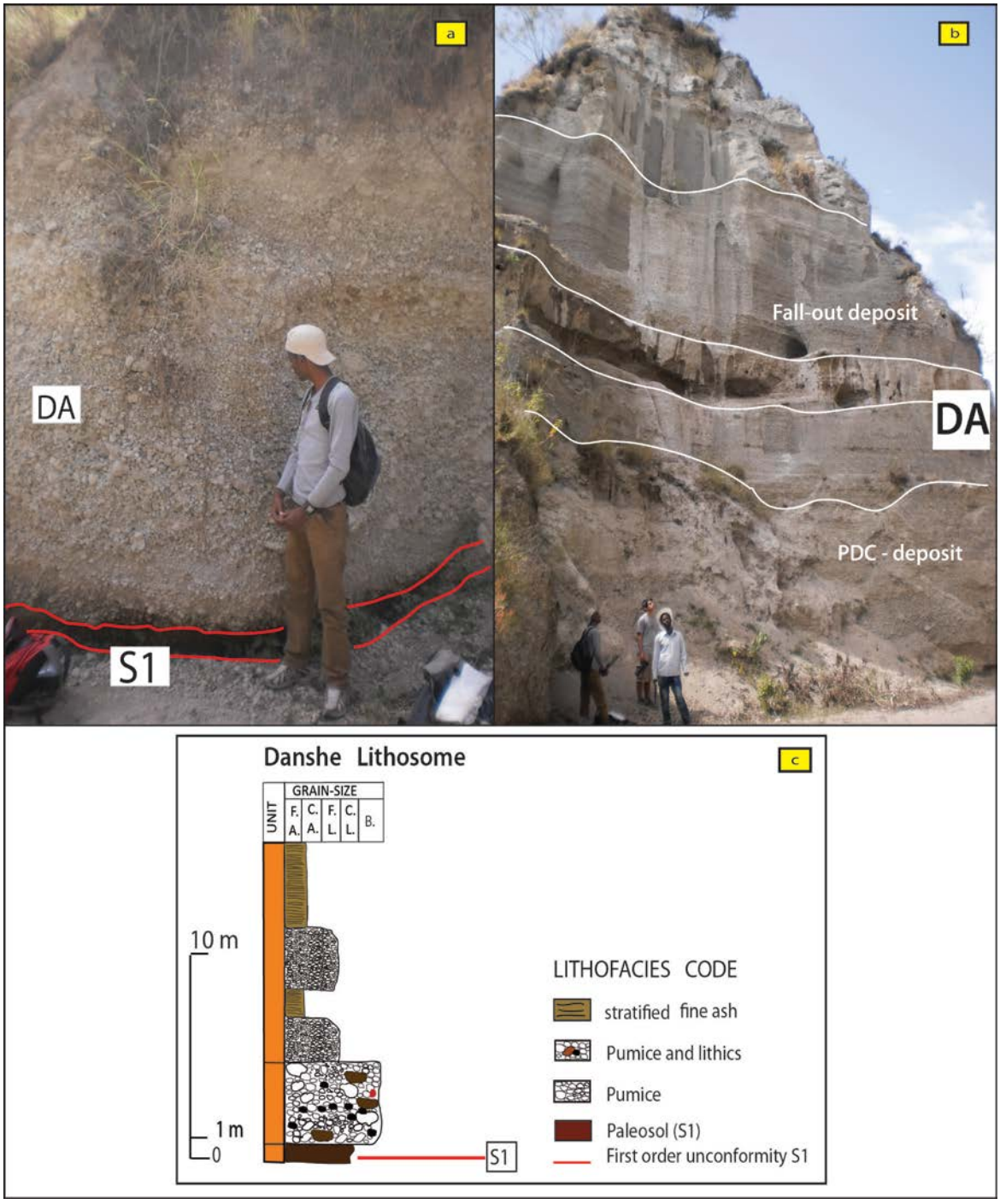

Fig. 2.12 : *Danshe Lithosome* deposits at sampling site n.17 in the central sector of caldera; **a)** pyroclastic density current facies in the lower part; **b)** PDC in the lower part and lapilli size-fine ash size fall-out deposit in the middle upper part; **c)** representative log of the deposits succession within the *Danshe Lithosome.*

Chabbi composite Lithosome

In agreement with Mohr (1966), Chabbi comprises seven different vents and related deposits , wich are here interpreted as seven different lithosomes included in the *Chabbi Composite Lithosome* (Fig. 2.5). It was not possible to establish for certain the relative temporal sequence of the seven lithosomes. However, on the basis of the reciprocal geometric organization of the deposits of each vents, as observed from LIDAR images and from the level of erosion observed using ortho-photos, the following temporal sequence, from the oldest to the newest volcano , might be hypothesized: Chabbi 1, which corresponds to the North East Vent II of Mohr (1966); Chabbi 2, which corresponds to the Norht East Vent I of Mohr (1966) and Chabbi 3 ,which corresponds to the North Vent of Mohr II(1966), located in the northern sector of *Chabbi Composite Lithosome*; Chabbi 4, corresponds to the Hot Vent to of Mohr (1966); Chabbi 5 , corresponds to the East Vent to of Mohr (1966); Chabbi 6 corresponds to the West Vent of Mohr (1966) and Chabbi 7 ,which corresponds to the Main Vent of Mohr (1966), located in the central-southern sector of *Chabbi Composite Lithosome.*

Suitable outcrops for a detail stratigraphic description were not found for all of the deposits of the seven lithosomes and only for Chabbi 5 and Chabbi 1 lithosomes, was possible to describe a detailed stratigraphic log of the deposits. However, field observations combined with observations of LIDAR images and ortho-photos, allowed a general stratigraphic description also for the Chabbi 2, Chabbi 3, Chabbi 6 and Chabbi 7 lithosome deposits.

The *Chabbi Composite Lithosome* is marked at the bottom by the deposits of Chabbi 1lithosome, CH1, (sampling site n. 26, 27, 28, 29 Fig.2.5) This deposit is characterized by four different lithofacies (Fig.2.13 (a), (b), (c), (d)). At the bottom the first lithofacies is a massive, poorly sorted, deposit (Fig.2.13 (a)). The clasts are represented by abundant (~75%) red-black lithics and a lower percentage (~ 25%) of pumice. The clasts range from lapilli to block size. In the upper part this facies shows a higher percentage of matrix with abundant fine lapilli to coarse lapilli size fragments of red litichs and sanidine phenocrysts. The total estimated thickness is ~ 30m. In the middle part the deposit is characterised by the second lithofacies (Fig. 2.13 (b)), represented by a laminated fine ashe deposit of ~ 30 m thickness. This fine ash deposit is interbedded with a thin (7cm) layer of grey pumice. In the upper part, CH1 lithosome deposit, is characterized by the third facies, represented by a massive, well sorted, grain-supported deposit 1.7 m thick (Fig.2.13 (c)), with fine lapilli to bomb size clasts of predominantly grey pumice (~90%) and a lower percentage (~ 10%) of red lithics.

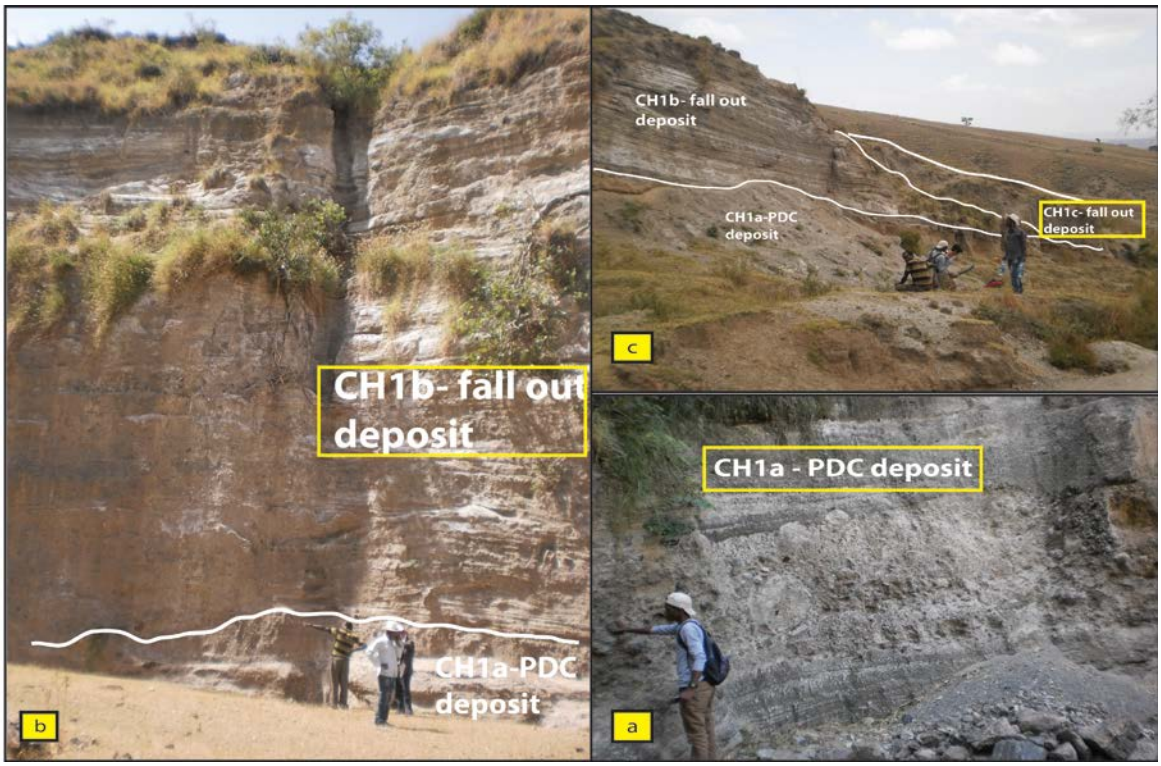

Fig. 2.13 : Chabbi 1(CH1) lithosome deposits at the sampling site n.26,27,28,29; **a)** pyroclastic density current facies at the bottom of the stratigraphic sequence; **b)** fine ash –fall out facies in the middle part of the stratigraphic sequence ; **c)** lapilli fall-out deposit in the upper part of the stratigraphic sequence.

At the top, the eruptive sequence of the CH1 lithosome ends with a fourth lithofacies, represented by an obsidian lava flow of 10 m estimated thickness (Fig.2.14)). The Chabbi Composite Lithosome sequence continues with the deposits of the Chabbi 2 and Chabbi 3 lithosomes respectively in the northern sector of Chabbi volcano (Fig2.5).

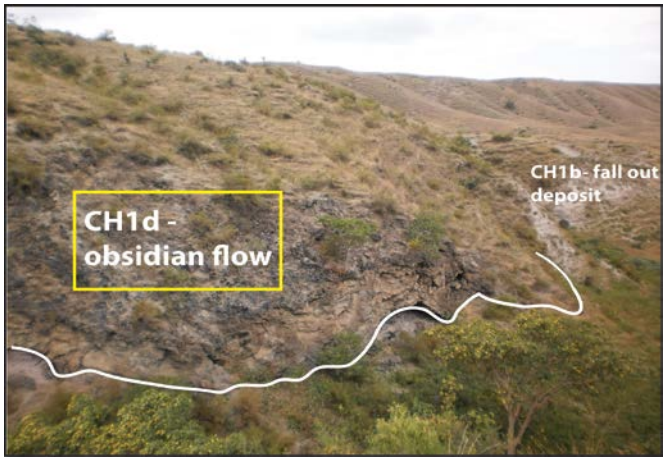

Fig.2.14 : Chabbi 1(CH1) lithosome deposits at the sampling site n. 29. Obsidian flow facies at the top of the stratigraphic sequence.

It was not possible to observe and describe the deposits of these two lithosomes directly, however from the observation of LIDAR images it was possible to anlayse the morphology of the deposits and to extrapolate the their features. The CH2 lithosome is characterized by the emplacement of large pyroclastic deposits probably occurring with the emplacement of two pyroclastic flows .

The CH3 lithosome is characterized by an older large pyroclastic flow deposit (CH3a Fig. 2.5 and 2. 15 (a)) extending toward the north and north-west, overlaid by a considerable obsidian field (CH3bO) associated with another pyroclastic flow deposit (CH3bP) (Fig.2.5, 2.15 a), b)). The obsidian field contains several different flows that extended mainly toward the north, while the pyroclastic flow extended toward the south. The CH4 lithosome outcrops in the central sector of Chabbi volcano (Fig. 2.5) and it is made up of PDC deposits (CH4a Fig. 2.15 (a), (b)), strongly altered by fumarolic activity (Fig.2.15 (c)) and of obsidian flow deposit (CH4b, Fig. 2.5). In the stratigraphic sequence, the CH4 lithosome is probably contemporary to the deposits that characterized the CH5 lithosome in the eastern sector of Chabbi volcano.

The CH5 (Fig.2.5) lithosome consists in the lower part of a thin (40 cm) layer of massive, well sorted, grain deposits. Most of the clasts (~85%) are grey pumice with small amount of lithics (~ 10%) and obsidian shards (~5%). The clasts range from fine to coarse lapilli size. In the middle part the deposit is a massive and poorly sorted deposit with a higher percentage of matrix and a slightly higher percentage of lithics than in the lower part. Most of the clasts comprise grey pumices and range from fine lapilli to block size. The maximum measured thickness is ~ 1.5 m at the outcrop n. 22 (Fig.2.5). In the upper part, the deposit is defined by an aphyric banded obsidian-lava flow with an estimated thickenss of ~ 20 m (Fig.2.15 (d)).
Chabbi 5 and Chabbi 1 lithosome deposits were the only stratigraphic sequences within the *Chabbi Composite Lithosome* that it was possible to study completely and in detail at the sampling site, and that it was possible to make a representative stratigraphic log (Fig. 2.16).

The *Chabbi Composite Lithosome* sequence ends with the deposits of CH6 and CH7 lithosomes in the southern sector of *Chabbi volcano* (Fig. 2.5). The CH 6 lithosome is also characterized, as the other Chabbi lithosomes, by two different facies. The lower part of the lithosome constists of PDC deposits (CH6a Fig. 2.5, sampling site n.19,20, Fig. 2.17 (a)) which shows a poorly sorted grain-supported deposit of grey pumice (Fig. 2.17 (b)). In the middle –upper part, CH6 is defined by several flows of banded obsidian (sampling site n.18 Fig. 2.5 and Fig.2.17 (c)).

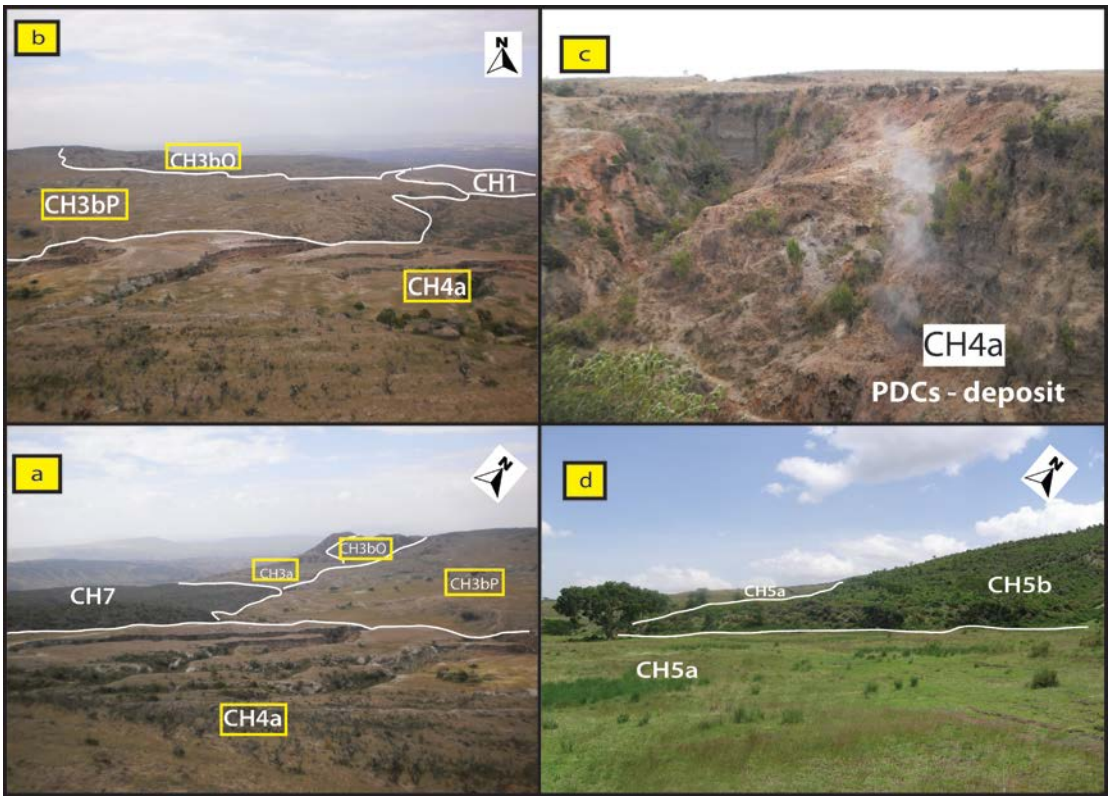

Fig.2.15: *Chabbi Composite Lithosome.* **a)-b)** Morpho-stratigraphic boundaries between Chabbi 1, 3, 4 and Chabbi 7 lithosomes; **c)** fumarolic activity within the PDC deposit of Chabbi 4 lithosome (CH4a), stop n.30; **d)** Chabbi 5 lithosome deposits (CH5a-CH5b). Sampling site n. 25

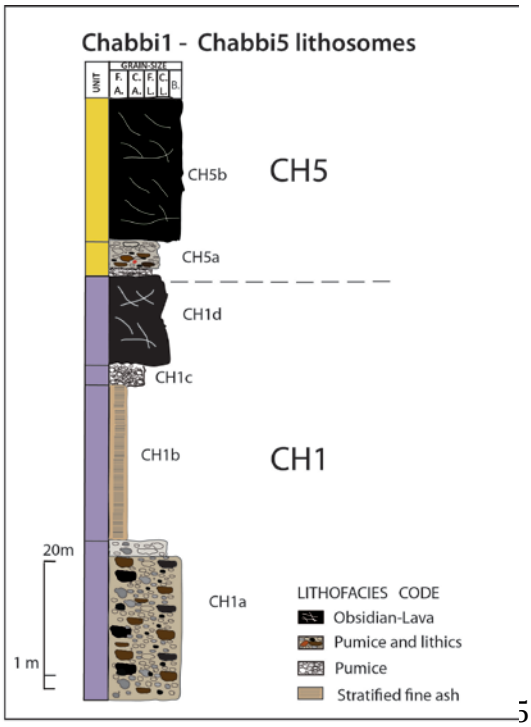

Fig.2.16: representative log of the stratigraphic sequence of the deposits within Chabbi 5 lithosome (W-SW sector of *Chabbi Composite Lithosome* Fig. 2.5) and Chabbi 1 lithosome (NW sector of *Chabbi Composite Lithosome* Fig. 2.5).

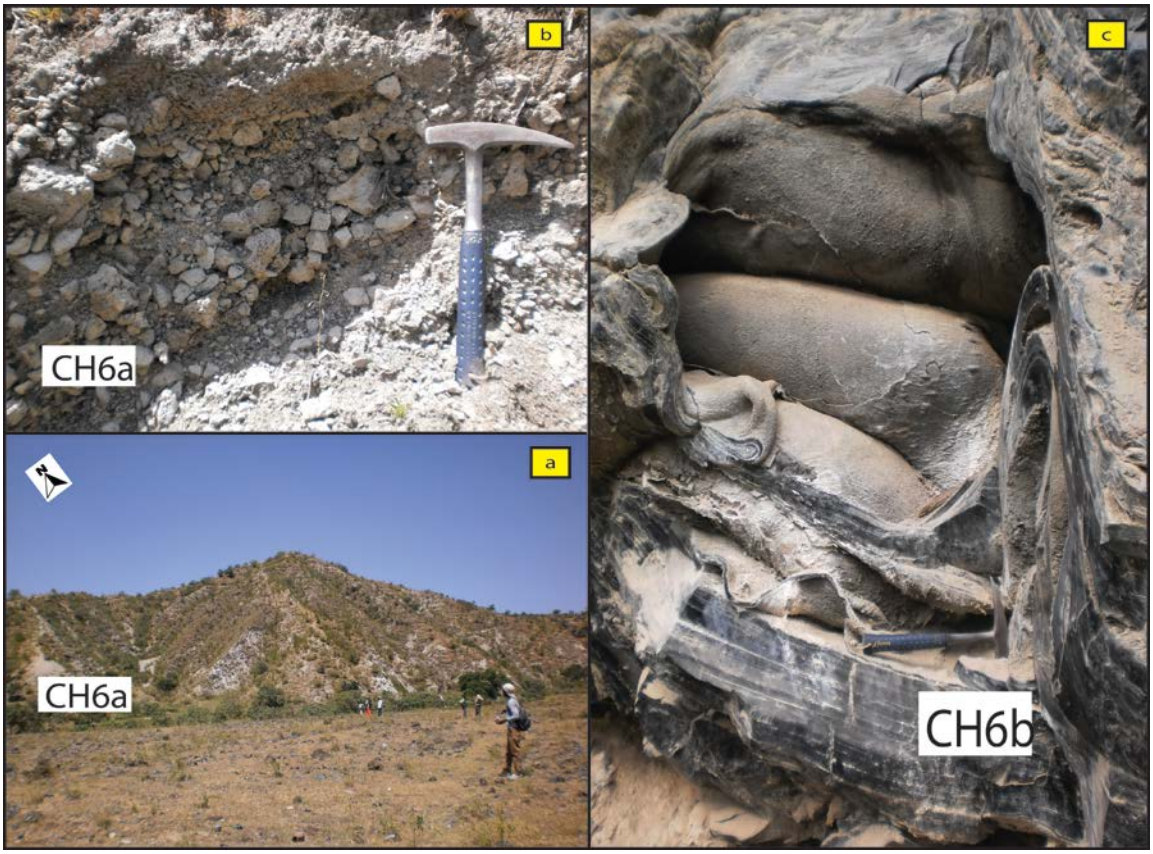

Fig. 2.17: *Chabbi Composite Lithosome,* southern sector. **a)**PDC deposit of Chabbi 6 lithosome (CH6a), stop n.20; **b)** detail of the PCD deposit (CH6a) at sampling site n. 21 ; **c)** banded obsidian flow deposit (CH6b) of Chabbi lithosome 6 at stop n.18 Fig. 2.5

The final eruption of Chabbi volcano emplaced the huge obsidian field, which characterises the deposits of CH7 lithosome in the southern sector of Chabbi volcano (Fig. 2.5, 2.18 (a),(b)). The CH7 obsidian field comprises several aphyric obsidian flows extended partially toward the north and mostly toward the south. Chabbi 7 lithosome is formed only by obsidian flows (Fig. 2.18 (b)).

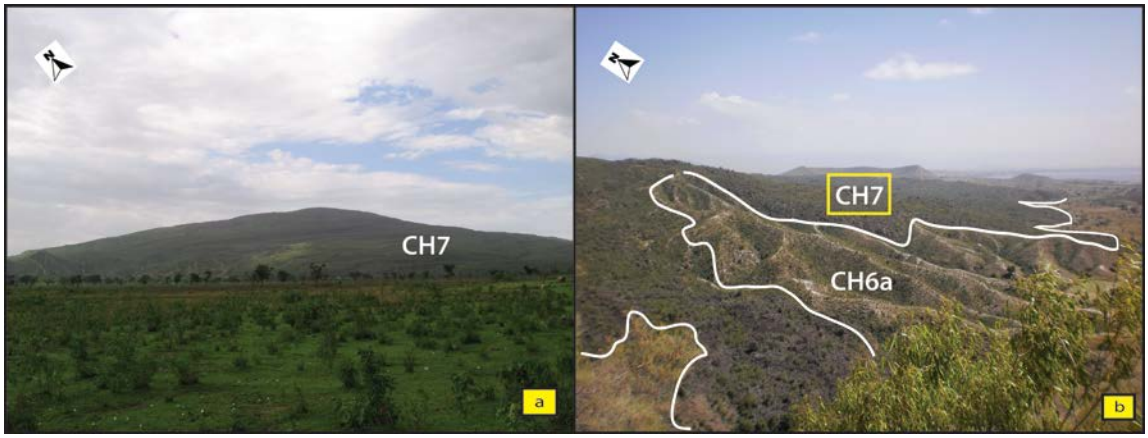

Fig.2.18: a) Chabbi 7 lithosome in the southern sector of *Chabbi Composite Lithosome*; **b)** Chabbi 7 obsidian flow in the southern sector of *Chabbi Composite Lithosome.*

2.3.3 $^{40}Ar/^{39}Ar$ Corbetti dating

At Corbetti caldera , the most suitable crystal for $^{40}Ar/^{39}Ar$ dating is the alkali-feldspar, sanidine. We attempted to use seperates of this mineral to date the products of Corbetti caldera from each lithosomes identified by the stratigraphic work, *Corbetti Composite Lithosome, Danshe Lithosome, Urji Lithosome, Chabbi Composite Lithosome*. However, the very low content (5-10 vol %) of crystals in Corbetti deposits and the presence of crystallized MIs in sanidine crystals, eventually resulted in reliable dates being obtained for only two eruptions, the caldera forming eruption (COR2 eruptive unit) and the oldest Chabbi's eruption from Chabbi 1 lithosome deposits (CH1).

The ages are reported as weighted mean ± standard error of the mean. In this work, the deposit from the caldera forming eruption, COR2, within the *Corbetti Composite Lithosome*, has been dated for the first time., and in particular we dated the PDC facies within the COR2 eruptive unit. The pre-caldera eruptive unit, COR1, was not possible to date due to the lack of suitable sanidine crystals, as well as most of the deposits from the post-caldera eruptive epoch. Only the PDC deposit, CH1, from the Chabbi 1 lithosome was possible to date.

The syn-caldera deposit COR2, yielded an $^{40}Ar/^{39}Ar$ age of 176.8±4.1ka (Fig.2.19), whereas the early post- caldera deposit from Chabbi 1 lithosome, yielded an $^{40}Ar/^{39}Ar$ age of 18.4±4.3ka (Fig.2.20)-

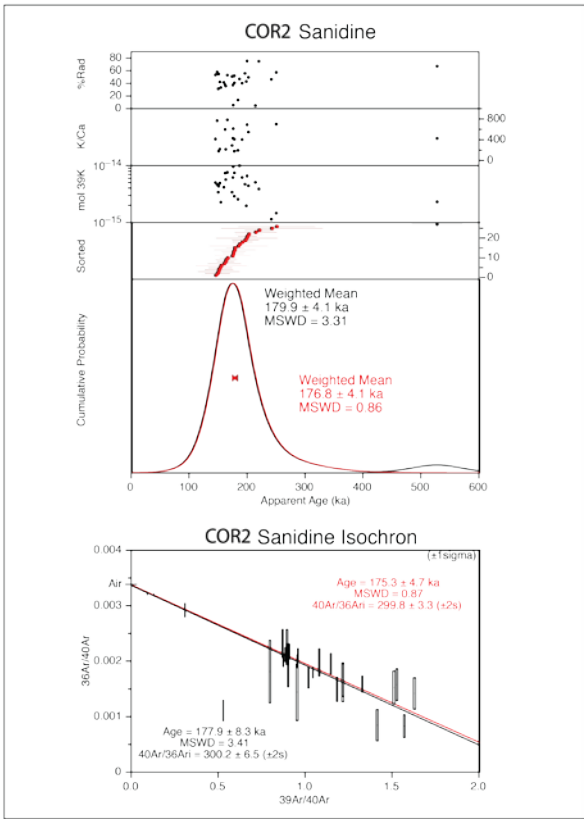

Fig.2.19 Age probability spectrum for USGS $^{40}Ar/^{39}Ar$_ sanidine analyses from syn- caldera products (COR2 EU, Corbetti Composite Lithosome).

Ages shown are the weighted mean ± standard error of the mean (1σ).

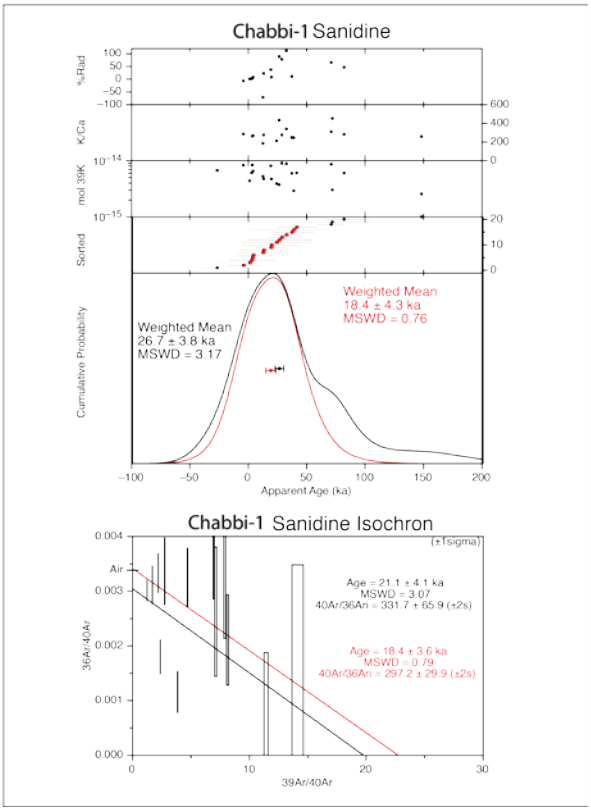

Fig.2.20 Age probability spectrum for USGS $^{40}Ar/^{39}Ar$_ sanidine analyses from post- caldera products (Chabbi1Lithosome). Ages shown are the weighted mean ± standard error of the mean (1σ).

2.4 Discussion

2.4.1 Reconstruction of the Corbetti Caldera eruptive activity

Corbetti Caldera volcano is an elliptical caldera (long axis 18 km, short axis 11km) associated with the Quaternary volcanism developed in the Main Ethiopian rift along with the Wonji faults segment, oriented ~N 12^0 in the central MER (Corti 2008).
Like other Quaternary calderas of the Main Ethiopian Rift (Fantale, Kone, Gedemsa), Corbetti shows a E-W elongation (Acocella et al., 2003).

The application of the UBSU criteria to the Corbetti caldera, revealed the value of using this methodology to reconstruct the eruptive activity of a volcano complex (Coltelli et al. (1994), Calvari et al. (1995), Maneti et al. (1995), Rossi et al. (1996), De Rita et al. (1997), Calanchi et al. (1999), Tranne et al. (2002a), Tranne et al. (2002b), Lucchi et al. (2003), De Astis et al. (2006), Giordano et al. (2006); Cimarelli et al. (2013); Di Traglia et al., (2013), Fusillo et al.(2015)).
The recognition of the first order unconformity allowed the identification of the volcanological evolution of Corbetti Caldera characterized as two eruptive epochs, the pre- and syn-caldera activity, represented by the *Corbetti Composite Lithosome (CCL)* deposits, and the post-caldera activity represented by the deposits of three different lithosomes, *Urji Lithosome*,*Danshe Lithosome* and *Chabbi Composite Lithosome.*

The recognition of second order unconformities (S2) allowed the identification of the main eruptive units that marked the eruptive epochs, as well as the identification of the temporal sequence within both the *CCL* lithosome and the three lithosomes, of the post-caldera activity. From the stratigraphic reconstruction, I hypothesize that the older activity of Urji (UR1 Eruptive Unit) and the Danshe activity, were the first expression of the resurgent volcanism followed by the younger expression of Urji ‘s activity (UR2 Eruptive Unit) and the Chabbi volcano activity as the later and the last expression of the post-caldera volcanism at Corbetti. The stratigraphic record of the pre-caldera activity is represented by a massive lava deposit, the COR1 Eruptive Unit, characterized by a structure of columnar jointing. The features of the columnar jointing suggests an E-W direction of the lava flow that might have been emplaced by an fissure eruption.

After a time break marked by reworked deposits (S2 unconformity), the Corbetti activity restarted with a big explosive eruption that likely ended with caldera formation. Syn-caldera activity emplaced the deposits of the COR2 Eruptive Unit.

The three facies that characterize this eruptive unit suggest they are proximal deposits. In particular the spatter bombs outcroppings along the north-western rim suggest that the vent was located in that sector of the caldera (Carey et al., 2008 a,b). The lack of accidental cobbles and boulders in the deposits of the COR2 unit, suggests that the Corbetti Caldera collapse occurred at the end of the eruption. The planar geometry of the deposits along with no significant thickness variation of the intra-caldera eruptive unit, also suggests a symmetric collapse that involved the subsidence of a coherent block of rock (plate/piston collapse, Lipman 2000b).

After a period of rest marked by a first order unconformity S1, the volcanic activity resumed within the caldera depression with the Urji, Danshe and Chabbi volcanoes and their deposits (*Urji, Danshe and Chabbi Composite lithosomes*). The first stage of the post-caldera volcanism was characterized by Urji and Danshe volcanic activity. The products of *Danshe lithosome (DA)* were emplaced by explosive eruptions of Danshe volcano. The three different facies of the products, PDC deposit, fall-out lapilli-size deposit and fall-out fine ash -size deposit, indicate a variation of the eruptive style of the parent eruption.
None effusive eruption characterized the Danshe volcano as also reported in Altaye (1984).

Explosive activity also characterized the eruptions that emplaced the products of the eruptive unit UR1 from the older Urji's activity, as suggested by the PDCs deposit in the lower part and fall-out deposit in the upper part. The grain size of the fall-out deposit in the upper part of UR1 EU, might suggest a phreatomagmatic eruption, which might have occurred during the lapse of time when there was still a local lake within the caldera depression (Altaye, (1984). It is likely that during this same period of time characterized by the local lake, the basaltic deposit COR3 within the *CCL* lithosome, has been emplaced as the pillow shapes suggest. The lack of any higher rank unconformity between the deposits of the Danshe and Urji volcanoes, might suggest that a short period of time elapsed between their activity and the high erosion of Danshe products, indicating that Danshe activity may have preceded the older activity of Urji (UR1).

After a time break marked by a paleosol (S2 unconformity), the Urji volcano activity resumed with the emplacement of the products of the eruptive unit UR2, characterized by fall-out deposits associated with obsidian lava flows. The emplacement of the obsidian flows marked the end of Urji activity as expression of magma completely degassed.

The last manifestation of the post-caldera activity was comprised in the *Chabbi Composite Lithosome,* as also suggested by the current fumarolic activity at Chabbi volcano. Chabbi volcano is located in the east sector of the caldera structure and, as Danshe deposits, Chabbi products overlap to the east sector of the caldera rim and they extend both inside and outside the caldera depression.

Although it was not possible to establish for certain the temporal relationship between Urji- Danshe and Chabbi lithosome activity, since no paleosol was found between the lithosomes, however the fresh morphology and the presence of fumaroles suggests that last activity of Chabbi (Chabbi 4, Chabbi 5, Chabbi 6, Chabbi 7 volcanoes) was probably following the second stage of Urji activity. Whereas from the fieldwork and LIDAR imagery observation, it can be also asserted that the first Chabbi activity started with the emplacement of the CH1, CH2 and CH3 lithosomes deposits in the northern sector and that may have been contemporary with the first Urji's activity (UR1) and before of the second one (UR2). Regarding the last volcanism that emplaced the deposits of *Chabbi Composite Lithososme,* it is likely that the activity of the Chabbi 4 and Chabbi 5 eruptive centers was contemporary, and that the Chabbi volcanism ended with the emplacement of the obsidian lava fields deposits of CH 6 and CH7 lithosomes (Fig.2.5).

The Chabbi volcano activity would have then occurred in two periods of time. The first period, characterized by the emplacement of the deposits of Chabbi 1, Chabbi 2 and Chabbi 3 lithosomes in the northern sector and the second period characterized by the emplacement of the deposits of Chabbi 4, Chabbi 5, Chabbi 6 and Chabbi 7 lithosomes in the southern sector. Most of the Chabbi volcanic eruptions (Chabbi 1, 3, 4, 5, 6) were characterized by a first phase of explosive activity followed by a second phase of effusive activity.

In particular, the explosive activity that emitted the Chabbi 1 lithosome was characterized by four different phases that emplaced four different lithofacies, (CH1a, CH1b , CH1 c and CH1d ,) within a pyroclastic density current deposit.

Only the eruption that emplaced the deposits of Chabbi 2 lithosome had exclusively an explosive phase, whereas on the contrary, the most recent activity of Chabbi was characterized by only effusive eruptions as expression of magma completely degassed. This is also confirmed by the size of the obsidian field that characterized the effusive activity of the Chabbi 6 and Chabbi7 volcanoes in the southern sector of *Chabbi Composite Llithosome.*

The activity of Corbetti caldera was characterized mostly by monogenetic centres with the exception of the vent that emplaced the COR1 and COR2 eruptive units and the Urji volcano. All Corbetti caldera deposits are of peralkaline composition (Chapter 3) with the exception of the basaltic lava deposit (COR3) included in the *Corbetti Composite Lithosome*. The position of this deposit, which covers the syn-caldera deposits on the western caldera rim, suggests that it was emplaced during the post-caldera volcanism and it is not correlated with the pre- and syn-caldera activity. The pillow lava could have been emitted during the phase when there was still a lake in the caldera depression (Altaye (1984)). This lava deposit outcropping on the caldera wall may be linked with a fault activity where current fumaroles are located.

Altaye (1984) describes a basaltic deposit on north-western part of caldera wall that may be correspond to the COR3 of this work and that is part of the **Qb** –unit, characterized by 'basaltic lava flows and scoria cones' within the ' Volcanic rocks post-caldera' sequence. He reports this deposit as a dyke, whereas other deposits of the same unit outcropping outside the caldera depression are reported as scoria cones and fissure flows. Altaye interprets this unit as the products of basaltic volcanism associated with the 'Corbetti-Shalla–sector' of the Wonji fault belt. A similar scenario has also been observed at Kone caldera (Rampey et al. 2010) where the genesis of a basalt lava flow (Kone B1, Rampey et al.2010), that is placed on the ignimbrite deposits along the caldera wall , is interpreted to be linked to a faults' activity near to area of the main direction (toward west) of the faults that cut the caldera wall.

Overall the Corbetti's eruptive history was characterized by four different cycles of activity, associated to four different volcanoes active in different periods of time. The volcanic activity was characterized mostly by monogenetic centres and was marked throughout the eruptive history by explosive eruptions with the emission of obsidian lava flows as expression of the last degassed magma.

Data presented here suggest a decrease of the explosivity in the volcanic eruptions of Corbetti activity, from the first manifestation of the resurgent volcanism characterized by the activity of Danshe and Urji volcano, to the last manifestation marked by the activity of Chabbi volcanoes.

In particular, the last activity of Corbetti produced the obsidian lava fields of Chabbi 6 and Chabbi7 lithosomes within the *Chabbi Composite Lithosome*, and this suggests a sub-volcanic system at the final stage with a magma completely degassed.

Corbetti caldera is currently at a quiescent stage and its activity is now represented by fumarolic gases.

The UBSU methodology along with the Lihosome concept allowed the identification of a relative temporal sequence of the volcanic activity of Corbetti volcano system and mostly important , helped to put in relationship the deposits with the different vents. The reconstruction of the temporal sequence of the volcanic activity and the relationship of the deposits with the different vents, are presented in this work for the first time. Indeed in the previous works the authors were not able to provide a temporal sequence of the volcanic events and to understand the relationship between the deposits and the different vents (2.4.2 'New stratigraphic reconstruction and comparison with previous works').

In this work it is also presented for the first time an absolute dating of some of the major eruptions in the Corbetti caldera history. The first interesting inference emerging from these data is that a period of time of about 158 ka, elapsed from the caldera forming eruption and one of the first eruptions of the resurgent volcanism in Corbetti caldera. The age of the Corbetti caldera forming eruption is comparable with the age of caldera –forming eruption of other Quaternary calderas along the rift. Recent $^{40}Ar/^{39}Ar$ age determinations carried out on Alutu caldera (Hutchison et al. 2016), comparable with the age of caldera collapse of other Quaternary volcanoes along the rift, suggest that a major pulse of explosive volcanic activity occurred along the rift between 320–170 ka. Among the Quaternary calderas, four distinct volcanic centers (Gedemsa, Alutu, Shalla, Corbetti) underwent large volume (> 10 km3) caldera-forming eruptions during this period of time. At Shalla, caldera collapse occurred at 240 ± 30 ka (K/Ar dating) , whereas at at Gedemsa, K/Ar dating showed "that pre- and post- caldera rocks bracket an age of 320–260 ka for collapse events" (Hutchison et al.2016).

The caldera forming eruption of Corbetti volcanic history therefore, took place in the same span of time when in other three silicic volcanic complexes (Gedemsa, Alutu, Shalla) along the MER, occurred the biggest explosive eruptions in a period of time (between 320 and 170 ka) considered a geologically short time-span .On the basis of these data, it has been hypothesized that in the Middle Pleistocene (300–200 ka) in the Main Ethiopian Rift, an intense silicic volcanism occurred along with a paroxysm of crustal extension, as also Mohr et al. have already speculated (Hutchison et al. 2016), and that would have also involved the magmatic system of Corbetti caldera.

The age of 18.4±4.3ka found for the early post- caldera activity of Chabbi 1, with $^{40}Ar/^{39}Ar$ dating, is consistent with the age of 0.02± 0.01 Ma, for the more recent obsidian flow from Chabbi 5, as reported in Woldegabriel et al. (1991). From both these data, although acquired by two different analytical techniques , it can be stated that the post-caldera activity of Chabbi eruptive center, within Corbetti volcanic complex, occurred at least about 20ka B.P. Also the new $^{40}Ar/^{39}Ar$ dating and the dating of Woldengabriel on Chabbbi's products, confirm the stratigraphic reconstruction , that is the deposits of Chabbi 1 lithosome were emplaced earlier than the deposits of Chabbi 5 lithosome, and that therefore Chabbi 1 vent was active earlier than Chabbi 5 vent.

In the stratigraphic reconstruction presented in this work the activity of some of the vents of Chabbi volcano, has been interpreted to be one of the early manifestation of the resurgent volcanism, probably occurred after the Danshe activity and before the more recent activity of Urji ,that produced the UR2 eruptive unit. The deposits of the Chabbi 1, Chabbi 2 and Chabbi 3 lithosomes therefore, would have been emplaced in a span of time contemporary to the first activity of Urji (UR1), whereas the deposits of Chabbi 4, Chabbi 5, Chabbi 6 and Chabbi 7 lithosomes, would have been emplaced by the last activity of Chabbi volcano, after the second eruption of Urji. If the K/Ar dating of Woldegabriel et al. (1991) of the Chabbi 5 obsidian flow, is taken into account, then the radiocarbon dating of the second eruption of Urji from Rapprich et al. (2105) (chapter 1) would not be consistent with this sequence.

It has been seen that Rapprich et al. (2015) (chapter1) dated a paleosoil located between the pumices of the Urji (Wendo-Koshe) eruption and a tuff deposit that was supposed to be emplaced by the Fike volcano, another volcanic center of the area, and that they sampled the paleosoil in two sites far ~14 km from Wendo-Koshe/Urji vent within Corbetti caldera. The lack of stratigraphic correlations of this paleosoil with other exposures inside and around the caldera, and the assumption that the deposit identified in the sampling sites 14 km far from Corebtti is the same deposit identified as " younger pumice " close to the Urji/ Wndo-Koshe vent, adds some uncertainty to the interpretation of Rapprich et al.2015 that report the second activity of Urji occurred in a ge of 396 ± 38 years B.C.

Overall it can be stated that Corbetti activity occurred more than 200ka B.P, and that after a period of rest of about 158 ka a resurgence in volcanism occurred within caldera at about 20 ka .

2.4.2 New stratigraphic reconstruction and comparison with previous works

The stratigraphic architecture proposed here well agrees with the stratigraphy proposed by Mohr (1966) regarding the newest lithosome Chabbi, whereas shows some differences with the geology and volcanology of the area as proposed by Di Paola (1972) and some difference with the post-caldera volcanism as proposed by Rapprich et al. (2015) . There are also significant differences with the previous stratigraphic reconstruction of the entire activity of Corbetti Caldera as proposed by Altaye (1984).

The main differences with the previous works regard the position and the interpretation of the ignimbrite and the pyroclastics deposits on the caldera rim and the temporal sequence and the interpretation of some of the deposits of the pot-caldera volcanism (Urji, Danshe and Chabbi lithosomes) .

Another important difference with the previous works concerns the application of the UBSU method based on the recognition of the unconformity surfaces and their meaning, since this method was used to reconstruct a temporal sequence of the main volcanic events that characterized the Corbetti Caldera eruptive history. The application of the lithosome and composite lithosome concept, also helped the identification of the deposits from the different vents improving the understanding the volcanic history of Corbetti caldera and especially the realization of the geological map there where for some deposits it was not possible to report them on the map because of the scale.

For example Rapprich et al. (2015) on their geological map, on the caldera rim, they only show the ignimbrite deposits omitting the lava deposit and the relationship between the two products. Altay (1984) in his geological map shows on the caldera rim the lava deposit and the ignimbrite and " pumiceous ignimbrite" deposits, but it is not clear their relationship.

On the contrary the composite lithosome concept allowed the mapping of the pre and syn caldera deposit, their relationship and the description of the different facies of the PDC deposit. This was of great advantage in knowledge and our understanding of the volcanic history of Corbetti caldera.

In this work the deposits related to the pre- and syn-caldera volcanism and post caldera volcanism are separated by an important unconformity of the first order (S1), identified as both the caldera wall and an erosive surface associated with reworked material/paleosol on the caldera floor. The rank of this unconformity marks two different eruptive epochs of the Corbetti volcanic history, pre- and syn-caldera volcanism and the post caldera volcanism.

Di Paola (1971) (Chapter1) described the caldera structure of Corbetti for the first time. However, he did not provide any detailed description and interpretation of the deposits that characterized the activity pre and post caldera collapse. He mentions fissure eruptions as activity preceding the volcanic tectonic – collapse and a typical ignimbrite formation as the most ancient product of the area. The author did not relate the ignimbrite deposit to the caldera forming eruption, as he pointed out that it was not possible to clearly identify any centre of eruption for this product. He also claimed that it was not possible to establish any relationship between the ignimbrite deposit and the "pumice layers" on the caldera rim.

The application of the UBSU method on the contrary, allowed the identification of the unconformity S1. The identification of the S1 unconformity allowed to understand the clear relationship between the pre and syn caldera deposits and especially allowed to make the stratigraphic description and correlation at each sampling site (Fig. 2.4 n.1,2,3,4,9,10,11,12,15, 16, Fig.2.6). This allowed in turn to understand that those deposits were emplaced by a volcanic center that was in the place of the caldera, before the caldera forming eruption (as the bomb facies, recognized within the COR2 eruptive unit, the syn caldera deposit, well show), and that the ignimbrite and the "pumice layers" on the caldera rim, were two different facies of the caldera forming eruption deposit, the COR2 eruptive unit of this work.

The "ignimbrite" of Di Paola (1971), the COR2 EU of this work, would not be then the most ancient product of Corbetti, as Di Paola suggests, since it is separated from the lava deposit (COR1) by a second order unconformity surface (S2, reworked material), and it would be related to the caldera forming eruption. An ignimbrite deposit (Qawi) is also identified in the stratigraphic reconstruction of Altaye (1984), who described the Corbetti products as 'Caldera and pre – Caldera Rocks' and ' Volcanic rocks post-caldera'. However, he does not provide the criteria by which he identified each rock unit and classified some of the deposits as pre - syn caldera and some as post- caldera.

The ignimbrite deposit (Qawi) in Altaye (1984) is the oldest deposit within the 'Caldera and pre – Caldera Rocks' sequence and is reported outcropping on the western and northern caldera rim. These outcrops of the ignimbrite deposit (Qawi) of Altaye reconstruction, well agrees with the outcrops (n. 15, 16 Fig.2.4) where the pyroclastic density current deposits have been observed (COR2 EU) in this work, and with the location of the ignimbrite as reported in Di Paola (1971).

However, the stratigraphic position and the interpretation of the ignimbrite deposit within the pre-syn caldera sequence as proposed by Altaye (1984), disagrees with the stratigraphic position and interpretation as proposed here.

Indeed in the Altaye reconstruction the ignimbrite is overlaied by the rhyolitic lava unit (Qr1) (Fig. 2.21) outcropping on the southern caldera rim, whereas in the stratigraphic reconstruction here proposed the rhyolitic lava (COR1 EU) is a pre-caldera unit and therefore precedes the ignimbrite deposit. Di Paola (1972) also hypothesized that the ignimbrite deposit observed on the Corbetti caldera rim, may be a product (Shibibo ignimbrite Qi_4,Mohr et al., 1980) of a the big eruption that formed the Shalla lake caldera(O'A Caldera to the north Corbetti). In this case the ash flow would have reached the north-northwest part of Corbetti only, depositing onto the rhyolitic lava deposit. According to this interpretation the ignimbrite deposit would not be associated with the caldera forming eruption of Corbetti.

However, the several levels of agglutinated deposits (spatter bombs) that characterizes the main body of the COR2 EU products and the fiamme structures, suggest that the PDC products are proximal deposits and this would rule out the Di Paola hypothesis.

Finally, the recognition of the second order unconformity surface S2, well constrains the relationship between the rhyoltic lava as a product that precedes the emplacement of the PDC deposits connected with the caldera forming eruption. The relationship between the rhyolitic lava and the products of the caldera forming eruption, were not understood in the previous studies on Corbetti caldera, whereas the application of the UBSU methodology allowed to understand this important relationship in order to know the volcanic evolution of Corbetti caldera.

Regarding to the deposits associated with the syn-caldera volcanism, Altaye (1984) identifies within the succession of the 'Caldera and Pre-Caldera Rocks' a 'pumiceous ignimbrite' deposit (Qp1 unit) (Fig.2.21) as the products of the caldera forming eruption. However, no lithological characterization of this deposit is provided and the location of the unit (some 'deep gorges' of Chabbi) is not discussed. This unit is then overlaid by a 'layered pumices pyroclastics' deposit (Qqwp) (Fig. 2.21) that would have been the last unit emitted from the 'Caldera and Pre-caldera rock' period on the basis of the Altaye reconstruction. The 'layered pumices pyroclastics' (Qqwp) is reported to outcrop on the southern, northern and western slope of the caldera rim.

Altaye also does not specify any relationship between the 'pumiceous ignimbrite' deposit (Qp1) and the subsequent 'layered pumices pyroclastics' (Qqwp), and he only reports that the Qqwp unit was probably emplaced by Corbetti volcano without clarifying if it was associated with the caldera forming eruption. Di Paola (1972) reported a similar unit of several layers of 'un-welded pumices' with maximum thickness (> 200 m) on the west part of the rim. Also this author claimed it was not possible to establish any relationship between the ignimbrite deposit and this pumice layers and once again claimed that no clear centres of eruption were recognized for the emplacement of this unit.

One again the application of the UBSU methodology and the recognition of the second order unconformity S2 and the first order unconformity S1 within the deposit of the Corbetti Composite Lithsome, allowed the stratigraphic correlation and description of the deposit at each sampling site along the caldera (Fig. 2.4 n.1,2,3,4,9,10,11,12,15, 16, Fig.2.6), and allowed to understand that products of the caldera forming eruption, the eruptive unit COR2, have different lithofacies that correspond to the "units" of Altaye (1984). In terms of the reconstruction of the volcanic history of a volcano, it is important to understand if some deposits are from the same eruption, so they represent the same eruptive unit or they are from different eruptions, so they are different eruptive units. It is also important to understand the relationship between the deposits and the volcanic center that emplaced them.

The application of the lithosome concept also allowed the recognition that the products of the caldera forming eruption, the eruptive unit COR2, the "ignimbrite" and the "pyroclastics" reported in the previous works, were therefore emplaced by the same eruptive centre, that emplaced all the products of Corbetti Composite Lithosome. It has been seen as the UBSU method also allowed both the reconstruction of the relative temporal sequence of the post-caldera activity (Urji, Danshe and Chabbi volcanoes) within the second eruptive epoch, and a better interpretation of the post-caldera deposits (Urji, Danshe and Chabbi lithososmes). In this regard there are significant disagreement with the previous works.

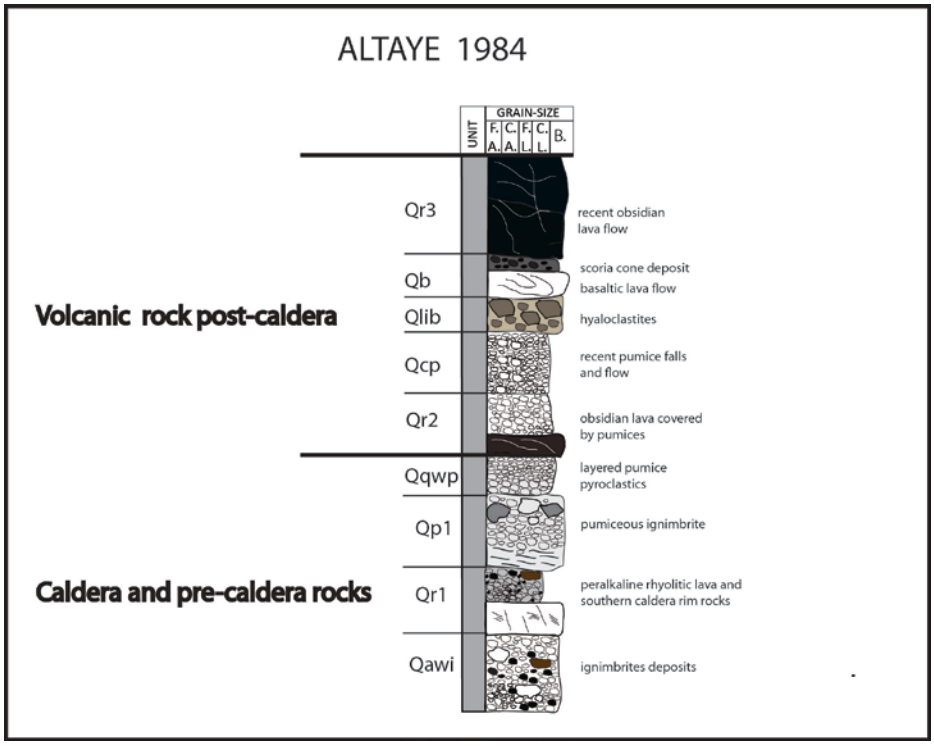

Fig.2.21: representative log of the Altaye (1984) stratigraphic sequence.

In his work, Di Paola (1971) hypothesizes that Urji and Chabbi activity were contemporary although he describes the development of Urji vent as the most important event of the post-caldera volcanism. He also provides a general description of the Urji and Chabbi deposits, whereas he does not report the existence of the Danshe vent. Altaye (1984) reports in general that the activity of the three recent volcanoes (Urji, Chabbi, Danshe) started to grow within the caldera floor after caldera collapse, but does not describe the temporal sequence of their development. In Rappich et al. (2015), the Danshe activity is reported as the first manifestation of the post caldera volcanism and they hypothesize some contemporary activity of Urji and Chabbi.

According to the stratigraphic reconstruction as proposed here based on the UBSU methosology, after a time break (marked by a S1 unconformity) following the caldera collapse, the activity resumed with the eruptions that emplaced the Danshe and Urji lithosome products, where the high erosion characterizing the Danshe products suggests that this volcano might have been active earlier than Urji. In the Altaye (1984) reconstruction the post-caldera activity starts with the emplacement of the Qr2-unit made up by ‘obsidian lava covered by pumices’(Fig. 2.21).

This unit seems to include the Urji second eruptive unit, UR2, within the Urji activity. The Altaye reconstruction omits all the deposits that are here interpreted as the eruptive unit UR1from the first Urji's activity. Indeed the UBSU methodology and the recognition of the first order unconformity S1 and the second order S2, at the bottom and in the middle of the stratigraphic sequence of Urji lithosome, allowed the identification of the deposits of the UR1 Eruptive Unit emplaced by the first Urji activity.

The Qcp unit that in Altaye reconstruction follows the Qr2 unit and that comprises 'recent pumice falls and flows' in different places within the Corbetti caldera, is interpreted produced by 'a number of centres'. This unit seems to consist of both the eruptive unit UR1 and the Danshe lithosome products (DA) as well as the products from several Chabbi lithosomes (CH1, CH2, CH3a, CH3bP) included in the *Chabbi Composite Lithosome,* according with the reconstruction presented here. There is therefore a strong disagreement about the interpretation and position of these deposits within the post- caldera activity of the second eruptive epoch of Corbetti volcanic history.

Rapprich et al. (2015) do not mention at all the products from the pre-syn caldera eruptions and from Danshe acitivity, as they focus only on the Urji activity. However, they also do not provide any interpretation of the deposit related to the first activity of Urji (UR1) since they described them as consisting "of thick accumulations of pumice with a monotonous appearance and that therefore the history and the evolution of Wendo Koshe (Urji) is difficult to reconstruct".

On the contrary, the application of the UBSU methodology and the recognition of the unconformity S2 as paleosoil within the deposit of Urji lithosome , allowed to identification of two different eruptions in the history of Urji volcano, and therefore the recognition of the PDCs - UR1, from the first Urji's activity and the obsidian flow and fall-out deposit, - UR2 as the product from the second activity of Urji. The Eruptive units UR1and UR2 could correspond to the " Older pumices" and the "Younger pumices" respectively of Rapprich et al. (2015) reconstruction. However, Rapprich et al. do not specify by which criteria they present this distinction and indeed they report that below the "Older pumice" there is a " freatomagmatic lapilli- tuff deposit of uncertain origin". They missed therefore that what they interpreted as two fall-out deposits, the "Older" and the "Younger" pumices, are from the same eruption and both of them correspond to the UR2 eruptive unit as interpreted here.

The recognition of the S2 unconformity clearly suggests that the deposits that in Rapprich et al. (2015) are defined " of uncertain origin" are from the eruption that characterized the first Urji activity and they are here interpreted as UR1 eruptive unit, so they are from Urji vent.

The UBSU methodology therefore ,along with the lithosome concept, allowed a clear distinction of the deposits from the different vents and most of all, allowed the reconstruction of the temporal sequence of the activity of each vent within the Corbetti caldera history. Indeed, the absence of any criteria in the previous works led to a misinterpretation of the deposits and consequently a misinterpretation of the reconstruction o the volcanic history.

Regarding the last activity within the post-caldera volcanism, there is a general agreement that it was represented by Chabbi volcano. However, there are also some important differences with the previous works concerning the interpretation of the deposits and the timing of the eruptions of Chabbi.

In Altaye's reconstruction the 'Volcanic rocks post-caldera' sequence ends with the Chabbi effusive activity that emplaced a generic 'recent obsidian lava flows' (Qr3-unit). In the Altaye reconstruction, therefore, there is not a distinction between the different lava flows emplaced from the seven different vents but they are interpret as emplaced from only one vent. On the contrary, from our fieldwork and morphological analyses of Chabbi deposits, carried out by the observation of the high resolution LIDAR imagery (2m pixel) , we identify, in agreement with Mohr (1966), seven eruptive centers that were active in different periods of time and that emplaced the products of the seven different lithosomes as recognized here.

The Qr3 unit of Altaye therefore includes obsidian flows from five different lithosomes (CH3bO, CH6b, CH4b, CH5b, CH7,) within the *Chabbi Composite Lithosome*.

Different eruptive centers, active in different time, are also identified in Rapprich et al. (2015). However, there are strong disagreements concerning the interpretation of the deposits and their position within the stratigraphic reconstruction as proposed in this work.

Rapprich et al. (2015) describe Chabbi deposits as " accumulation of obsidian lavas" and they define Chabbi volcano as an example of " obsidian shield volcano". On the contrary from the fieldwork along with morphological analyses of LIDAR imagery and ortho-photos , in agreement with Mohr (1966), I found that *Chabbi Composite Lithosome* consists of several PDCs associated with obsidian lava flows.

In Raprich et al. (2015) they identify two obsidian lava flows , COX and CO2 corresponding to the CH2 and CH3a lithosomes of this work as the products of the early Chabbi activity. Although I agree that these deposits were emplaced from the early Chabbi activity, however from the observation of the high resolution LIDAR imagery along with the orthophotos, I found that these deposits are pyroclastics, in agreement with what was already described in Mohr (1966). Another deposit identified in Rapprich et al. (2105) as the obsidian lava flow CO1, corresponds to the deposit of the CH5a lithosome of this work , interpreted as a PDC deposit on the basis of our fieldwork and sampling.

In terms of understanding a volcano behaviour , it is important to understand, from the interpretation of the deposits, the type of activity that characterized the eruptions.

There is instead agreement regarding the identification of the obsidian lava flow CO3 of Rapprich et al. (2015), that corresponds to the obsidian lava flow CH3bO of this work. However, there is disagreement concerning the position of the deposit in the stratigraphic reconstruction. Indeed in Rapprich et al.(2015) they interpret this deposit as one of the recent Chabbi products, whereas from the high resolution of LIDAR imagery and ortho-photos, I interpreted this deposit , in agreement with Mohr (1966), as one of the oldest of Chabbi activity.

Rapprich et al. (2015) also used radiocarbon dating for the eruption that emplaced the "Wendo Koshe Younger pumices" ,corresponding to the UR2 eruptive unit of this work, and they found an age of 398±38 B.C. They dated a paleosoil identified between this pumices and underlying a yellowish tuff supposed to be emplaced by the Fike volcano located to the north of Shalla lake. They sampled the paleosoil in two sites far about 14 km from Wendo-Koshe/Urji vent within Corbetti caldera.

However, the lack of any stratigraphic correlations of this paleosoil, using an recognizable unconformity surface on the basis of the UBSU methodology, which assures that the deposit identified in the sampling sites 14 km far from Corebtti (WKSC14 A, WKSC14b Rapprich et al.2015) is the same deposit identified as " younger pumice " close to the vent (HSRVRO69,C,D – Rapprich et al. (2105)) within Corbetti, makes uncertain the date of Rapprich et al.(2015). A careful stratigraphic correlation indeed is required especially in volcanic terrain that are still scarcely studied as the case of the volcanic deposits in the central-southern sector of the Main Ethiopian Rift.

In this regard the UBSU methodology and the application of the recognition of unconformity surfaces, is a very suitable method for investigations in such volcanic areas. In addition to this, on the basis of Rapprich et al. (2015) reconstruction, the "Wendo- Koshe younger pumices" would have been covered by the Chabbi obsidian lava flow CO4 corresponding to the CH5b obsidian lava flow of this work.

Rapprich et al. (2015), however, missed that the obsidian lava flow has been dated by Woldegabriel et al. 1991 with K/Ar method and resulted to be 0.02± 0.01 m.y.B.P.

Furthermore the $^{40}Ar/^{39}Ar$ dating analyses carried out on the PCD deposit of Chabbi1 lithosome and resulted to be 18.4±4.3 ka, agree with the Woldegabriel et al.1991 dating.

On the basis of the stratigraphic reconstruction proposed here I hypothesize that the Urji's activity was contemporary or just a bit earlier than the first Chabbi eruptions. Therefore the " Wendo Koshe younger pumices" of Rapprich et al. (2105), that correspond to the UR2 eruptive unit of this work, would be much older than 396±39 years B.C.

The stratigraphic reconstruction, and the volcanic evolution as proposed in this work on the basis of the USBU methodology along with morphological analyse of LIDAR imagery, and the lithosome concept, offer in comparison with the previous works, an improved knowledge and understanding of the Corbetti caldera volcanic history, highlighting the temporal sequence of the main volcanic events and the relationship between the different deposits and the deposits and the different vents that emplaced them. (Fig. 2.22,2.23) . This new scenario also has important implications in regard to the assessment of the volcanic hazard of the area. In the following section the main outcomes are summarized.

<table>
<tr><th>Lithosome/Composite Lithosome</th><th>Description</th><th>Eruptive Unit</th><th>Age</th><th colspan="4">Supposed contemporaneity of activity</th></tr>
<tr><td>Chabbi composite lithosome - Lithosomes CH 4, CH5, CH6, CH7</td><td>Succession of four different lithosomes (CH4, CH5, CH6, CH7) characterised by alternation of pyroclastics deposits with obsidian lava flows</td><td></td><td></td><td colspan="4"></td></tr>
<tr><td rowspan="2">Urji Lithosome</td><td rowspan="2"></td><td>UR2 - This unit is constituted by massive well sorted grain supported deposits in the lower part and by banded -aphyric obsidian lava flow in the lower part
S2 second order unconformity surface</td><td>CH1 lithosome
18.4 ± 4.3ka</td><td>Lithosome/Composite Lithosome</td><td>Description</td><td colspan="2">Post- caldera deposits</td></tr>
<tr><td>UR1 - This unit is constituted by massive poorly sorted grain-supported deposit of pumice and lithics in the lower part and by laminated bedding fine ash interbedded with massive poorly sorted layers of pumice and lithics in the upper part.</td><td></td><td>Chabbi Composite Lithosome - Lithosomes CH 1, CH2, CH3</td><td>Succession of three different lithosomes characterised by alternation of pyroclastics deposits with obsidian lava flows</td><td>PSC
pyroclastics deposits (tuff-ring)</td><td>BA
basaltic lava deposit</td></tr>
<tr><td>Danshe Lithosome
S1 first order unconformity surface</td><td>Danshe lithosome is constituted by massive poorly sorted grain supported deposits of pumices and lithics in the lower part and by succession of massive well sorted grain supported deposits with fine ash deposits in the upper part.</td><td></td><td></td><td colspan="4"></td></tr>
<tr><td rowspan="2">Corbetti composite lithosome</td><td rowspan="2"></td><td>COR2 - This unit is constituted by red massive matrix supported, welded deposit with fiamme in the lower part. In the middle part is constitued by massive poorly sorted deposit of pumices and lithics. In the upper part this unit is constituted by poorly sorted grain supported deposit ofpumices and lithics. The deposit is interbedded with layers of spatter bombs.
S2 second order unconformity surface</td><td>176.68± 4.1ka</td><td colspan="4" rowspan="2"></td></tr>
<tr><td>COR1 - This unit is constituted by massive lava deposit showing columnar jointing. Pre-caldera deposit</td><td></td></tr>
</table>

Fig. 2.22 Recapitulatory scheme of the Corbetti caldera stratigraphy of this work based on the Unconformity Bounded Stratigraphic Units (UBSU) methodology, lithosoma concept and $^{40}Ar/^{39}Ar$ dating analyses

Mohr (1966)		Di Paola (1971)			Altaye (1984)			Rapprich et al. (2015)		
volcano	deposits	volcano	activity	deposits	volcano	activity	deposits	volcano	activity	deposits
Chabbi : 7 vents (Main Vent, East Vent, North East Vent I, North East Vent II) Hot Cone, West Vent,	pyroclasctic deposits followed by lava flows	1) Chabbi- 2)Urji	last activity of Corbetti caldera	1)-pyroclastics and massive lava flows 2) - pyroclastics	Danshe- Urji-Chabbi	Volcanic rock - post caldera activity	Qr3-recent obsidian lava Qb- basaltic lava flow Qlib- hyaloclastites Qcp- recent pumices fall and flows Qr2- obsidian lava covered by pumices	Chabbi	effusive activity post-caldera	COX, CO2, CO3, CO6 lava flows
								Wendo Konshe (Urji)	one explosive eruption from post-caldera activity	Wendo Konshe younger pumices deposit (398±38 B.C - C^{14}dating) paleosoil Wendo Konshe older pumices deposit
		caldera vents	ancient activity of Corbetti caldetra	several pumice flows and air-fall deposits associated unwelded ignimbrite deposit covered by a typical ignimbrite formation	caldera vents	caldera and pre - caldera activity	Qqwp- layered pumice pyroclastics Qp1-pumiceous ignimbrite Qr1-peralkaline rhyolite lava dome Qwb- basaltic deposit Qawi-ignimbrite deposit	(uncertain origin)	phreatomagmatic activity	bedded to laminated phreatomagmatic lapilli-tuff

Fig. 2.23 Recapitulatory scheme of the Corbetti caldera stratigraphy from the previous works

2.5 Concluding Remarks

Corbetti volcano is a Quaternary caldera (long axis 18 Km, short axis 11Km) lying in the southern sector of Main Ethiopian rift between the Shalla lake in the north and Awaasa lake in the south. As other Quaternary calderas along the rift, Corbetti volcanism is associated with the development of Wonji Fault Belt along the Main Ethiopian Rift. However if the volcanism of other calderas (Fantale, Kone, Boseti, Gedemsa) along the main axis of the rift is well studied (Gibson et al.(1970), Cioni et al.(2001), Ayalew et al.(2003), Williams et al.(2004), Orsi et al.(2007), Rampey et al.(2010)), the volcanic history of Corbetti caldera is still poorly constrained and there is only limited published work on this complex (Mohr (1966), Di Paola (1971), McDonald 1969, Wodelgabriel et al.1991, Rapprich et al.2015).

The application of UBSU methodology based on the recognition of unconformities along with the use of lithsosome concept revealed a complex volcanic activity that characterized the eruptive history of Corbetti volcano. The UBSU method also allowed a better constraints on the temporal sequence of the main eruptions that characterized Corbetti eruptive history.

The main results can be summarized as follow:

- using the UBSU architecture, two hierarchical–order unconformities were recognized. The S1-first order unconformity identifies 2 eruptive epochs, the S2-second order unconformity identifies 4 eruptive units;
- the concept of lithosome (Girordano et al., 2006; Fusillo et al., 2015) applied to Corbetti deposits allowed the identification of four lithosomes (*Corbetti Composite Lithosome*, Urji, Danshe and *Chabbi Composite Lithosome*) and a clear relationship between the deposits and the eruptive centres that emplaced them;
- the first order unconformity (S1) divides deposits of pre- and syn-caldera activity from the post- caldera activity;
- the *Corbetti Composite Lithosome* includes the deposits of the pre-caldera activity,the syn-caldera activity and the basaltic deposit COR3 from the post- caldera activity;
- the pre-caldera activity is characterized by effusive eruption and 1 eruptive unit (COR1 EU) deposit, likely emplaced by fissure eruption;
- The syn-caldera activity is characterized by explosive eruption and 1 eruptive unit (COR2 EU). The absence of a proximal breccia suggests that the syn-caldera activity was

characterized by an eruption that triggered a symmetric collapse (piston/plate Lipmann 2000b) of the eruptive centre with consequent development of caldera structure;

- the post-caldera activity was characterized by the deposits of three different lithosomes (Urji, Danshe, Chabbi);
- the post-caldera activity was characterized by a decrease of the explosivity in the eruptions;
- the post-caldera volcanism resumed with Danshe and Urji volcanoes activity and continued subsequently with the activity of Chabbi volcano. A second order unconformity (S2, here characterized by a paleosoil of 2 m thickness) separates the first Urji activity characterized by the UR1 eruptive unit, from the second Urji activity characterized by the UR2 eruptive unit;
- Danshe volcano activity was characterized by only explosive eruptions that emplaced the products of Danshe lithosome;
- the *Chabbi Composite Lithosome* comprises the deposits of seven different eruptive centeres that emplaced the products of seven different lithosomes.
- the analysis of LIDAR imagery allowed the identification of the geometric organization of Chabbi products and to hypothesize the temporal sequence of Chabbi lithosomes from the oldest to the newest as follows: CH1, CH2, CH3, CH4, CH5, CH6 CH7;
- Most of the lithosomes consist of pyroclastics deposit overlaid by obsidian flow deposits with the exception of CH2, CH6 and CH7. The CH 2 lithosome is characterized by only pyroclastics deposits whereas CH 7 and CH6 lithosomes are characterized mostly by obsidian flow deposits;
- the analysis of LIDAR imagery also allowed the interpretation that Chabbi volcano activity started in the northern sector and ended in the southern sector of *Chabbi Composite Lithosome*;
- the location of the deposits of the Danshe lithosome and *Chabbi Composite lithosome*, in the eastern caldera rim, suggests that part of the post- caldera activity may have been fed by a magma rising along a NNW-SSE sinistral strike -slip faults ;
- the Corbetti caldera volcanic history was characterized mostly by monogenetic eruptive centres with the exception of the vent that emplaced the COR1 and COR2 eruptive units within the *CCL* lithosome and the Urji volcano, that emplaced the UR1 and UR2 eruptive units.
- Corbetti Caldera volcano is currently at quiescent stage and fumarolic activity

References-

Acocella, V., Korme, T., Salvini, F., Funicello, R., 2002. Elliptical Calderas in the Ethiopian Rift: control of pre-existing structures. Journal of Volcanology and Geothermal Research 119, 189–203.

Agostini A., Marco B., Giacomo C., Federico S., Piero M., 2011. Distribution of Quaternary deformation in the central Main Ethiopian Rift, East Africa. Tectonics, v. 30 p.

Altaye, E., 1984. Geology and Surface Alteration of the Corbetti Caldera Area, Ethioia. Geothermal Institute, University of Auckland. (Project for Diploma in Energy Technology).

Ayalew, D., Di Vito, M.A., Isaia, R., Orsi, G., Yirgu, G., 2003. The Gedemsa caldera (Main Ethiopian Roft): an example of interplay among regional tectonism, volcanism and volcano-tectonics. E.G.S.–A.G.U.–E.U.G. Joint Assembly, Nice, France, April 6–11 2003, Geophysical Research Abstracts 5

Barberio, M.R., Donati, C., Donato, P., Yirgu, G., Peccerillo, A., Wu, T.W., 1999. Petrology and geochemistry of Quaternary magmatism in the northern sector of the Ethiopian Rift between Debre Zeit and Awash Park. Acta Volcanologica 11 (1), 69–81.

Bastow, I. D., S. Pilidou, J.-M. Kendall, and G. W. Stuart (2010), Melt- induced seismic anisotropy and magma assisted rifting in Ethiopia: Evi- dence from surface waves, Geochem. Geophys. Geosyst., 11, Q0AB05, doi:10.1029/2010GC003036.

Biggs, J., Bastow, ID., Keir, D. and Lewi, E., 2011. Pulses of deformation reveal frequently recurring shallow magmatic activity beneath the Main Ethiopian Rift. Geochemistry Geophysics Geosystems 12, ISSN: 1525--2027

Bompressi, E., 2001. Trachyte-pantellerite syn-eruptive magma mixing evidence from the caldera-forming ignimbrites at Gademsa (Main Ethiopia Rift). GEOITALIA 2001, 3rd Forum Italiano di Scienze della Terra, Chieti, Italy, Federazione Italiana Scienze della Terra, Abstract Volume, pp. 711–712.

Calanchi, N., Tranne, C. A., Lucchi, F., RossiI, P. L. and Villa, I. M. (1999) Explanatory notes to the geological map of Panarea and Basiluzzo islands (Aeolian arc, Italy), Acta Vulcanologica, 11, 223–243.

Calvari , S., Groppelli, G. and Pasquare, G. (1995) Preliminary geological data on the sou- thernwestern walls of the Valle del Bove, Mt Etna (Sicily), Acta Vulcanologica, 5, 15–30

Carey, R.J., Houghton, B.F., Thordarson, T., 2008. Contrasting styles of welding observed in the proximal Askja 1875 eruption deposits I: regional welding. Journal of Volcanology and Geothermal Research 171, 1-19.

Carey, R.J., Houghton, B.F., Thordarson, T., 2008. Contrasting styles of welding observed in the proximal Askja 1875 eruption deposits II: regional welding. Journal of Volcanology and Geothermal Research 171,20-44.

Chang, K. H. (1975) Unconformity bounded stratigraphic units, Geological Society of America Bulle- tin, 86, 1544–1552, doi:10.1130/0016-7606(1975)86⟨1544:USU⟩2.0.CO;2.

Chernet, T., Hart, W.K., 1999. Petrology and geochemistry of volcanism in the northern Main Ethiopian Rift-southern Afar transition region. Acta Vulcanol. 11, 21-42.

Cimarelli, C., Di Traglia, F., De Rita, D., Gimeno Torrente D., Fernandez Turiel J-. L. 2013. Space–time evolution of monogenetic volcanism in the mafic Garrotxa Volcanic Field (NE Iberian Peninsula). Bulletin of Volcanology 75 :758

Cioni, R., Cristiani, C., De Rosa, R., Marianelli, P., Mazzuoli, R., Ayalew, D., Yirgu, G., Bompressi, E., 2001. Trachyte-pantellerite syn-eruptive magma mixing evidence from the caldera-forming ignimbrites at Gademsa (Main Ethiopia Rift). GEOITALIA 2001, 3rd Forum Italiano di Scienze della Terra, Chieti, Italy, Federazione Italiana Scienze della Terra, Abstract Volume, pp. 711–712.

Cole J.W. , Milner D.M., Spinks K.D. 2005. Calderas and caldera structures: a review. Earth-Science Reviews 69 ,1–26

Coltelli, M., Garduno, V. H., Neri, M., Pasquare` , G. and Pompilio, M. (1994) Geology of the northern wall of Valle del Bove, Mt Etna (Sicily), Acta Vulcanologica, 5, 55–68.

Corti, G. (2008), Control of rift obliquity on the evolution and segmenta- tion of the main Ethiopian rift, Nat. Geosci., 1, 258–262.

Dalrymple, G.B., 1989, The GLM continuous laser system for $^{40}Ar/^{39}Ar$ dating; description and performance characteristics, in Shanks, W.C., III, and Criss, R.E., eds., New frontiers in stable isotopic research; laser probes, ion probes, and small-sample analysis: U.S. Geological Survey Bulletin 1890, p. 89-96.

Dalrymple, G.B. and Duffield, W.A., 1988, High precision 40Ar/39Ar dating of Oligocene rhyolites from the Mogollon-Datil volcanic field using a continuous laser system, Geophy. Res. Lett., v. 15, 463-366.

Dalrymple, G.B., Alexander E.C., Jr., Lanphere, M.A., and Kraker, G.P., 1981, Irradiation of samples for 40Ar/39Ar dating using the Geological Survey TRIGA reactor. US Geol. Surv. Prof. Paper 1176.

David J. Ferguson , Andrew T. Calvert , David M. Pyle, Jon D. Blundy , Gezahegn Yirgu & Tim J. Wright , 2013. Constraining timescales of focused magmatic accretion and extension in the Afar crust using lava geochronology. Nature Communications, DOI: 10.1038/ncomms2410.

Deino, A. and Potts, R., 1992, Age-probability spectra for examination of single-crystal $^{40}Ar/^{39}Ar$ dating results: Examples from Olorgesaille, southern Kenya Rift, Quaternary International, v. 13-14, p. 47-53.

De Astis, G., Dellino, P., L a Volpe, L., Lucchi, F. and Tranne, C. A. (2006) Geological map of the Island of Vulcano (Aeolian Islands), L.A.C. Firenze.

De Rita, D., Giordano, G., and Milli, S., 1998, Forestepping - backstepping stacking patterns of volcaniclastic successions: Roccamonfina volcano, Italy: Journal of Volcanology and Geothermal Research, v. 80, p. 155–178.

Di Paola, G. M. 1970. Geoloogy of the Corbetti Caldera Area (Main Ethiopian Rift Valley). Bulletin of Volcanology 35, 497---506.

Di Traglia, F., Pistolesi, M., Rosi, M., Bonadonna, C., Fusillo, R., Roverato M. , 2013. Growth and erosion: The volcanic geology and morphological evolution of La Fossa (Island of Vulcano, Southern Italy) in the last 1000 years. Geomorphology 194, 94-107

Fisher, R.V., 1979. Models for pyroclastic surges and pyroclastic flows . Journal of Volcanology and Geothermal Research 6, 305---318.

Fisher, R.V. and Schmincke, H.---U., 1984. Pyroclastic rocks. Springer---Verlag Berlin. Heidelberg, 472pp.

Fusillo, R., Di Traglia, F., Gioncada, A., Pistolesi, M., Wallace, P.J., Rosi, M., 2015. Deciphering post-caldera volcanism: insight into the Vulcanello (Island of Vulcano, Southern Italy) eruptive activity based on geological and petrological constraints. Bulletin of Volcanology 77:76 DOI 10.1007/s00445-015-0963-6

Gibson, I.L., 1970. A pantelleritic welded ash-flow tuff from the Ethiopian Rift valley. Contributions to Mineralogy and Petrology 28, 89–111.

Giordano, G., De Benedetti, A.A., Diana, A., Diano, G., Gaudioso, F., Marasco, F., Miceli, M., Mollo, S., Cas, R.A.F., Funiciello, R., 2006. The Colli Albani mafic caldera (Roma, Italy): stratigraphy, structure and petrology. Journal of Volcanology and Geothermal Research, 155, 49–80

Hutchison W., Fusillo, R., Pyle, D.M., Mather, T.A.,Blundy, J., Biggs, J., Yirgu, G., Cohen, B.E., Brooker, R., Barfod, D.N., and Calvert A.T. A pulse of mid- Pleistocene rift volcanism in Ethiopia at the dawn of modern humans. Nature Communications, DOI: 10.1038/ncomms13192

Kendall, J. M., G. W. Stuart, C. J. Ebinger, I. D. Bastow, and D. Keir (2005), Magma assisted rifting in Ethiopia, Nature, 433, 146–148, doi:10.1038/nature03161.

Lipman, P.W., 2000b. Calderas. In: Sigurdsson, H. (Ed.),Encyclopedia of Volcanoes. Academic Press, San Francisco,pp. 643–662.

Lucchi, F., Tranne, C. A., Calanchi, N., Keller, J. and RossiI, P. L. (2003) Geological map of Panarea and minor islets (Aeolian Islands), L.A.C. Firenze.

Macdonald, R., Gibson, I. L., 1969. Pantelleritic Obsidians from the volcano Chabbi (Ethiopia). Contributions to Mineralogy and Petrology 24, 239--244.

Maneti, P., Pasquare, G. and Tsegaye, A. (1995) A new geovolcanological map of Filicudi Island (Aeolian Arc, Italy), Acta Vulcanologica, 7, 1–5.

Manville, V., Németh, K., Kano, K., 2009a. Source to sink: A review of three decades of progress in the understanding of volcaniclastic processes, deposits, and hazards. Sedimentary Geology, 220, 136-161, doi: 10.1016/j.sedgeo.2009.04.022

Mazzarini, F., Keir, D., Isola, I. , 2013. Spatial relationship between earthquakes and volcanic vents in the central-northern Main Ethiopian Rift. Journal of Volcanology and Geothermal Research, 262, 123-133.

Mohr , P.A. 1966. Chabbi Volcano (Ethiopia). Bulletin of Vulcanology 29, 797--815

Mohr, P.A., Mitchell, J.G., Raynolds, R.G.H., 1980. Quaternary volcanism and faulting at O'A caldera, central Ethio-pian Rift. Bulletin of Volcanology 43, 173^189.

Orsi, G., Ayalew, D., Dell'Erba, F., Di Vito, M.A., Yirgu, G., 2007. Can the Fantale area in Ethiopia, be counted among the cities on volcanoes? I.U.G.G. XXIV 2007, Perugia, Italy, July 2–13 2007, Abstract volume V, p. 6873 (ISBN 978-88-95852-24-6).

Rampey M. L., Oppenheimer C., Pyle D. M. Gezahegn Y. 2010. Caldera-forming eruptions of the Quaternary Kone Volcanic Complex, Ethiopia. Journal of African Earth Sciences 58 ,51–66

Rapprich, V., ÊáÊek,V. Verner, K., Erban V., T. Goslar, Y.Bekele , Legesa F., Hroch T., Hejtmánková P. 2015. Wendo Koshe Pumice: The latest Holocene silicic explosive eruption product of the Corbetti Volcanic System (Southern Ethiopia). Journal of Volcanology and Geothermal Research 310 (2016) 159–171.

Rossi, P. L., Tranne, C. A., Calanchi, N. and Lanti, E. (1996) Geology, stratigraphy and volcanological evolution of the island of Linosa (Sicilian Channel), Acta Vulcanologica, 8, 73–90.

Salvador, A., 1987. Unconformity bounded stratigraphic units. Geol. Soc. Amer. Bull. 98, 232–237.

Salvador, A., 1994. A guide to Stratigraphic Classification, Terminology and Procedure. In: IUGS-GSA (Ed.), International Stratigraphic Guide. 214 pp.

Simkin, T., Siebert, L., Mcclelland, L., Bridge, D., Newhall, C., and Latter, J.H., 1981. Volcanoes of the World. In: , Smithson. Inst., Hutchinson Ross, Stroudsburg, pp. 1–232.

Soriano, C., Zafrilla, S., Marti; J., Bryan, S., Cas, R., Ablay, G., 2105. Welding and rheomorphism of phonolitic fallout deposits from the Las Can˜adas caldera, Tenerife, Canary Islands. Geological Society of America Bulletin*;* July 2002; v. 114; no. 7; p. 883–895;

Sparks, R.S.J., Walker, G.P.L. 1973. The ground surge deposit: a third type of pyroclastic flow. Nature, 241, 62-64.

Sparks, R.S.J., 1976. Grain size variation in ignimbrites and implications for the transport of pyroclastic flow. Sedimentology 23, 147-1488.

Tranne, C. A., Lucchi, F., Calanchi, N., Lanzafame, G. and Rossi, P. L. (2002a) Geological map of the Island of Lipari (Aeolian Islands), L.A.C. Firenze.

Tranne, C. A., Lucchi, F., Calanchi, N., Rossi, P. L., Campanella, T. and Sardella, A. (2002b) Geological map of the Island of Filicudi (Aeolian Islands), L.A.C. Firenze

Trua, T., Deniel, C., Mazzuoli, R., 1999. Crustal control in the genesis of Plio-Quaternary bimodal magmatism of the Main Ethiopian Rift (MER): geochemical and isotopic (Sr, Nd, Pb) evidence. Chem. Geol. 155, 201^231.

Valentine, G.A., Fisher, R.V., 1986. Origin of layer 1deposits in ignimbrites. Geology vol 1, 146-148

Walker ,G.P.L. 1973. Explosive volcanic eruptions, a new classification scheme. Geol.Rund 62,431-446.

Walker, G.P.L. 1983. Ignimbrite types and ignimbrite problems. Journal of Volcanology and Geothermal Research 17, 65-88.

Williams, F.M., Williams, M.A.J., Aumento, F., 2004. Tensional fissures and crustal extension rates in the northern part of the Main Ethiopian Rift. Journal of African Earth Sciences 38, 183–197.

Woldegabriel, G., Aronson, J., L., Walter, C., R. 1990. Geology, geochronology, and rift basin development in the central sector of the Main Ethiopia Rift. Geological Society of American Bulletin 102, 4, 439---458

3 The geochemical characterization of Corbetti caldera products (Main Ethiopian Rift)

3.1 Introduction

The Corbetti caldera volcanic history, although have been characterized by a complex activity, as the stratigraphic reconstruction has revealed, shows a geochemistry with a compositional gap, typical of bimodal magmatism as found elsewhere in the Ethiopian Rift (Alutu, Gedemsa, Boseti, Fantale). However, while the other volcanic centres erupted intermediate products, Corbetti caldera only produced the most evolved products with the exception of a single basalt deposit.

Whole rocks' major and trace element analyses from deposits of both pre-syn caldera and post- caldera eruptive epochs, show a composition of a large range of silica content (SiO_2 46.21 - 75.40 wt%), if the rare basalt (COR3) is included. The rhyolitic products can be further classified as peralkaline on the basis of the value of the agpaitic index ($[NaO]+[K_2O]/Al_2O_3$), AI= 1.5,and as pantellerite on the basis of Al_2O_3 and FeO^T wt% content (MacDonald 1974). The Corbetti rhyolites belong to a high-K calc-alkaline series, whereas the basalt sample falls in a medium-K calc-alkaline series.

Trace elements concentrations (LILE vs HFSE and HFSE vs HFSE) confirm the stratigraphic reconstruction (chapter 2), showing two distinct groups with an enrichment in incompatible elements from the pre- and syn-caldera deposits to those from the post-caldera epoch. When comparing the Corbetti trace element trends with data from Alutu, Gedemsa, Boseti and Fantale calderas (Peccerillo et al. 2003, Giordano 2006, Ronga et al. 2010 , Giordano et al. 2013, Hutchison 2015), there is close agreement and a similar petrogenesis could be hypothesized (fractional crystallization plus crustal contamination) for all five systems. However, the lack of intermediate deposits in Corbetti stratigraphy, the value of ratio of incompatible elements such as Rb/Nb, the very low Sr concentration (~8ppm) and the geochemical features of the basalt COR3 (similar to Gedemsa basalts interpreted from a deep ,~60km, peridotite mantle source), may also suggests a different magma source for the petrogenesis of the post caldera basalt COR3.

In this chapter the geochemistry of the products from all the eruptions from Corbetti caldera eruptive history is presented, along with the basalt deposit.

The Corbetti geochemistry is then compared with the geochemistry of the other Quaternary calderas along the rift (Alutu, Gedemsa, Boseti, Fantale), and trace elements modelling is tested for a better understanding of the magmatic evolution and the petrogenesis of the rhyolites.
A mineralogical characterization of Corbetti products is also presented.

3.2 Analytical methods

Major element concentration have been investigated by Inductively Coupled Plasma Optical Emission Spectroscopy analyses (ICP-OES) and the trace element content by Inductively Coupled Plasma Mass Spectroscopy analyses (ICP-MS). The analyses and the second stage of the sample preparation were carried out at the School of Earth and Ocean Sciences of University of Cardiff (UK). Standards (SY-3, BR, RGM-1, JB1a) were run alongside the samples to check the accuracy, and a couple of samples were run as blind duplicates, to check the precision of the analysis. All the major elements analyses were normalized to sum to 100% on an anhydrous basis.

3.2. 1 Whole rock analyses

The first step of the sample preparation was carried out in the sample preparation laboratories at the School of Earth Science of University of Bristol. In order to get a rock powder of 1μm size using a Retsch Agate Planetary Ball Mill, the selected fresh samples were previously reduced to chips of 2-3mm size in a jaw crusher after being manually crushed on an acetone –cleaned steel plate.

The standard ICP analysis and the sample preparation procedures and instrument parameters used, are those from McDonald and Viljoen (2006). The main steps of the procedure are summarized as follows. We have analysed Si, Ti, Al, Fe, Mg, Mn, Ca, K, Na P Ni, Cu, Co, Cr, Ba, Sr, Zr, Y, Sc and V using a JY Horiba ULTIMA2 ICP- OES system.
From each sample we have heated approximately 2.0 g of the rock powder up in a muffle furnace to remove H_2O, CO_2 and other volatiles. The Corbetti samples needed to be heated firstly at 750 ^oC and successively at 900 ^oC in order to avoid total melting of the powder rock due to their peralkaline composition. The loss on ignition (LOI) has then been calculated. The residue powder was then mixed in amount of 0.100 g with 0.400 g of Li metaborate flux .

An amount of about 0.5ml of 25% lithium iodide solution was then added to the mixture and

this was fused. The melted mixture was then added to a solution of 50 ml of 4% HNO_3 contained in a 250 ml Teflon beaker. In order to have a rock solution with 2% HNO_3, a 1 ml of a 100 ppm Rh spike solution was put in as internal standard, along with 18.2 MΩ deionized water to make it up to 100ml.

The instrument parameters used for ICP-OES analyses (major elements) were as follows (McDonald and Viljoen 2006) :

- "plasma gas - Argon;
- Forward power = 1000W;
- Ar purge gas flow rate, 2 liters min^{-1};
- Auxiliary Ar gas flow rate, 12 liters min^{-1};
- Sheath gas flow rate (for K analysis), 8 liters min^{-1};
- Nebuliser – Meinhard;
- Amplifier gain setting, G1 (G3 for K analysis)".

In the same way the blanks were prepared without sample material.
For the calibration we used solutions of the standards (SY-3, BR, RGM-1) along with a reagent blank. The solutions of the standards was analysed every 6 unknowns.

For measuring the concentration of the REEs and Ti, V, Cr, Mn, Co, Ni, Cu, Zn, Ga, Rb, Sr, Y, Zr, Nb, Mo, Sn, Cs, Ba, Hf, Ta, Pb, Th ,U, we carried out ICP-MS analyses and we used the same solutions as for ICP-OES analyses.
However with respect to the ICP-OES analyses , the solution is made 10 times more watery with 2% HNO_3, and 5 ppb of In and Tl internal standards are added to set right the instrumental drift.
A Thermo Elemental X Series (X7) ICP-MS system machine, was used and the calibration and accuracy were checked by the same international certified reference materials (SY-3, BR, RGM-1) as for ICP-OES.
The instrument parameters used for ICP-MS analyses (trace elements) were as follows (McDonald and Viljoen 2006) :

- "plasma gas - Argon;
- Forward power = 1200W;
- Nebuliser – Meinhard with impact bead spray chamber;
- Pump speed = 15 rpm;
- Sample uptake ~ 0.5 ml min^{-1};

- Nebuliser gas flow rate = 0.95 l min^{-1};
- Auxiliary gas flow rate = 0.7 l min^{-1};
- Coolant gas flow rate = 13.0 l min^{-1};
- Cones – nickel. Lens parameters optimized to achieve >50,000 cps per ppb for ^{103} Rh and ^{115} In and to achieve <1% CeO/Ce. Analysis mode = peak jumping. Dwell times from 1ms (for Ti and Mn) to 20ms (for REE, Hf, Ta, Th and U)".

The standard JB1 was analysed as unknown for each sample batch and the standards BR basalt, RGM-1 rhyolite and SY-3 syenite, were also analysed (Table 1, 2, 3) in order to assess the accuracy and precision of the analyses .

3.2. 2 Mineralogical analyses

Major element compositions in phenocryst and matrix glass have been determined by electron microprobe analyses (EMPA) at the School of Earth Sciences of University of Bristol (UK), using a Cameca SX 100 equipped with five wavelength-dispersive detectors. Three different set-ups have been used :

1. Accelerating voltage of 20 kV, a probe current of 10 nA and a beam spot diameter of 5 μm, have been used for alkali feldspar to reduce Na loss;
2. Accelerating voltage of 20kV, a beam current of 10 nA and a beam spot diameter of 1 μm, have been used for olivine , clinopyroxenes, and Fe-Ti oxides;
3. Accelerating voltage of 20kV, 10nA and a beam spot diameter of 10 μm, have been used for matrix glass. A probe current of 4 nA and a beam spot diameter of 20 μm have been used for Cl and F;

The standards used were Amelia-albite for Na and Si, Eifel-sanidine for Al and K, wollastonite for Ca, ilmenite for Fe and Ti, St. Johns olivine for Mg, synthetic Cr_2O_3 for Cr, synthetic MnO $_{18}$ for Mn, synthetic MgF_2 for F, Durango apatite for P and synthetic $BaSO_4$ for Ba.

Trace-element contents in mineral phases and matrix glass were determined on 100 μm thick sections by Laser Ablation-Inductively Coupled Plasma-Mass Spectrometry (LA-ICP-MS).

The analyses were carried at the laboratories of the School of Earth and Ocean Sciences of Cardiff University. New Wave Research UP213 UV laser system coupled to a Thermo X Series 2 ICP-MS was used . The beam diameter was 100 μm, and the laser beam was at a frequency of 10 Hz and a power of ~ 6 J/cm-2. Helium (flow ~ 0.7 L min-1) was used as carrier gas and the resulting vapour was combined with Ar (flow rate 0.65-0.75 L min-1) .

Precision and accuracy were assessed by means of repeated analyses of NIST SRM 610, 614, and BIR1, BCR2, BHVO, BHVO-2, KE12 standards. The composition of the glass beneath the thin section was documented before the sample analysis to recognize the piercing of the rock and to eliminate any glass contribution. The gas background was measured for 60 s, whereas signals during ablation were acquired for approximately 20–50 s.

Si was used as internal standard. The following isotopes were measured : ^{29}Si, ^{44}Ca, ^{45}Sc, ^{47}Ti, ^{51}V, ^{60}Ni, ^{65}Cu, ^{66}Zn, ^{71}Ga, ^{75}As, ^{85}Rb, ^{88}Sr, ^{89}Y, ^{90}Zr, ^{93}Nb, ^{95}Mo, ^{121}Sb, ^{133}Cs, ^{137}Ba, ^{139}La, ^{140}Ce, ^{141}Pr, ^{146}Nd, ^{147}Sm, ^{153}Eu, ^{157}Gd, ^{159}Tb, ^{163}Dy, ^{165}Ho, ^{166}Er, ^{169}Tm, ^{172}Yb, ^{175}Lu, ^{178}Hf, ^{181}Ta, ^{208}Pb, ^{232}Th, ^{238}U.

A quantitative point counting has been carried out on the analyzed samples to determine the percentage of the phenocrysts in the rock samples. An average of about 1000 points were counted on the thin sections for each sample.

3.3 Data

3.3.1 Corbetti caldera samples

Whole rocks' major and trace element analyses were carried out on deposits of the COR1 eruptive unit (lava deposit) for the pre- caldera eruptive epoch.

From the syn-caldera activity the products of the COR2 eruptive unit (pyroclastic density current deposit) unit were analysed , whereas the products of the three lithosomes Danshe, Urji and Chabbi were analysed for the post-caldera activity.

The Danshe samples include the pyroclastic density current (PDC) deposits DA, whereas from Urji's activity, the products of both the eruptive units of UR1 (PDCs) and the mixed explosive and effusive rocks of UR2 (UR2P-PDCs, UR2O-obsidian lava flow) were analysed.

From the *Chabbi Composite Lithosome*, the products of the Chabbi 1(CH1-PDCs) , Chabbi 5 (CH5a-PDCs, CH5b- obsidian lava flow,) Chabbi 6 (CH6a- PDCs, CH6b-obsidian lava flow) and Chabbi7 (obsidian lava flow) lithosomes were analysed.

3.3.1.2 Corbetti mineralogy

All the rhyolitic products show a low phenocryst content (5-10 vol%) with a mineral paragenesis, in order of abundance of sanidine, augite, aengimatite, fayalite and Fe-Ti oxides. The dominant mineral phase is the alkali- feldspar that occurs as homogeneous tabular phenocrysts, 1-2 mm long (Fig.3.1-3.2). They show a similar composition amongst the deposits of all of four lithosomes, Corbetti, Danshe, Urji and Chabbi, and all can be classified as sanidine ($An_{0-0.2}Ab_{52.1-60.7}Or_{39.2-47.9}$, Fig. 3.3 a). They also show a very low concentration range of Sr (1.4- 3.7ppm).

The second most abundant phase is clinopyroxene, that also occurs as homogeneous well-formed phenocrysts 100-200um long. They show a narrow compositional range ($Ca_{36.3-38.9}$ $Mg_{0.5-4.2}$ $Fe_{57.1-63.2}$) amongst the products of the four lithosomes and can be classified as augite (Fig.3.3 b). The rest of the mineral phases are: fayalite, aenigmatite, quartz and Fe-Ti oxides.

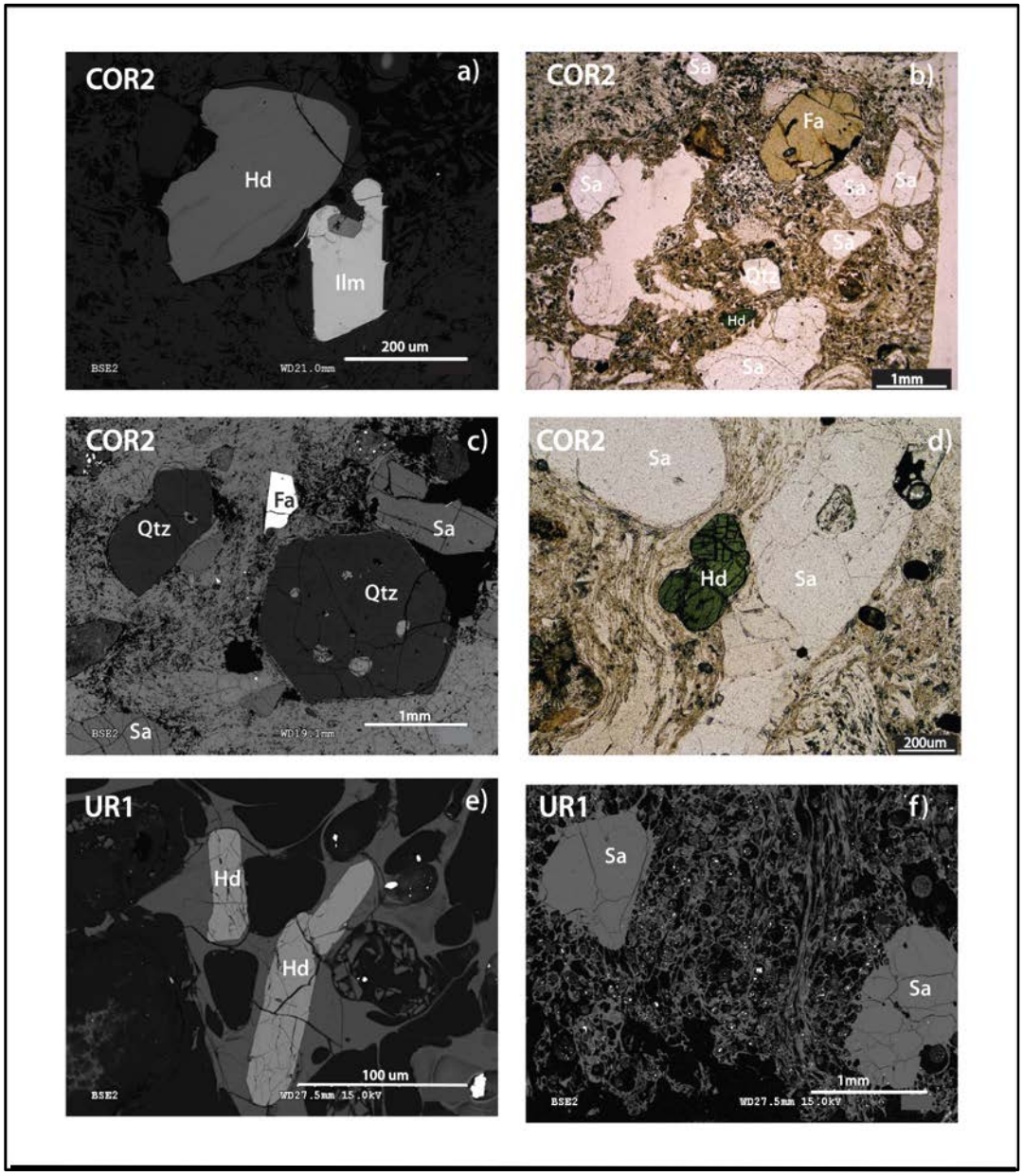

Fig. 3.1 Thin section microphotographs (b, d, plane-polarized light) and backscattered electron images (a, c, e, f) showing the mineral phases of COR2 EU (Corbetti Composite Lithosome, syn-caldera activity) and UR1 EU (Urji Lithosome, early post-caldera ctivity). **(a)** Phenocrysts of clinopyroxene (augite) and ilmenite. **(b)- (c)- (d)** Assemblage of phenocrysts of alkali feldspar (sanidine) , fayalite, clinopyroxene (augite) and Quartz in the welded facies with the typical fiamme of COR2 eruptive unit. **(e) - (f)** Phenocrysts of alkali feldspar (sanidine) and clinopyroxene (augite) in pumices of UR1 PDC deposit.

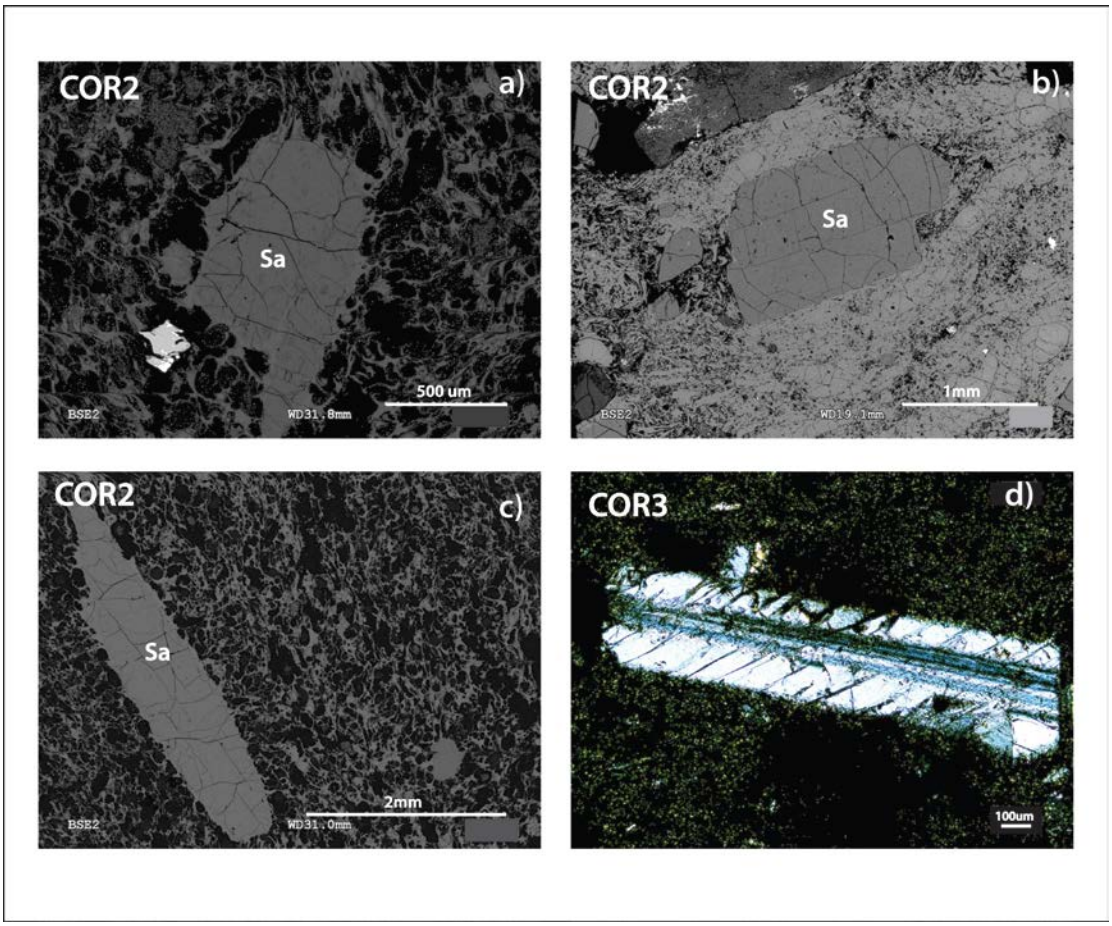

Fig.3.2 **(a)- (b)- (c)** Backscattered electron images showing phenocryst of alkali-feldspar (sanidine) in both facies (welded with fiamme and pumiceous) of COR2 eruptive unit (Corbetti Composite Lithosome, syn-caldera activity) **(d)** Thin section microphotograph (plane-polarized light) showing plagioclase phenocryst (labradorite) in COR3 basalt sample (Corbetti Composite Lithosome, post-caldera activity).

Fayalites occur as rare, well-developed phenocrysts ($Fo_{2.1}$) (Fig. 3.1 b) only in the PDC deposit COR2 from the caldera forming eruption. Phenocrysts of aenigmatite 1 mm long occur in all of the products of Corbetti, and show a well formed lamellar habit . Quartz is also present as euhedral penocrysts of 1mm size in all deposits, although is mainly present in the syn-caldera products (Fig.3.1c). Fe-Ti oxides occur mainly in the syn-caldera deposits as accessory small phenocrysts, and they can be classified as ilmenite and Ti-magnetite.

The basaltic lava deposit COR3 shows a porphyritic texture in vitrophyric groundmass of microphenocrysts and glass. The phenocryst assemblage is dominated by plagioclase, which occurs with a subhedral tabular habit (Fig.3.2 d), and with subordinate clinopyroxene and Fe-Ti oxides .The microphenocrysts found in the matrix, are plagioclase and rare opaque oxides. The plagioclase feldspars show a labradorite composition ($An_{66.3}Ab_{32.8}Or_1$), whereas the clinopyroxenes have a diopside composition ($Ca_{64.3}Mg_{25}Fe_{9.9}$) (Fig.3.3). The opaque oxides occur as ilmenite and ulvospinel.

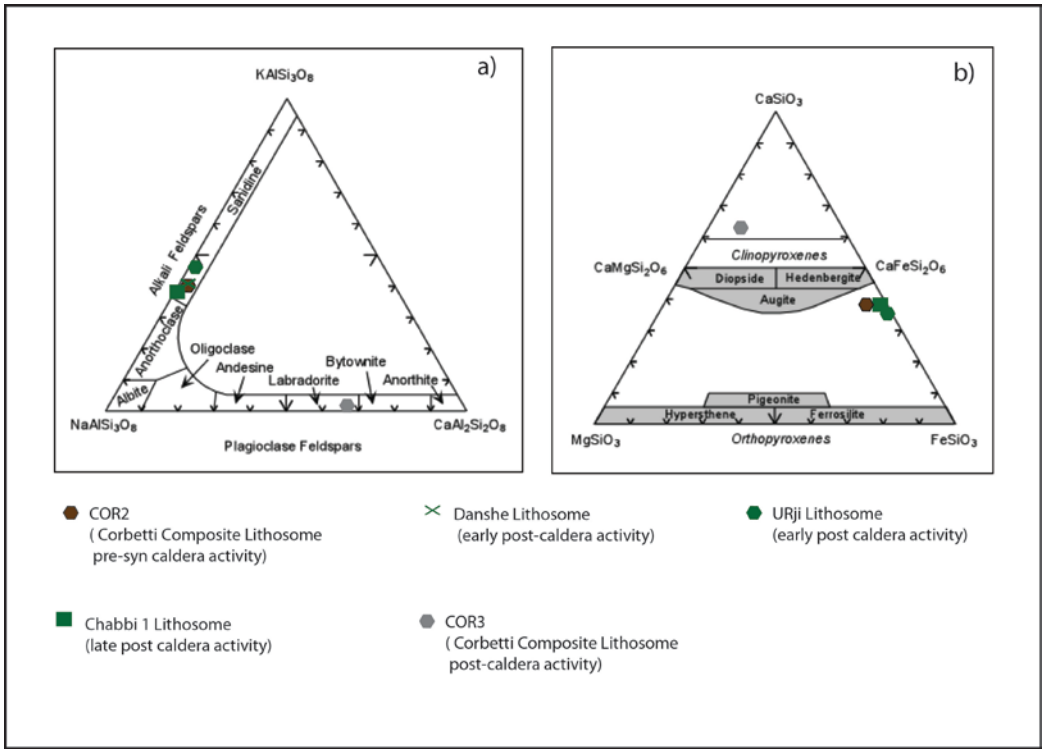

Fig.3.3 Triangular diagrams showing alkali- feldspar **(a)** and pyroxene **(b)** composition from syn-caldera deposits (COR2 eruptive unit, *Corbetti Composite Lithosome*) and post- caldera deposits (*Danshe, Urji and Chabbi 1Lithosomes* and basalt deposit COR3 *from Corbetti Composite Lithosome*).

3.3.2 Major element content in whole rock

Corbetti products show a large range of silica content (SiO_2 46.2 - 75.4 wt%) if the rare basalt deposit, COR3, (*Corbetti Composite Lithosome)* is included. They show a wide silica content gap of about 28 wt %. However, if considering only the rest of the products from the four lithosomes (*Corbetti Composite Lithosome, Urji Lithosome , Danshe Lithosome and Chabbi Composite Lithosome*) ,the range of SiO_2 concentration (73.7-75.4 wt%) becomes very narrow and all the products show a rhyolite composition when plotted on total-alkali vs silica diagram (Fig.3.4). The rhyolites are peralkaline (AI=1.5) and can be further classified as pantellerites on the basis of the Al_2O_3 and FeO^T content (Fig. 3.5). Corbetti caldera products do not appear to have any intermediate composition between basalt and rhyolite in terms of major element concentrations, and they clearly have a wide compositional gap.

Although the range of silica content in Corbetti rhyolites is limited, it is possible to observe some variation in major element concentrations as illustrated in Fig 3.6, 3.7

When plotted against the narrow range of increasing SiO_2, there is a slight decrease of MgO, FeO^T, CaO, TiO_2 and MnO (Fig.3.6, 3.7) between the products of the two different eruptive epochs, the pre-syn and post-caldera epochs, possibly due to a different proportion of crystals.

In particular the FeO^T, TiO_2 and MnO content of the pre/syn- and post-caldera deposits, are clearly clustered into two distinct groups. Al_2O_3 and Na_2O concentrations tend to show the opposite trend with a slight increase. For Al_2O_3, the pre/syn and post caldera products are distinct, but they are basically clustered together. Na_2O and P_2O_5 are the only two major elements that do not appear in the pre-syn caldera deposit (COR1 and COR2) as a distinct defined group. For Na_2O content, the two *Corbetti Composite Lithosome* samples (COR1, COR2) are split between the two clusters at 4.5% and 5.5% Na_2O (Fig.3.6).

The K_2O content of Corbetti samples does not show any particular trend within the rhyolites samples, ranging from 4.6%, the lowest content in the post-caldera deposits (Chabbi 1 lithosome), to 5.2 %, as the highest in the syn-caldera deposit (COR2).

The Corbetti rhyolites belong to a high-K calc-alkaline series, whereas the basalt sample falls in a medium-K calc-alkaline series (Fig. 3.8), although it should be noted that the analyzed basalt sample was altered (weathered) to some extent.

Among the latest products of the post-caldera epoch, the Chabbi 1 lithosome sample (CH1), moves away from the general trend in regard to the MgO, TiO_2, CaO and P_2O_5 concentration.(Fig. 3.6)

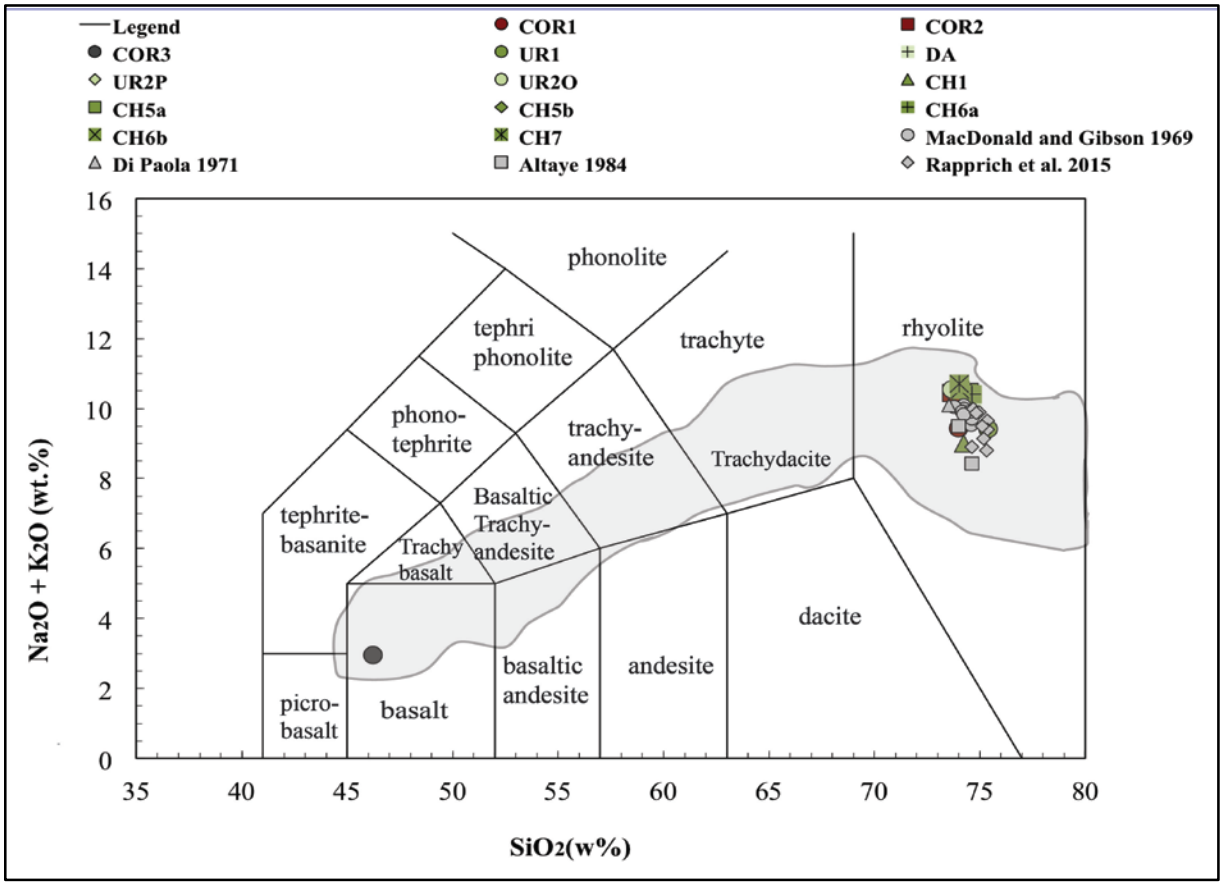

Fig.3.4 Diagram showing total alkalis (Na2O+K2O) vs SiO2 (TAS classification diagram , Le Bas et al.(1986)) in whole rock samples from Corbetti Caldera deposits of this work and previous works (Macdonald and Gibson (1969)-circles; Di Paola (1972)-triangles; Altaye (1984) –squares; Rapprich et al. (2015)-diamonds).In red are the samples from the pre and syn caldera activity (*Corbetti Composite Lithosome,* COR1, COR2) whereas in green are the samples from the post- caldera activity (*Urji Lithosome* -UR1,UR2P, UR2O, *Danshe Lithosome* - DA and *Chabbi Composite Lithosome* - CH5a, CH5b, CH6a, CH6b, CH7) of this work. The dark grey circle is the basalt sample (COR3) from the *Corbetti Composite Lithosome*. All analyses of whole rock samples have been normalized to sum to 100% on an anhydrous basis with all iron as FeO. The grey field has been drawn on the basis of literature data on MER volcanic rocks (Barberio et al., (1999); Boccaletti et al., (1995), (1999); Brotzu et al.(1974); Chernet and Hart, (1999); Furman et al., (2006a); Gasparon et al., (1993); Gibson, (1972); Peccerillo et al., (2003), (2007); Ronga et al., (2010); Trua et al., (1999)).

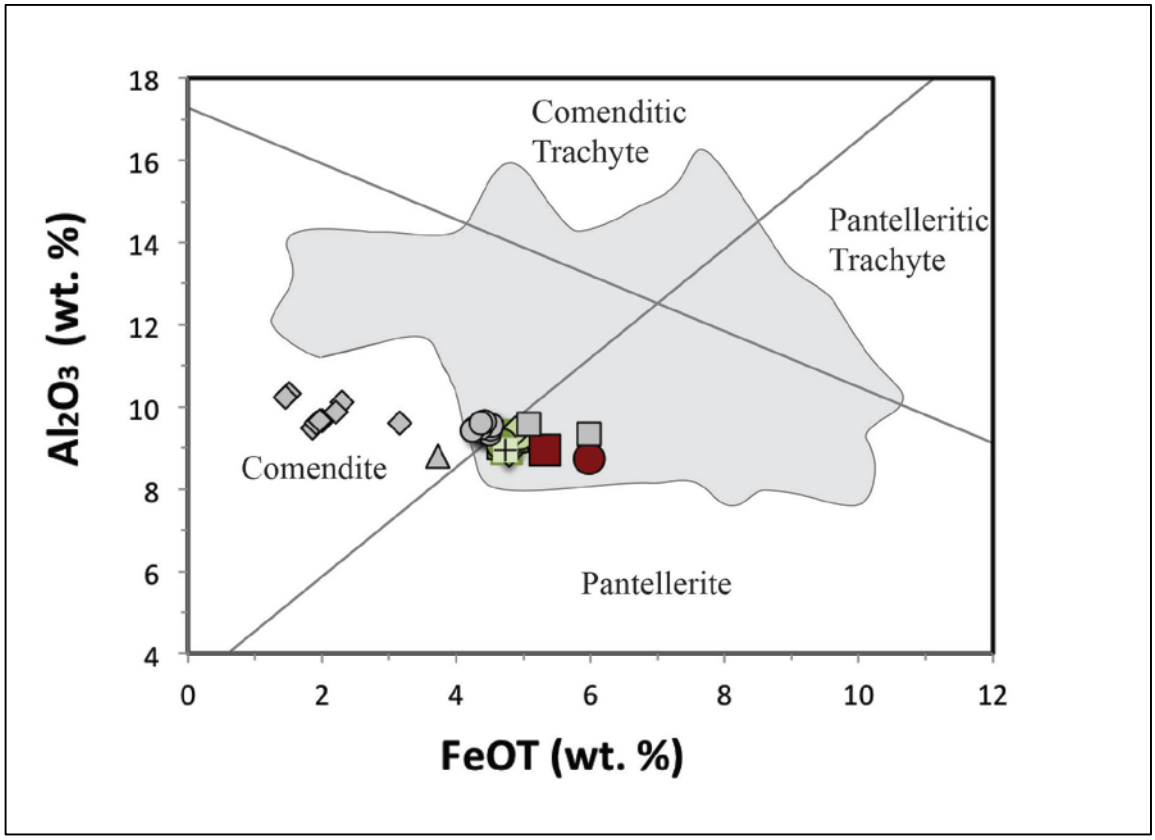

Fig.3.5 Diagram showing Al_2O_3 vs FeOt for peralkaline rhyolitic rocks (Macdonald, (1974)). In red are the samples from the pre and syn caldera activity (*Corbetti Composite Lithosome,* COR1, COR2*,*) whereas in green are the samples from the post- caldera activity (*Urji Lithosome* - UR1,UR2P, UR2O, *Danshe Lithosome* - DA and *Chabbi Composite Lithosome* - CH5a, CH5b, CH6a, CH6b, CH7). The grey symbols are from the previous works: the circles are data from Macdonald and Gibson (1969), the triangle is from Di Paola (1972), the squares are from Altaye (1984) and the diamonds are from Rapprich et al. (2015).All analyses of whole rock samples have been normalized to sum to 100% on an anhydrous basis with all iron as FeO. The gray field has been drawn on the basis of literature data on MER volcanic rocks (Barberio et al., (1999); Boccaletti et al., (1995), (1999); Brotzu et al., (1974); Chernet and Hart, (1999); Furman et al., (2006a); Gasparon et al., (1993); Gibson, (1972); Peccerillo et al., (2003), (2007); Ronga et al., (2010); Trua et al., (1999))

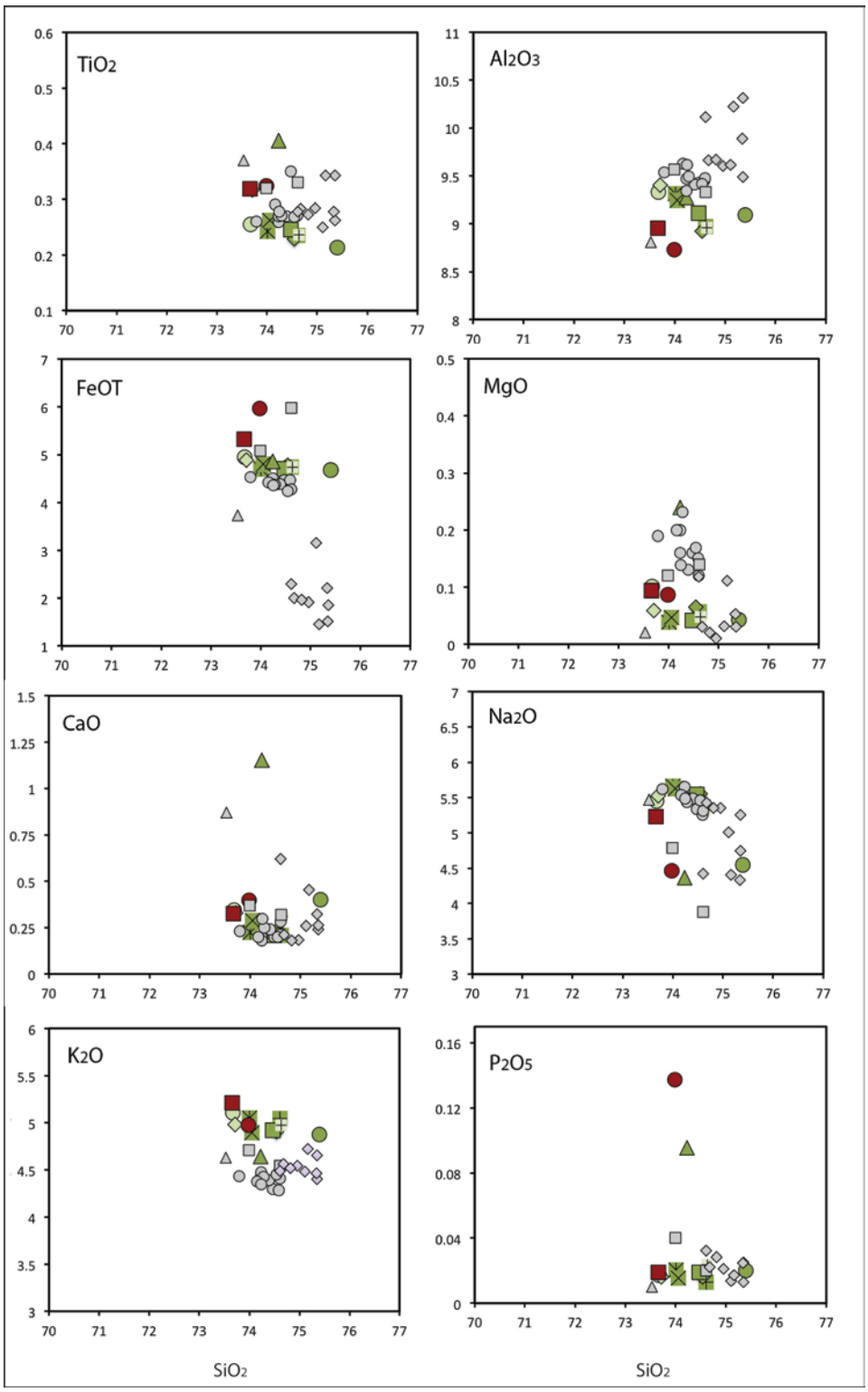

Fig.3.6

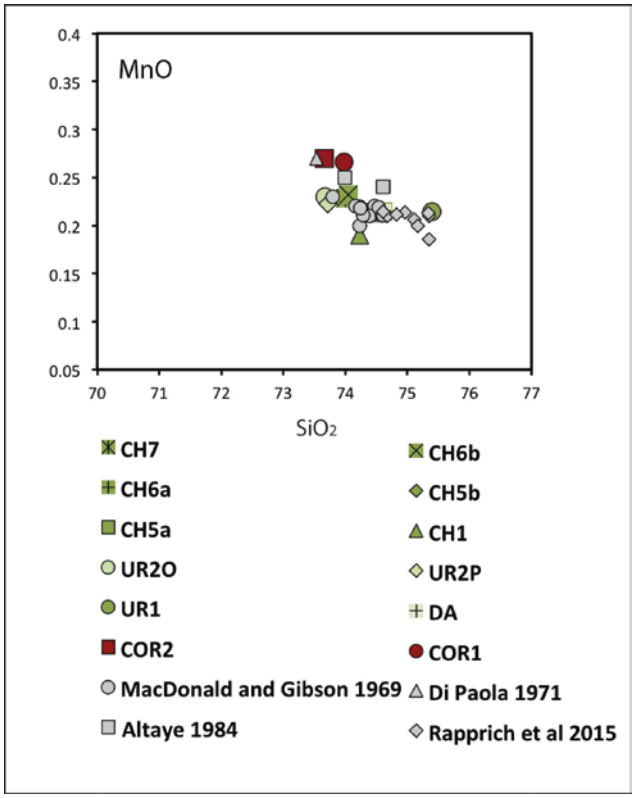

Figure 3.6- 3.7 Major element Harker diagrams for rhyolites samples of Corbetti caldera from this work and previous works. Symbols are as in figure 3.4 and 3 .5 All analyses of whole rock samples have been normalized to sum to 100% on an anhydrous basis with all iron as FeO. Major elements concentrations are in %wt.

The TiO_2 content is slightly higher than the others with 0.4 wt% , whereas MgO, CaO and P_2O_5, show concentrations higher than the other deposits.

When comparing Corbetti major elements with data from previous works, there is a general agreement with the exception of a few elements; our data show slightly higher K_2O and slightly lower MgO (Fig.3.6). There is then a difference regarding the FeO^T and Al_2O_3 concentrations, between our data and those of the previous works, in particular with those from Rapprich et al. 2015. This difference leads to a different classification when plotted on the Al_2O_3 vs FeO^T diagram (Fig.3.2, MacDonald 1974). The Corbetti rhyolites are classified as comendite in Rapprich et al. (2105) whereas in this work as well as in Di Paola (1972)and Altaye (1984), they are classified as pantellerite. The data from Macdonald and Gibson 1969 fall on the transition line between comendite and pantellerite composition (Fig.3.5).

The difference in the concentration for some major elements between our data and the previous works, may be due to the different analytical technique and standards adopted (see next sections)

Overall, from the trend of the major elements content in Corbetti caldera deposits, it is difficult to understand any possible magmatic evolution that links the basalt to the rhyolitic products, or any clear fractional crystallization that produced the pantellerite composition. However, the lack of samples of intermediate compositions (Daly gap) is a typical feature at Corbetti and other MER volcanic centres. The lack of any intermediate composition products at Corbetti, might suggest that the rhyolites are not the result of fractional crystallization process from a parental basalt as the basalt of the *Corbetti Composite Lithosome* COR3. Other hypotheses would include an immiscible separation of high and low silica melts, or some flat 'liquidus' curve that produced a big change in SiO_2 content (or melt productivity) for a small change in temperature (Melekhova et al., 2013).

It is also worth noting that in the case of Corbetti caldera all the products of both pre-syn caldera and post- caldera activity, are all of rhyolite composition, with the exception of the basalt sample COR3 , and this monotonous compositional range for >90% of the erupted products presents a challenge for interpreting .

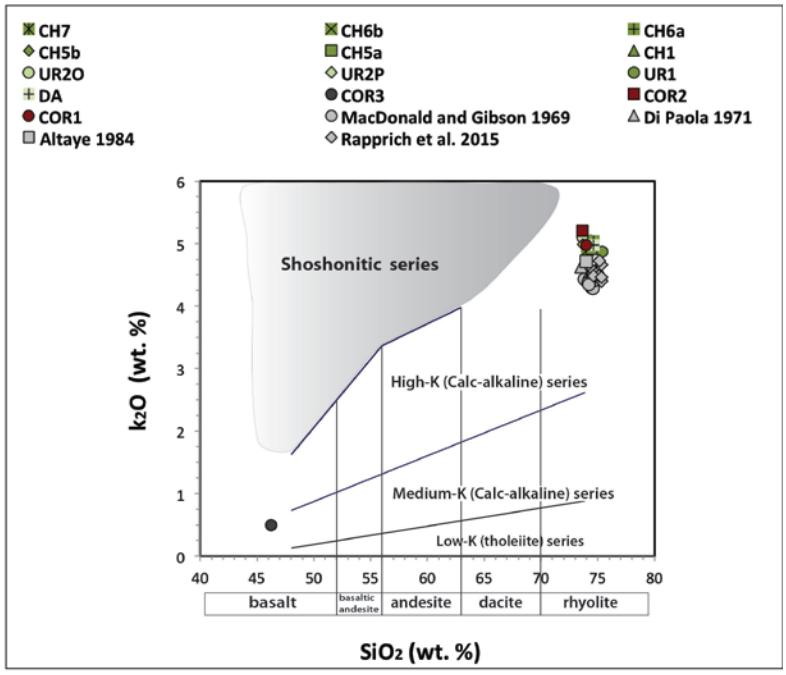

Fig.3.8 K2O vs. SiO2 (wt%) classification diagram (Peccerillo & Taylor, (1976)). Symbols are as in figure 3.4 - 3.5 .All analyses of whole rock samples have been normalized to sum to 100% on an anhydrous basis

3.3.3 Trace element content in whole rock

The small range of SiO_2 content in whole rocks precludes any clear interpretation about the processes that might have produced evolved magmas. The trace elements concentration then it can provide a more insightful or sensitive record of the magmatic process.
A comparison with the trace elements trend from other Quaternary calderas (Alutu, Gedemsa, Boseti, Fantale) , also helps to better understand the possible magmatic evolution of the Corbetti caldera volcanic system. The selected incompatible elements are both LILE (Rb, Sr, Ba, La, Ce) and HFSE (Nb, Ta, Zr,Y, Hf, U).

3.3.3.1 Trace elements content in rhyolite deposits of Corbetti caldera

The analyses of the trace elements in the rhyolite deposits, allows a better investigation of the magmatic processes occurred in Corbetti sub-volcanic system, in relation to the stratigraphic reconstruction as proposed in this work.
When the rhyolites are considered in terms of pairs of incompatible element contents such as LILE vs HFSE and HFSE vs HFSE, they clearly show two distinct groups between the deposits of the pre/syn caldera epoch (*Corbetti Caldera Lithosome*) and the deposits of the post-caldera epoch (*Urji, Danshe and Chabbi Composite Lithosome*) (Fig. 3.9, 3.10). This agrees with the stratigraphic reconstruction of Corbetti activity as proposed in chapter 2. The trace elements therefore show that a 'magmatic evolution' occurred within the peralcaline- rhyolitic magma of the Corbetti plumbing system.

The HFS incompatible element Zr, has been chosen as proxy for melt fraction for incompatible elements. Zircon saturation indeed is typically delayed in alkaline rocks because of its high solubility. Among the post-caldera epoch deposits, the concentration of incompatible elements
(Ta, Y, La, Ba,) show further grouping. For example in the Ba vs Zr concentration diagram (Fig.3.9), the UR1 (Urji lithosome) and DA (Danshe lithosome) samples, show a Ba content lower than the deposits of the other lithosomes.

This agrees with the stratigraphic reconstruction where the eruptive unit UR1 of Urji activity and the Danshe deposits, have been interpreted as the first manifestation of the resurgent volcanism after the caldera collapse (chapter 2). Among the LILE elements, Ba and Rb behave as more incompatible elements than Sr. Indeed the Ba and Rb concentration show an enrichment from the pre-syn- caldera to the post- caldera epoch, whereas Sr shows a small variation with respect to increasing Zr for all samples, with the exception of the CH1 sample (Fig. 3.9). This is a particular geochemical feature of Corbetti rhyolites and will be further discussed in the next sections.

Regarding the incompatible elements Ta, U, Hf, Nb, Y, all diagrams show an increase from pre-syn caldera to post-caldera epoch suggesting an 'magmatic evolution' within the peralcaline-rhyolitic magma, from the oldest to the newest deposits within the Corbetti rhyolite magma (Fig.3.9, 3.10). The same pattern of a clear enrichment in incompatible elements from the pre-syn caldera to the post-caldera epoch, is also shown when plotted on primordial mantle-normalized trace element diagram (Fig. 3.11). In this diagram a strong decrease in Sr concentration is apparent, that would be explained by about 90% crystallization of alkali feldspar in the Corbetti magmas. However, it has been seen that all Corbetti rhyolitic deposits show a low percentage (5-10 % vol) of phenocrysts and this percentage does not explained the low content of Sr. In addition to this, if there had been a fractionation of alkali feldspars during the evolution of the Corbetti felsic magma, this would have resulted in a wider range of Sr concentration along the different samples from the different lithosomes. On the contrary the limited range of a very low Sr content (3 – 12 ppm) might suggest that the Sr would have been already included in some crystals removed and forming a cumulate before the eruptions. In this scenario the magma erupted during both the eruptive epochs that characterized Corbetti volcanic history , would have been already depleted in Sr.

However, before formulating further considerations regarding the magmatic processes that took place in Corbetti sub-volcanic system, the analyses of the trace elements of both the basalt sample and the rhyolites, especially in comparison with those from other Quaternary volcanoes (Alutu, Geemsa, Boseti, Fantale, Boina Centre –Afar) provide more inferences for possible petrogenesis and evolution of Corbetti magmas.

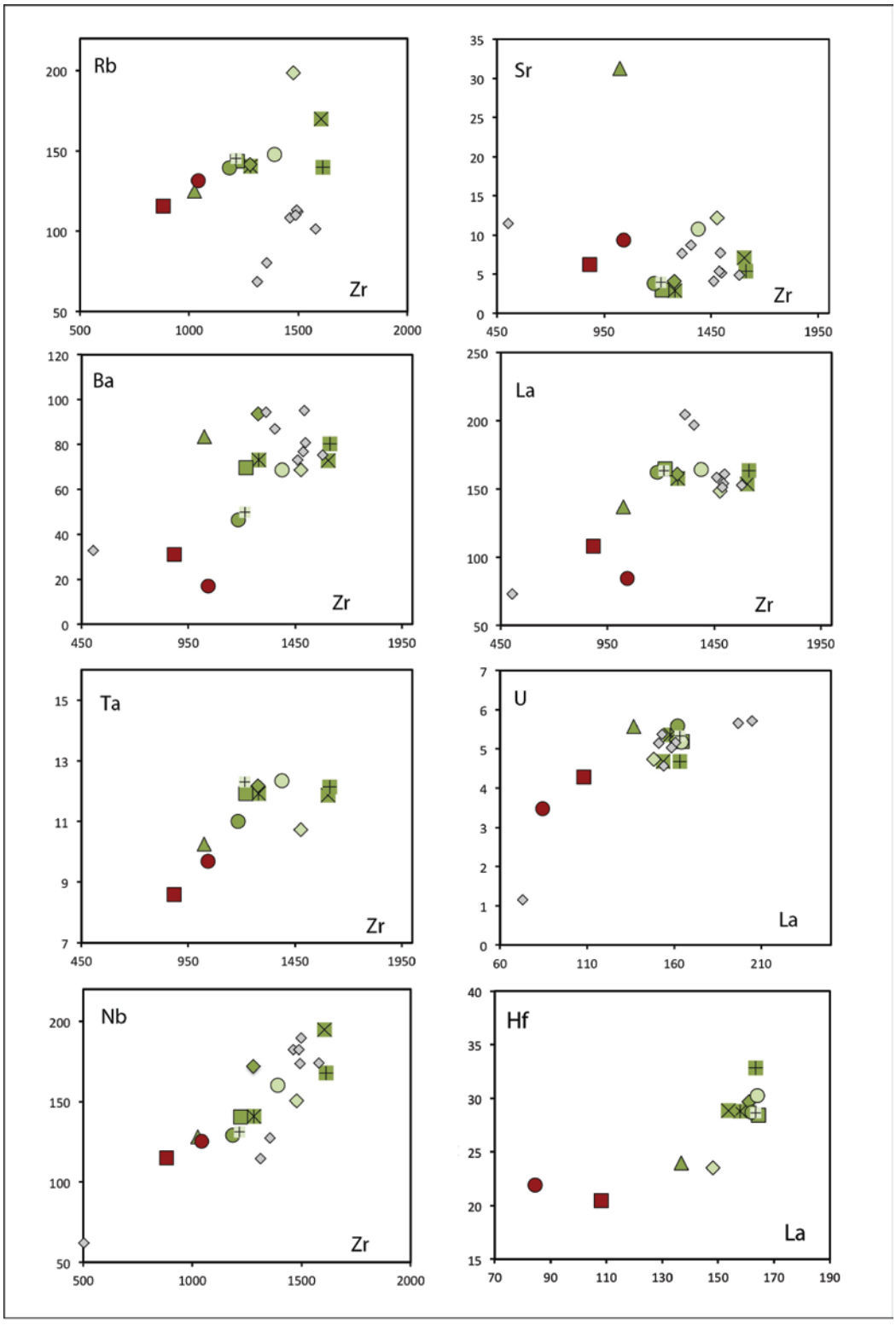

Fig.3.9

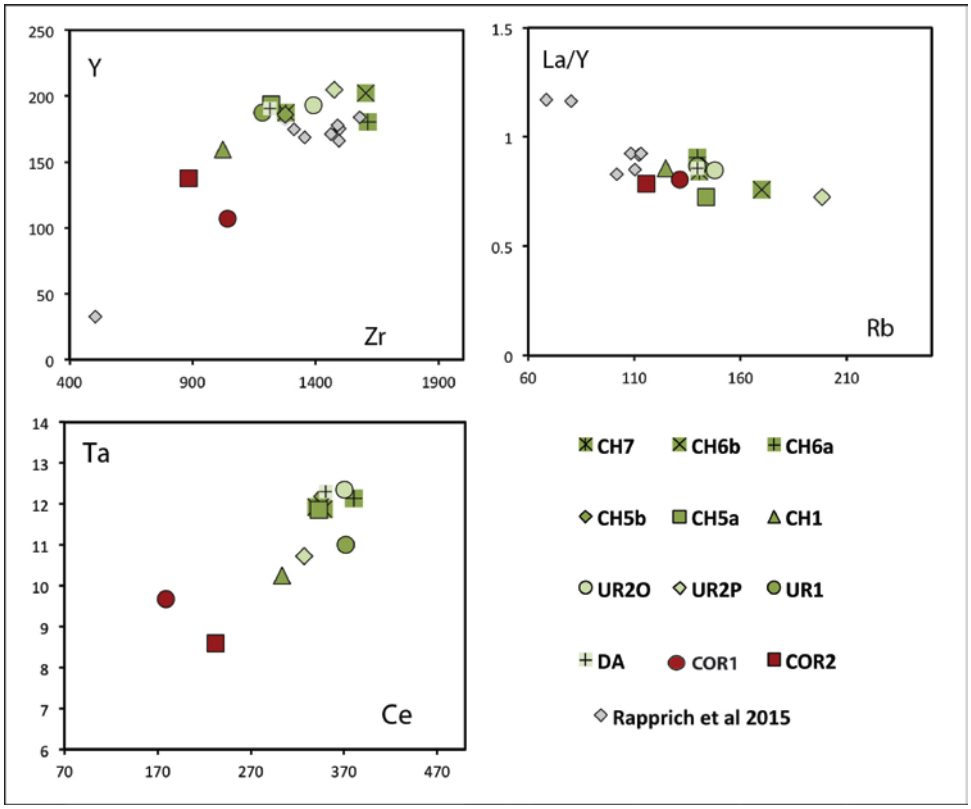

Fig.3.10

Figure 3.9 – 3.10 Harker variation diagrams for selected trace elements in Corbetti rhyolites of this work and Rapprich et al. (2015). In red are the samples from the pre and syn caldera activity (*Corbetti Composite Lithosome,* COR1, COR2*,*) whereas in green are the samples from the post- caldera activity (*Urji Lithosome* - UR1,UR2P, UR2O, *Danshe Lithosome* - DA and *Chabbi Composite Lithosome* - CH5a, CH5b, CH6a, CH6b, CH7). The grey diamonds are from Rapprich et al. (2015). All concentration are shown in ppm.

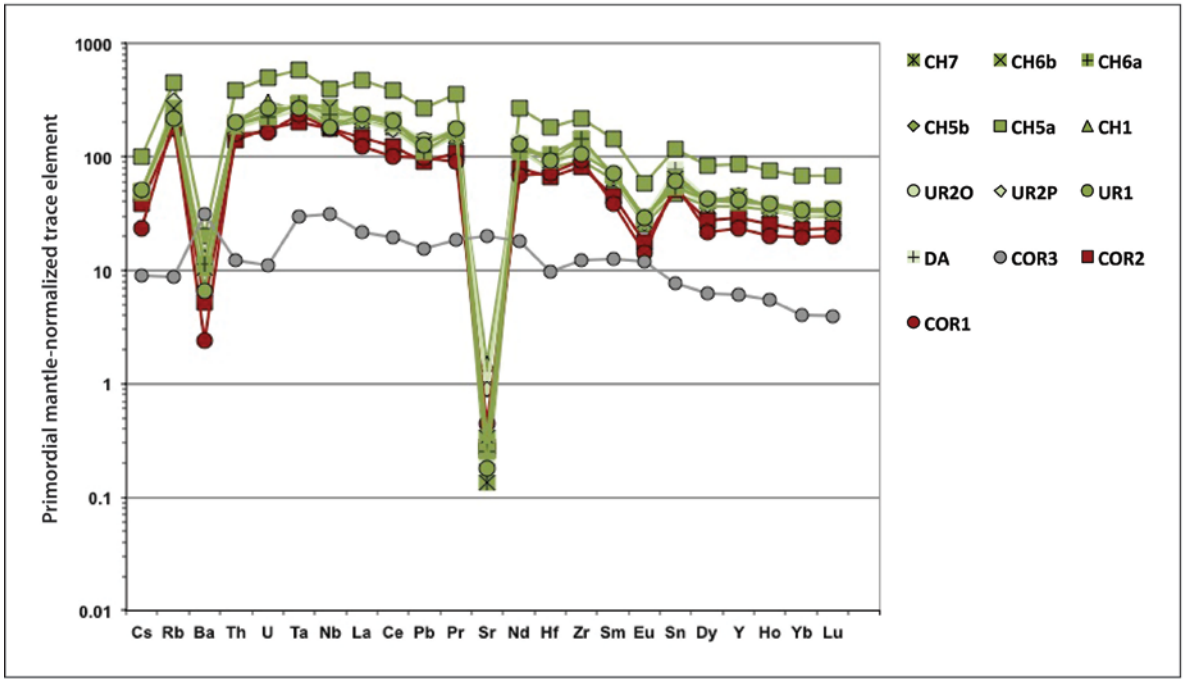

Fig.3.11 Primordial mantle-normalized trace element diagram for Corbetti Caldera products. Normalizing values are from McDonough et al. (1992). In red are the samples from the pre and syn caldera activity (*Corbetti Composite Lithosome,* COR1, COR) whereas in green are the samples from the post- caldera activity (*Urji Lithosome* - UR1,UR2P, UR2O, *Danshe Lithosome* - DA and *Chabbi Composite Lithosome* - CH5a, CH5b, CH6a, CH6b, CH7). The dark grey circle is the rare sample of basaltic composition (COR3) from the *Corbetti Composite Lithosome*

3.3.3.2 Trace elements content in rhyolite and basalt deposits of Corbetti Caldera. Comparison with other Quaternary calderas along the rift.

The behaviour of some trace elements can offer key insights into the magmatic processes that produced the high silica rhyolites, when considered both the basalt and rhyolite deposits and especially when compared with those from other Quaternary volcanoes along the rift. The composition of Corbetti caldera rocks have been compared with those from Alutu (Hutchison, PhD thesis 2015), Gedemsa (Peccirillo et al. 2003), Boseti (Ronga et al. 20010), Fantale (Giordano et al. 2013, Giordano PhD thesis 2006) ,Boina Centre-Afar (Barberi et al. 1975), from the central to the north part of the Main Ethiopian Rift up to the Afar region.

The behaviour of selected incompatible elements might distinguish between fractional crystallization process only, or production by partial melting and crustal assimilation. A strong positive correlation between pairs of incompatible elements which have low values of solid/liquid partition coefficient (D<<1) such as U, Ta, Hf, Zr, La, Ce, Nb, Y, suggests that only fractional crystallization occurred, as only this process tends to maintain the concentration ratio of the incompatible elements. Indeed the concentration of incompatible elements will not keep a positive correlation in other processes, as for example crustal contamination, partial melting and gas transfer, which would not produce a composition of the volcanic rocks typical of a fractional crystallization process.(Treuil 1973, Ferrara & Taruil 1974, Barbieri et al.1975).

The selected volcanoes for comparison, show intermediate composition in the products along their volcanic history whereas, as it has been seen, there is not record in Corbetti products of intermediate rocks. It could be argued that Corbetti volcano emplaced intermediate deposits but that they have not been sampled. However, from the oldest works on Corbetti (Mohr (1966), Di Paola (1972)) to the newest (Altaye (1984), Rapprich et al.(2105)), not a single product with intermediate composition has been found. It can be stated that Corbetti volcano emplaced only the end-members of the chemistry composition of the volcanic rocks throughout its volcanic activity.

Comparing therefore Corbetti products with those of volcanoes along the MER, that emplaced some intermediate rocks and that, as it occurred at Boina-Centre (Afar), the products show all the geochemical sequence from basalt to rhyolite, allows a better understanding of the trace elements' trend of Corbetti caldera rocks.

It is possible to observe a strong positive correlation between pairs of the HFSE (Ta, Nb, Y) vs Zr, and between LILE vs HFSE , (Rb and La vs Zr and U and Hf vs La), where Corbetti basalt sample matches with the most primitive products, and Corbetti rhyolites match with the most evolved samples of the other volcanoes (Fig. 3.12, 3.13). However for Nb and Y content, Corbetti rhyolites deviate slightly from the general trend. The Sr and Ba content shows an opposite trend along the samples from all volcanoes, decreasing from the basaltic composition to the most evolved rocks with the higher Zr concentration (Fig.3.12). However, in this case the trend is more scattered in respect to the strong positive correlation observed for the other trace elements. Once again the Corbetti rhyolites match with the most evolved rocks of the other volcanoes, although for the Ba content, Corbetti samples group slightly apart, showing a relative increase of Ba from the pre-syn caldera deposits to the post-caldera deposits as already seen. It is interesting also to note that for the Sr concentration, the Corbetti rhyolites especially match with those from Alutu, that also shows a very low and limited content of Sr , whereas the samples from the other volcanoes , especially Gedemsa and Fantale, show a wider range of Sr from the basalt to the most evolved rocks.

Corbetti rocks also deviate from the general trend that characterizes rocks from the other volcanic centres when plotted on La/Y vs Rb diagram (Fig. 3.13). The trend is the same as the other volcanoes, although the values of the ratio La/ Y for Corbetti samples are lower, ranging between 0.5 to 1 instead of 1 to 1.5. Corbetti rhyolites also show the same ratios of incompatible elements of rhyolitic samples from Gedemsa, for which crustal contamination has been hypothesized in their petrogenesis (Peccirillo et al. 2003). This is also apparent on a Rb/Nb vs Rb diagram (Fig. 3.14), where are plotted the values of granofels, granitoids, gneiss and schists that form the Precambrian basement in Ethiopia (Peccirillo et al 1998). Corbetti rhyolites match with the most evolved samples of Gedemsa, Fantale and Alutu, that are thought to have experienced some crustal contamination in addition to the fractional crystallization, which is hypothesized as the main process for the petrogenesis of the magmas. The Corbetti basalt shows a lower values relative to the general trend of basalts from the other volcanoes. When comparing Corbetti products to those from the other volcanic centers on a primordial mantle-normalized trace element diagram (Fig. 3.15), it is also evident that Corbetti rocks match with the end-members, basalt and rhyolites, of the deposits from the other calderas along the MER. However, as already seen on the Harker variation plots (Fig.3.12), the Ba and Sr concentration of Corbetti rhyolites have a different trend and concentration in respect to the rhyolites of other calderas and this might have different implications for the petrogenesis of the Corbetti magmas

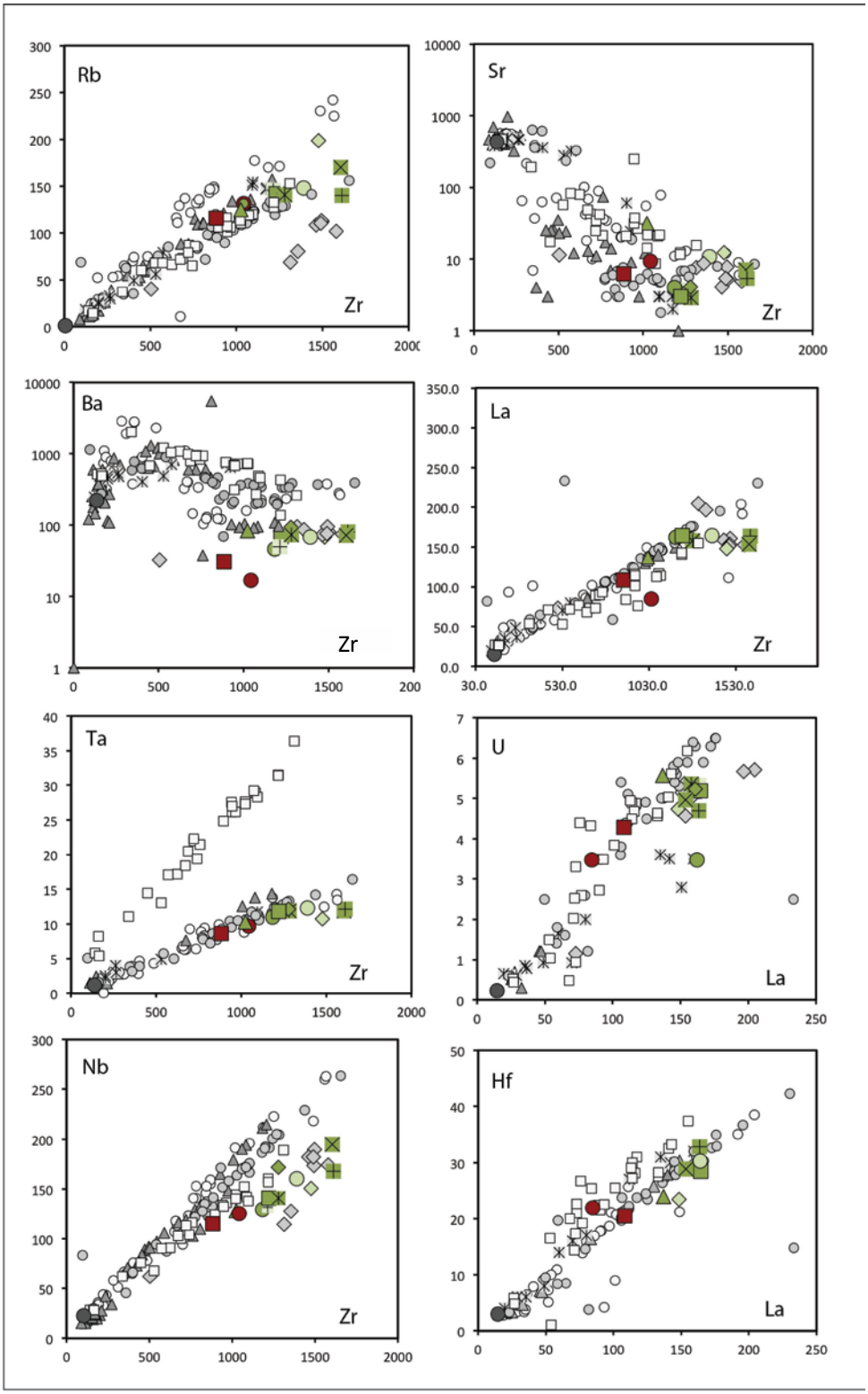

Fig.3.12

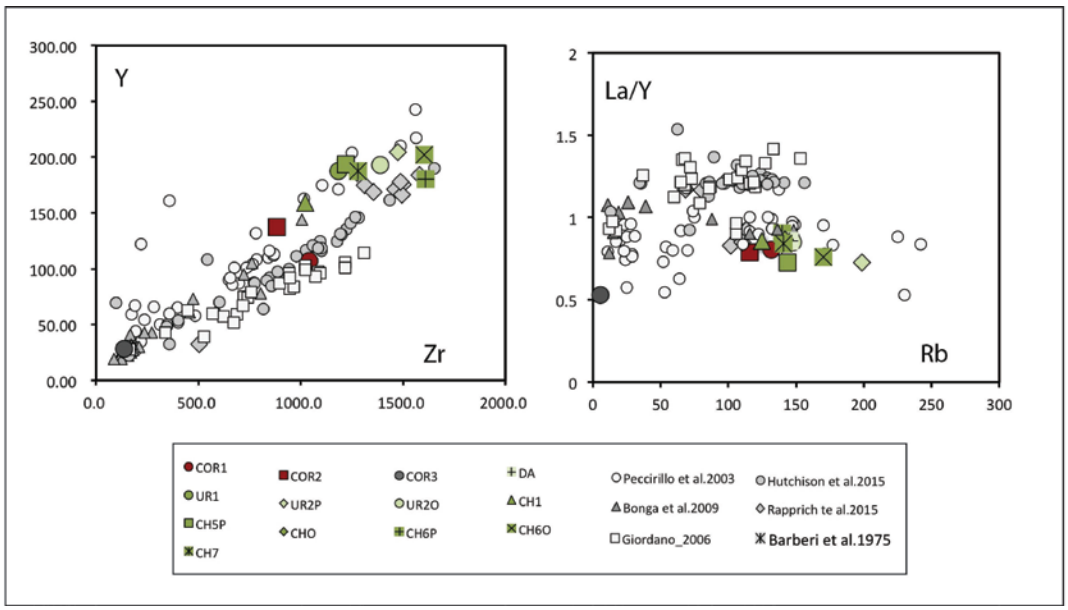

Fig.3.13

Figure 3.12-3.13 Harker variation diagrams for selected trace elements in Corbetti deposits from this work and from Rapprich et al (2015) and in volcanic rocks from other volcanic centres along the MER and Afar region. In red are the samples from the pre and syn caldera activity (*Corbetti Composite Lithosome,* COR1, COR) whereas in green are the samples from the post- caldera activity (*Urji Lithosome* - UR1,UR2P, UR2O, *Danshe Lithosome* - DA and *Chabbi Composite Lithosome* - CH5a, CH5b, CH6a, CH6b, CH7). The dark grey circle is the rare sample of basaltic composition (COR3) from the *Corbetti Composite Lithosome* whereas the grey diamonds are from Rapprich et al. (2015). For the other volcanic centres the symbols are as follows: the grey squares with a cross are data from Barberi et al. (1975)for the Boina-Center in Afar; the white circles are data from Peccirillo et al. (2013) for Gedemsa volcano; the white squares are from Giordano (2006), Giordano et al. (2013) for Gedemsa and Fantale volcanoes; the grey triangles are from Bonga et al. (2009) for Boseti volcano and the grey circles are data from Hutchinson (2015) for Alutu volcanic center. All concentration are shown in ppm. The Ba and Sr contents are shown in logarithmic scale.

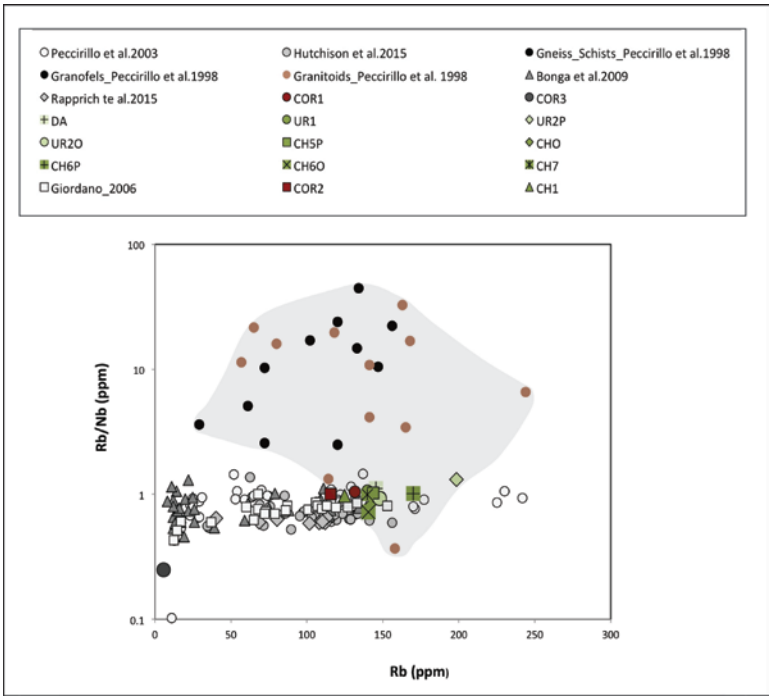

Fig.3.14 Rb/Nb vs Rb concentration diagram for Precambrian basement (Peccirillo et a. (1998)), Corbetti deposits from this work and from Rapprich et al. (2015)and for deposits from other volcanic centres along the MER : Alutu, (Hutchison (2015)), Gedemsa (Peccirillo et al. (20030), Fantale (Giordano et al. (2006)), Boseti (Bonga et al. (2009)) . All symbols are as in figure 3.12- 3.13

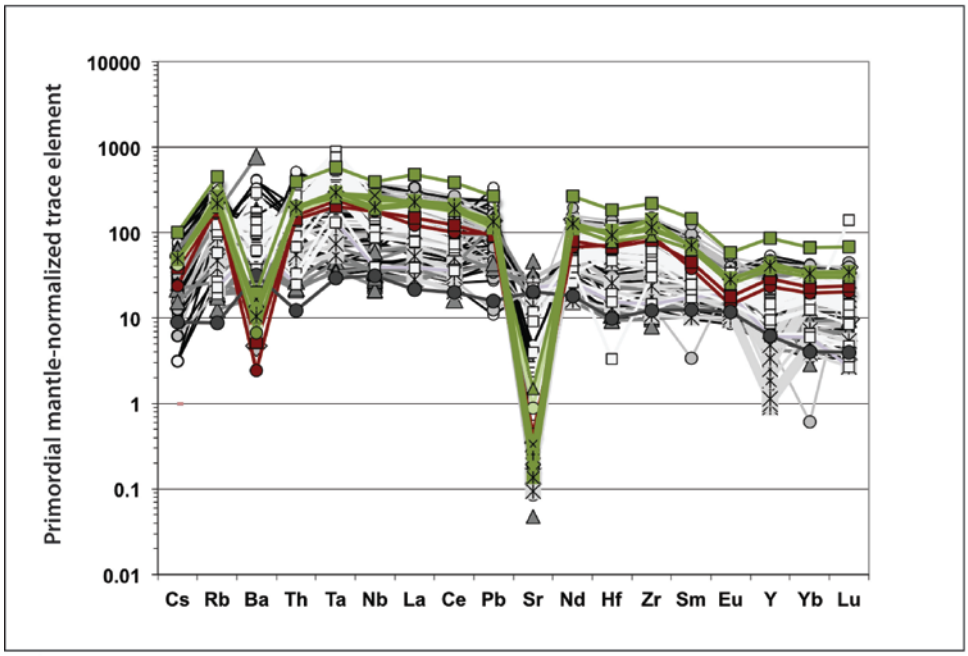

Fig.3.15 Primordial mantle-normalized trace element diagram for Corbetti Caldera products from this work and from Rapprich et al. (2015) and for volcanic rocks from Alutu (Hutchison (2015)) Gedemsa (Peccirillo et al. (2003), Giordano (2006)), Fantale (Giordano et al. (2013)), Boseti (Bonga et al. (2009)) and Boina volcanic center (Barberi et al. (1975)). Normalizing values are from McDonough et al. (1992). All symbols are as in figure 3.12 -3.13

3.3.3.3 Comparison between Corbetti basalt and basalts from the main Quaternary calderas along the MER

The sampling of the rare basalt COR3 among the products of Corbetti caldera allows a comparison with the basalts from the main Quaternary calderas along the Main Ethiopian Rift. This is an important comparison as any basaltic product from Corbetti activity was sampled and analysed in the previous works. The comparison helps in understanding and interpreting the evolution of the volcanic history of Corbetti caldera .

In the volcanic centres Alutu, Gedemsa, Boseti, and Fantale, the basalt products are from the newest post-caldera activity, with the exception of the Boina Centre, where the basalts are the exclusive products of the initial fissure activity (Barberi et al. (1975)).

In these Quaternary calderas along the Main Ethiopian Rift, the basalt deposits are from vents aligned along the direction of the Wonji Fault Belt and the activity is probably linked with the activation of the Quaternary fault system.

On the basis of the stratigraphic position of COR3 basalt within the stratigraphic reconstruction of Corbetti deposits (chapter 2), this primitive product of Corbetti magma system, has been interpreted to have been erupted during the post- caldera eruptive epoch, and it has been interpreted by Altaye (1984), as a deposit of basaltic volcanism associated with the 'Corbetti-Shalla–sector' of the Wonji fault belt.

When plotted on a MgO vs SiO_2 diagram, the basalts from the different volcanic centres show two distinct groups with different percentage of MgO for different SiO_2 content (Fig.3.16). One group shows a MgO content ranging from 10% to ~ 3%, for a higher content of SiO_2 (47% to ~ 52%),whereas the other group shows a lower range of MgO concentration, from 8% to 3% ,for a lower range of SiO2(46% to ~ 49%). The Corbetti basalt COR3 falls in the second one. However, a more evident grouping for the basalts from the calderas selected of the MER and the volcanic centre from Afar ,is visible when considered some compatible trace elements as Ni and Cr.

In a Ni vs MgO diagram (Fig. 3.16), the basalts show three different groups from higher to lower contents of Ni and MgO. The Alutu basalts and two basalt from Boina Centre, move away from the general trend showing a slightly lower content of Ni for a higher content of MgO. Corbetti basalt sample (COR3) falls in the group of higher Ni and higher MgO concentration. A similar pattern is visible in a Cr vs MgO diagram (Fig. 3.16), where all of the basalts samples are clustered in two groups. Corbetti basalt falls in the group with higher values of Cr and MgO.

Two basalt samples from Gedemsa volcano (GdM 125, GdM 139), analysed by Giordano (2006), as also other basalt samples investigated by Peccirillo et al. (2003), fall in the group showing higher Ni, Cr and MgO concentrations.

These basalts with MgO content ranging between 8-9% wt, and a high concentration of compatible trace elements, as well as a particular enrichment of incompatible elements and constant isotopic ratios, has been interpreted as basalts that did not undergo fractional crystallization process plus crustal assimilation, hypothesised for the other group (Peccirillo et al. (2003), (2007)). On the contrary ,it has been interpreted formed by partial fusion of a mantle more enriched of incompatible trace elements than the mantle that generated the group of transitional -basalts (Giordano (2006)).

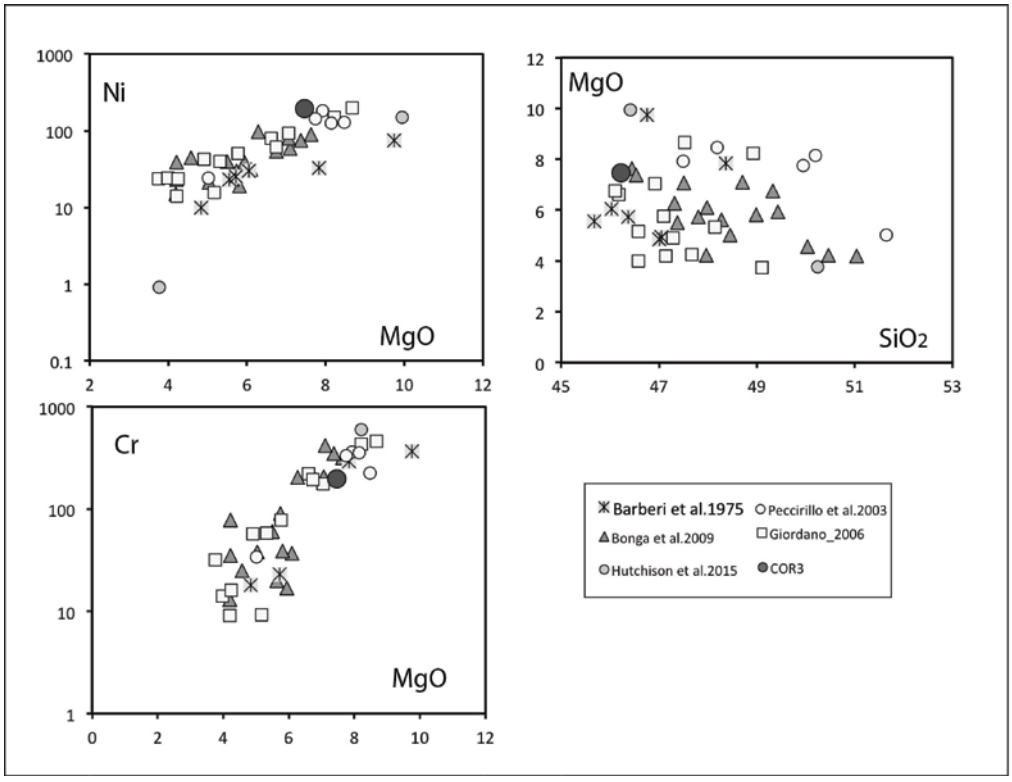

Fig. 3. 16 Harker variation diagrams for selected major and trace elements in Corbetti basalt (COR3) and in basaltic deposits from other volcanic centres along the MER and Afar region : Alutu, (Hutchison (2015)), Gedemsa (Peccirillo et al. (2003)), Fantale (Giordano (2006)), Boseti (Bonga et al. (2009)), Boina volcanic center (Barberi et al. (1975)). Symbols are as in figure 3.12-3.13- 3.14-3.15. Trace elements concentration are in ppm whereas major elements concentration are in %wt.

Although further investigation are necessary to well establish the relationship between the basalt sample COR3 and the rhyolitic products of Corbetti, the geochemistry here presented might suggest for Corbetti basalt COR3 from the post-caldera activity , a similar genesis of the basalt samples GdM 125, GdM 139 form Gedemsa volcano.

3.4 Discussion and conclusions from major and trace elements content in Corbetti caldera's whole rock

Corbetti caldera shows for all its volcanic history, from the pre-syn caldera epoch to the newest products of the post-caldera epoch, only peralkaline rhyolites, with the exception of the one deposit of basaltic composition.

No one product of any intermediate composition (trachy-basalt, basaltic-trachy-andesite, trachy-andesite, trachyte) has been recorded in Corbetti deposits. This is a very particular feature if compared with the geochemistry of other main Quaternary calderas along the Main Ethiopian Rift, as Alutu, Gedemsa, Boseti, Fantale, up to the Afar region with the Boina-centre (chapter 1,1.4).

Indeed, although the stratigraphic sequence of the deposits of all these Quaternary volcanoes is characterized by the lack of some products of intermediate composition, however they record along their volcanic history, a general compositional variation from basalt to rhyolites that is completed in the Boina rocks suite. In this scenario Corbetti caldera is the only one volcanic center showing only the end-member products of the entire geochemical sequence.

It could be argued that not all the deposits emitted from Corbetti volcano have been sampled, but it has been already seen that in all the previous works (Mohr (1966), Macdonald and Gibson (1969),Di Paola (1972), Altaye (1984), Rapprich et al. (2015)) any intermediate products has been sampled and that only basalt and rhyolites deposits have been found. Until proven otherwise therefore , Corbetti calderas can be consider the only volcano in the Main Ethiopian Rift that have produced only the end-member of the entire geochemical sequence. MacDonald and Gibson (1969), also defined Corbetti as 'unique volcano', due to the geochemical features of its products.

In this regard, a comparison and discussion of the Corbetti geochemistry with the geochemistry of the above mentioned volcanoes helps for a deep understanding of the volcanic history of this 'unique' volcano of the Main Ethiopian Rift.

3.4.1 The geochemistry and volcanic history of Corbetti caldera: similarities and differences with Alutu, Gedemsa, Boseti and Fantale calderas.

The intraplate volcanism is characterized by the lack of intermediate composition within a sequence of volcanic products (Daly Gap) , and this particular geochemical feature has been found in most of the products from the volcanism in the Main Ethiopian Rift. Two different hypothesis has been suggested to understand the origin of the peralkaline silicic rocks and their relation with the basaltic magmas: i) a process of protracted fractional crystallization of transitional basaltic magma along with crustal contamination; ii) peralkaline rocks and the associated basalts are formed by two different melts, where the mafic liquids are not the basaltic parents of the perlakaline – rhyolitic liquids.

In this scenario the basalts would form in the mantle whereas the silicic liquids would form by partial melting of old crust or young underplated basalts (Barberi et al., (1975), Davies & Macdonald, (1987), Lightfoot et al., (1987) , Macdonald et al. (1987), Mahood et al., (1990), Gasparon et al., (1993), Geist et al., (1995), Mungall & Martin, (1995), Black et al., (1997), Bohrson & Reid, (1997), Civetta et al., (1998), Trua et al., (1998) **).**

Corbetti caldera, like the other calderas selected for comparison , Alutu, Gedemsa, Boseti and Fanatele, shows this typical bimodal composition within the entire sequence of emplaced products However, while in Corbetti deposits the compositional gap covers a wide range, from~ 45% to 75% wt of SiO_2, without any intermediate rocks, the products of Alutu, Gedemsa, Boseti and Fantale, record some deposits of intermediate composition. In Alutu and Gedemsa the intermediate products are not only the juvenile deposits emitted from the pre and post – caldera activity, but also enclaves or lithichs found within the most evolved rocks of the resurgent volcanism (Peccirillo et al. (2003), Hutchison (2105)). In Fantale, the pre-caldera deposits show both rhyolitic and trachytic composition, whereas the ignimbrite deposits linked with the caldera forming eruption, shows a different composition from rhyolite in the lower part of the deposit to trachyte in the upper part. The post-caldera deposits of Fantale, as also those from Boseti volcano, show trachyte composition (Giordano (2006), Ronga et al. (2010)).

The enclaves, the compositional zonation in deposits of a caldera forming eruption, the more 'primitive' composition (trachyte) in the post- caldera activity and not only in the pre-caldera, have suggested the existence of a shallow zoned magma chamber (Peccirillo et al. (2007)), where the lighter silicic liquid floats above a more dense liquid of a more primitive composition.

This interpretation agrees well with the hypothesis proposed to explain the petrogenesis of the Gedemsa suite rocks (Peccerillo et al. (2003)), that invokes a fractional crystallization process plus a minor contribution from the Precambrian crust, that outcrops at the edge of the Ethiopian volcanic region and that constitutes the geological basement beneath the Tertiary-Quaternary volcanoes. The zoned magma chamber therefore would be the result of a low-pressure fractional crystallization process that begins from a mildly alkaline basalt.

The trend of the pairs of the selected incompatible elements (Rb, Sr, Ba, La, Ta, U, Nb, Hf, Y, Zr) in Gedemsa deposits matches with those from the rocks sequence of Boina centre (Fig.3.12, 3.13). In particular the Boina centre's rhyolites show a concentration of both major and many trace elements similar to that of the Gedemsa's rhyolites (Peccirillo et al. (2003)).

Since the suite from Boina center has been interpreted to be generated by a fractional crystallization process starting from transitional basalt (Barberi et al. (1975)), this further supports the fractional crystallization genesis also for the Gedemsa magmas.

However, in order to fully explain the petrogenesis of the Gedemsa rocks a contribution from the Precambrian crust has also been invoked, on the basis of trend of incompatible element and ratios (Fig. 3.14), (Peccirillo et al. (1998), Peccirillo et al. (2003))

This model for the petrogenesi of peralkaline magmas starting from transitional basalts and crustal contamination, has been also applied to Alutu, Boseti and Fantale on the basis of comparison with Gedemsa rocks and on the basis of fractional crystallization modelling for major and trace elements (Giordano (2006), Ronga et al.(2010), Hutchison (2015)).

The selected trace elements (Rb, Sr, Ba, La, Ta, U, Nb, Hf, Y, Zr) contents of Corbetti deposits plotted against those from Alutu, Gedemsa, Boseti, Fantale and Boina centre (Afar), have concentrations that mostly match with those of these other volcanic centres.

On the basis of this therefore, it could be hypothesized, as Rapprich et al. (2015) have done, that a similar petrogenesis occurred also for Corbetti magmas. However some further considerations are required.

It has been seen that in Corbetti volcanic history all the deposits both from the pre-syn caldera eruptive epoch and the post-caldera eruptive epoch, with the exception of a single basaltic product, show a rhyolite-pantellerite composition. In addition to this, the stratigraphic reconstruction (chapter 2) showed that all the eruptive centres from the vent that emplaced the *Corbetti Composite Lithosome*'s deposits, to the newest one of *Chabbi Composite Lithosome*, with the exception of Urji volcano, were monogenetic eruptive centres.

The presence of only two paleo-soils as second order unconformities surfaces (chapter 2) , also suggests that the eruptions in both the eruptive epochs of Corbetti volcano occurred in a relatively short span of time.

On the contrary, the volcanic history of Alutu, Gedemsa, Boseti and Fantale was characterized by the additional emplacement of intermediate deposits of trachy-andesite, trachyte composition in both the pre and post-caldera activity deposits, in some part of the caldera forming eruption deposits (Fantale), as well as in enclaves within both the syn-caldera and post-caldera rocks. Alutu and Gedemsa volcanoes also showed that their syn- caldera activity was characterized by polygenetic eruptive centeres (chapter 1, 1.4)

These differences that emerge from the stratigraphic investigations and comparison, plus those from the major elements analyses and comparison, might suggest a different eruptive dynamics linked with a different magmatic plumbing system for Corbetti caldera, that might have had a different scenario for the genesis and evolution of Corbetti magmas.

Looking at the trace element concentrations, it has been seen that Corbetti rhyolites overall match with the most evolved products of the other calderas and the Boina centre. However, in the Nb and Y vs Zr diagrams, the Corbetti rhyolites clearly move away from the general linear trend (Fig.3.12, 3.13).

It has been seen that a strong positive correlation is observed between pairs of incompatible elements, as for example elements like Nb and Y, which have a very low values of solid/liquid partition coefficient ($D<1$), during fractional crystallization process. Indeed this is the only petrogenetic process that keeps the concentration ratio of incompatible elements the same (Treuil, (1973); Ferrara & Treuil, (1974)),whereas other processes (gaseous transfer, crustal contamination , partial melting,) can change the concentration of the incompatible elements and this does not results in a strong positive correlation when plotting the trace elements content on a Harker diagram. (Barberi et al. (1975)).

The trend of incompatible elements in Corbetti rhyolites might suggest that other sub-volcanic processes, different from a single, prolonged fractional crystallization of a transitional basaltic melt, occurred during the magma petrogenesis.

The concentration of incompatible element ratios, such as Rb/Nb, vs Rb (Fig. 3.14), for Corbetti rhyolites, match with those from rhyolites from Alutu, Gedemsa, Fantale, that record signs of crustal contamination, (Peccirillo et al. (2003), Giordano (2006), Hutchison (2015)).

This might also suggest some crustal contamination or crustal melting for the genesis of Corbetti magmas. Indeed, in Peccirillo et al. (2003), it is reported that the Gedemsa rhyolite samples GD22, GD29, GD34 "have higher Sr and slightly lower Nd isotope ratios (comparable with those of the upper continental crust) respect to the other silicic rocks that have comparable Sr, Nd and Pb isotope ratios to the basalts". The data from Peccirillo et al. (2003) support the idea that rhyolitic magmas "may be formed by a partial melting process of basalt, along with a contribution from Precambrian crust". It has been also found that peralkaline rocks from the Kenya rift have variable isotope compositions and this suggests a "contribution from both underplated basalt and old crust" (Davies & Macdonald, (1987)).

The values of the Sr and Nd isotope ratios of the Gedemsa silicic rocks samples (GD 22, GD39, GD 34) interpreted as having had a crustal contamination in their genesis, are comparable with the values of the Sr and Nd isotope ratio, having an average value of 0.705 for $^{87}Sr/^{86}Sr$ and of 0.513 for $^{144}Nd/^{143}Nd$, measured by Rapprich et al. (2015) , for the syn-caldera deposits and for deposits from Urji (UR2O) and Chabbi (CH7, CH2) activity.

Another interesting observation emerges from the comparison of the Corbetti basalt sample (COR3) with those from the other Quaternary calderas, in particular with some basaltic samples from the post-caldera activity of Gedemsa (Giordano (2006)).

It has been seen in section 3.3.3.3 , that in Ni and Cr vs MgO diagrams, where the samples are clustered in two and three groups respectively (Fig.3.16), COR3 falls in the group of samples showing higher content of Ni, Cr and MgO. In this group also fall some basalts from the post-caldera activity of Gedemsa (GdM 125 , GdM 139 Giordano 2006) that have a MgO content between 8 and 9 wt.%, Ni content between 150 and 200 ppm and no evidence for olivine accumulation. They also show more radiogenic Sr isotopic composition with respect to the other analyzed mafic rocks (Giordano (2006)). Giordano et al. (2013) found that none other rocks investigated from Gedemsa and Fantale, derived from these mafic parent magmas by fractional crystallization processes.

These basalts, on the basis of their MgO content (8-9%), of the high content of compatible trace elements and enrichment of the incompatible trace elements, and on the basis of their constant isotopic ratios of Sr, Nd, Pb, are not considered to be the magma source of the rhyolites generated by fractional crystallization plus crustal contamination process, that has been instead hypothesized for the other basalts that have a lower MgO, Cr and Ni content.

The genesis of these basalts therefore, has been hypothesized by partial fusion of a mantle more enriched of incompatible trace elements (Giordano (2006), Giordano et al. (2013)). To test this hypothesis Giordano (2006) estimated the pressure and consequently the depth of the partial fusion process, using the Albarede (1992) model and on the basis of a partial fusion model, using the equations of the "non- modal batch melting" of Wilson (1989). They found pressures of 1.7±0.2 GPa and 2 ± 0.3 GPa, that correspond to a depth between 45 and 60 km. They also found that the composition of these two basalt samples from Gedemsa (GdM 125, GdM 139) matches with the compositional trend of experimental melts in equilibrium with mantle peridotite obtained at 1.5 and 2 GPa (Baker and Stolper (1994), Kushiro (1996)). These basalt samples from Gedemsa also fall in the compositional field of some Quaternary basalts of the rift, emplaced in the region of Debre Zeyit and Butajira (Rooney et al. (2005)) and that have been interpreted as resulting by 5-7% of partial fusion of a mantle peridotite with spinel.

Corbetti caldera basalt (COR3) might have had the same genesis by partial melting of a mantle peridotite with spinel occurred at a depth between 45-70 km. If so this basalt would not be the parental magma related to the rhyolites samples. In this scenario the rhyolites – pantellerites of Corbetti caldera, would have formed by fractional –crystallization process of transitional basalts with a different mantle source of the basalt COR3. The parental basalt to the rhyolites, might have been generated in the mantle, ascend into the crust and fractionate to evolved magmas depleted in compatible elements. During the protracted fractional crystallization the alkali feldspars would have been removed from the system and formed a cumulate.

This would be supported by the model that explains the geochemistry, petrology and stratigraphy of the rift volcanism by the emplacement of large magma body of basalt composition in the lower crust . Then zoned magma chambers would be developed by a low-pressure fractional crystallization process characterized by a magma of rhyolite composition in the upper part and magma of basaltic composition in the bottom. In this scenario the less abundant lavas of basaltic composition, that are associated with the more evolved deposits, would be emerged through regional faults, which slice through the lower part of the shallow reservoirs, or catch into the deeper magma storage of magma underplating at the Moho (Peccirillo et al. (2007))

An other interesting aspect concerns the Sr concentration in the whole rock samples. In the primordial mantle-normalized trace element diagram, Corbetti rhyolites match with the most evolved products from all the other calderas, and they show a strong decrease in Ba and Sr content. The Sr concentration in particular shows an extremely low value (Fig.3.11, 3.15).

In order to test the fractional crystallization process for Gedemsa magmas, Peccirillo et al (2003) carried out major elements mass balance and thermodynamic MELTS modelling (Ghiorso & Sack (1995)), and they found that with 70% fractional crystallization, starting from a magma of basaltic composition like the Gedemsa basalt, it is possible to have a magma of trachytic composition. This implies that an assemblage with the following abundance of plagioclase (~50%), olivine (~ 20%), clinopyroxene (~ 20%), magnetite (~ 10 %), apatite (~ 1%) must be removed from the system. They also found that in order to reach a magma of peralkaline rhyolite composition is necessary about 50-60% of further fractional crystallization, with the crystallization and removal of alkali feldspar (85-90%) , clinopyroxene (~ 10%), fayalite (2%) and Fe-Ti oxides (2%). Peccirillo et al. (2003) then have tested the fractional crystallization model based on major elements, with a trace elements model. Their results show that by ~ 70% of fractional crystallization of the most primitive basalt, it is possible to have concentration of incompatible trace elements in liquids of trachytic composition as they have found in Gedemsa rocks, and that by ~ 90-95% of fractional crystallization of the trachytic liquids, it is possible to reach a melt of peralkaline rhyolites composition.

The same proportions have been also proposed by Ronga et al. (2010) to explain the genesis of the pantelleritic rocks of Boseti volcano. The low Sr concentration in the whole rocks of Corbetti, would be explained by the extreme crystallization process necessary to reach the rhyolite melt and by the fact that most of the Sr had already entered in the crystal lattice of the alkali feldspar crystallized. However, one problem related to this model is where are the magma storages of the large volumes of the parental magmas, and the reason why there are so few evidences on surface (Peccirillo et al. (2003)).

Regarding Corbetti products, when considered also the low percentage of phenocrysts (5-10 vol%) in Corbetti rhyolites, this may support the hypothesis that Corbetti peralkaline melts formed by an alkali parental basalt that underwent fractional crystallization, generating evolved magmas, rich in phenocrysts and depleted in compatible elements. The phenocrysts were then removed from the system and formed a cumulate.

The comparison of Corbetti geochemistry with the geochemistry and models for the petrogensis of other Quaternary calderas along the central and northern sectors of the Main Ethiopian Rift , helped to understand the particular geochemical features of Corbetti deposits from the pre, syn and post caldera activity. The comparison also allowed the interpretation that the Corbetti basalts, COR3, might not represent the parental magma from which the rhyolites formed by fractional crystallization. The COR3 basalt may be formed from a deeper reservoir of mantle peridotite source.

3.4.2 The petrogenesis of Corbetti rhyolites

The main issue for understanding the volcanic activity of Corbetti caldera complex and for the assessment of volcanic risk of the area, is to understand whether or not the rhyolites formed by fractional crystallization from a magma of basaltic composition similar to the pillow lava sample COR3. This would imply the same feeding system for rhyolites and basalt deposits, and it would have different implications for the eruptive dynamics from the case that rhyolites and basalt represent the products of two different and independent magmatic systems.

Resurgent volcanism reveals the evolution of a magmatic system depending on the residual magma, and/or on the replenishment of the magma storage after the caldera collapse (Druitt et al. 2012). It has been seen that in the case of Corbetti caldera the resurgent volcanism has been characterized by the same composition that marked the pre and syn-caldera activity, whereas the activity of other Quaternary calderas along the rift (Alutu, Gedemsa, Boseti Fantale) have emplaced products of more primitive composition, or rhyolites with enclaves of trachytic composition, suggesting a zoned magmatic feeding system and a fractional crystallization process for the genesis of the rhyolites .

It has been also seen that, although Corbetti rhyolites overall match with the most evolved products of the other quaternary calderas, Alutu, Gedemsa, Boseti, Fantale, the concentration of residual elements as Nb, Y, Zr , Rb in the rhyolites, and Ni, Cr and Mg in Corbetti basalt, seem to suggest a different magma source for the rhyolites and the basalt.

Trace element models have been tested to investigate the petrogenesis of rhyolite products of Corbetti caldera.

3.4.2.1 Trace element models

Trace element models help to identify geochemical processes occurring in magmatic systems and the consequent magmatic evolution that characterized the activity of a volcanic complex. In petrogenetic modelling it is important to choose accurately the bulk partition coefficients (D) values of the trace elements to use.

It has been demonstrated that D-values are function of melt composition, temperature, fO_2, as well as whole rock and crystal composition (Mahood and Stimac 1990, Wood and Fraser 1976). Larsen (1979) also was the first to note the strong effect of peralkalinity on trace-elements partitioning.

In this regard trace elements partition coefficients in alkali feldspars in equilibrium with rhyolite peralkaline melt, have been considered for modelling trace elements of Corbetti magma. Alkali feldspars are the dominant phase in rhyolite rocks and during the fractional crystallization process they exert a strong impact on the bulk partition coefficient of the majority of the trace elements. For several authors (Nicholls and Carmichael 1969, Roux and Varet 1975, Nash and Crecraft 1985, Cameron and Cameron 1986, Mahood and Stimac 1990, Ewart and Griffin 1994; Holt 1998) using the equation for the equilibrium crystallization of Korringa and Noble 1971, it is possible to calculate a bulk distribution coefficients from the composition of the trace elements in whole rock and feldspars, that is representative of the alkali feldspar partition coefficients, and that therefore they can be used.

Fractional crystallization model has been tested using incompatible (Rb, Zr, Y, La, Ta) trace elements starting from the composition of Corbetti basalt COR3.

According to literature data (Mahood and Hildreth 1983, Mahood and Stimac 1990, Ewart and Griffin 1994, White 2000, White 2003, White et al. 2003, Fedele et al. 2015) values of partition coefficient for incompatible elements as Zr, Y, La and Ta, decrease with the increments of the silica content and have a range of D values between 0.0007 and 0.2 (Mahood and Stimac 1990, White 2003, Peccerillo et al. 2003, Ren 2004, Fedele et al. 2015), whereas partition coefficient of compatible elements in alkali feldspar are affected by variations in melt polymerization (Larsen 1979, Mahood and Stimac 1990, White 2003, White et al. 2003, Fedele et al. 2015).

However, it has been observed an increase for partition coefficient values for Sr and Ba in alkali feldspars in peralkaline melts. One explanation is that Sr and Ba may substitute for Na in a Ca-poor alkali feldspars and therefore, their partition coefficients increase as a consequence of the higher Ab content in the alkali feldspars, that typically crystallize in strongly peralkaline melts (White 2003, White at al. 2003, Fedele et al. 2015).

For a similar reason the value of partition coefficient for Rb has been observed to decrease, in a similar fashion to the decrease in partition coefficients of incompatible elements in peralkaline rhyolites (White 2003, White at al. 2003, Fedele et al. 2015). Indeed in the case of Rb, the decrease of the partition coefficient seems related to the lower content of the orthoclase molecule in the alkali feldspar, since Rb shows a great geochemical similarity to K (Mahood and Stimac 1990, Icenhower and London 1996, White 2003).

In order to investigate the fractional crystallization modelling for the petrogenesis of Corbetti rocks, the following partition coefficients for the selected elements in sanidine crystals, have been used, after having tested several values of partition coefficients for peralkaline - rhyolites rocks from the authors mentioned above:

- DZr- 0.03 (Nash and Crecrft 1985),
- DTa - 0.019 (Mahood and Hildreth 1983)
- DRb- 0.05 (Peccerillo et al. 2003)
- Dy - 0.01 (White et al. 2003, Peccerilo et al. 2003)
- DLa- 0.01 (White et al. 2003, Peccerilo et al. 2003).

The software Petrograph (Petrelli et al. 2005) and the Rayleigh fractionation equation, $C_L/C_O = F^{(D-1)}$, has been used for calculations and diagrams.

3.4.2.2 Fractional crystallization of Corbetti rhyolites

It has been seen that positive correlation between couple of incompatible elements, which have low values of partition coefficient (D<<1), suggests that a only fractional crystallization process occurred for rocks formed from the same magmatic system, as only with this process the content ratio of the residual elements remains constant. In this regard the fractional crystallization model has been tested using pairs of incompatible elements such as Ta, La , Y vs Rb.

Rb has been considered as incompatible since the concentration of the orthoclase molecule is lower in the alkali feldspar that form in peralkaline melts. The incompatible behavior for Rb is also confirmed when Corbetti pantellerite are plotted on Primordial mantle-normalized trace element diagram (Fig. 3.11).

Diagrams of incompatible vs incompatible trace elements for Corebtti rocks (Fig. 3.17), clearly show that a fractional crystallization process seems not to be occurred for Corbetti rhyolites to explain their genesis from a magma source of COR3 basalt. Another magmatic process therefore must be hypothesized or ,alternatively, the rhyolites are generated by fractional crystallization process starting from a different basalt from COR3.

From the first seminal study on the Corbetti geochemistry of Macdonald and Gibson (1969), it has been hypothesized a fusion of a peralkaline granite for producing homogeneous rhyolite magma, assuming that it was superheated and remained so up to the eruption.

Indeed, although peralkaline felsic rocks are explained for the majority of natural volcanic deposits by fractional crystallization of alkali or transitional basalts at low fH_2O content and low fO_2 (Scaillet and MacDonald 2001,Harris 1983, Caroff et al.1993), this petrogenetic scheme may not be applied to explain peralkaline volcanic deposits everywhere. Some authors (Davis and MacDonald 1987, MacDonald et al. 1987, Black et al. 1997) have shown that the peralkaline rhyolites of the Greater Olkaria Volcanic Complex (GOVC) in the Kenya Rift Valley, can be explained by a partial melt of the crust “triggered by alkali- bearing volatiles” and they have ruled out the possibility that the Olkaria peralkaline rhyolites are from the daughter magmas of associated basalt (Scaillet and MacDonald 2001).

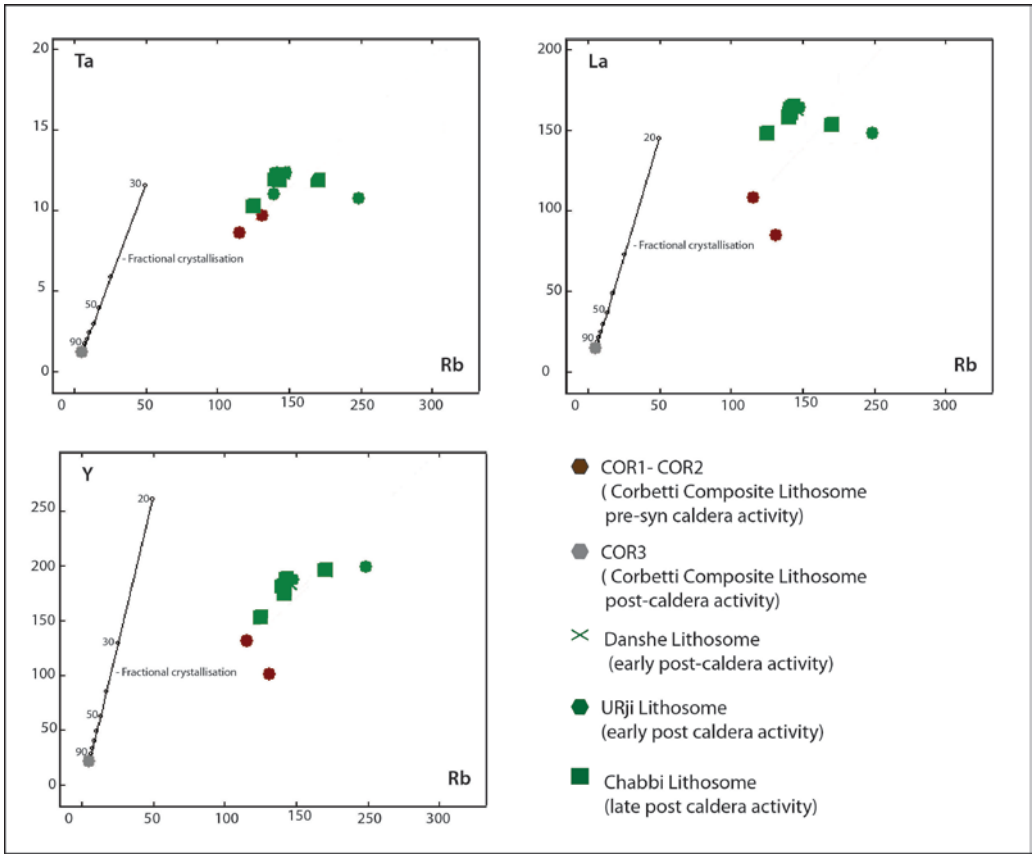

Fig.3.17 Rb vs Ta , Rb vs La and Rb vs Y concentration (ppm) diagrams in whole rock from Corbetti deposits. The black line is the fractionation crystallization model, starting from a magma of the COR3 basalt composition. Numbers on the line indicate the percentage of amount of melt. For the values of partition coefficients (DRb, DLa, DY) used see the text.

However, when comparing Corbetti products with those from Gedemsa volcano (Peccerillo et al. 2003) on the same incompatible vs incompatible elements diagrams and using same values of partition coefficients and considering the similarities in the geochemistry and mineral phases between the two volcanic complexes, what is shown is that Corbetti rhyolites might be the result of fractional crystallization process starting from a magma of basalt composition as that of the most primitive basalts of Gedemsa, rather than a magma with a composition as that of Corbetti basalt (Fig.3.18).

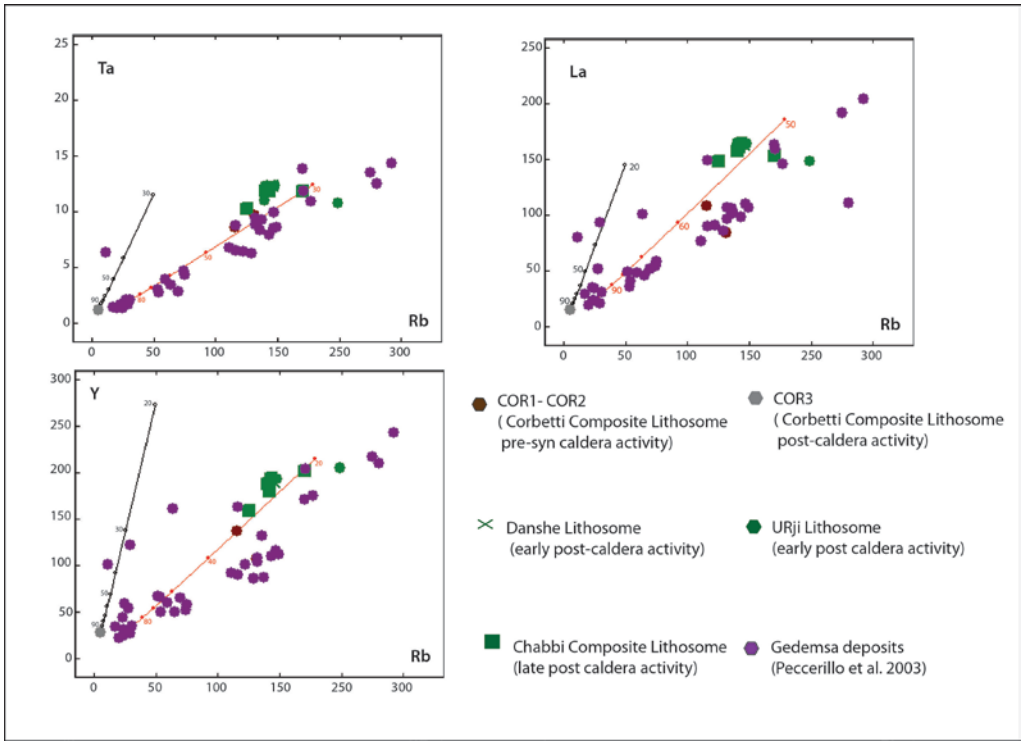

Fig. 3.18 Rb vs Ta , Rb vs La and Rb vs Y concentration (ppm) diagrams for Corbetti and Gedemsa (Peccerillo et al. 2003) whole rocks. Lines are fractionation crystallization models starting from the COR3 Corbetti basalt (black line), and from Gedemsa basalts with most primitive composition (red line). Numbers on the lines show the percentage of the total of melt. For the values of partition coefficients (DRb, DLa, DY) see the text.

Testing a fractional crystallization model for Corbetti rocks using pairs of compatible vs incompatible elements starting from a composition melt as that of Corbetti basalt (COR3), this process would require more than 90% of crystallization and this would imply that all the eruptions that characterized all the volcanic history of Corbetti, would have occurred with less than 10% of residual melt.

It could be then hypothesized that a fractional crystallization process occurred from a melt of composition like that of primitive basalt of Gedemsa and that as long as the crystallization of the mineral phases occurred until the formation of the alkali feldspar ,the crystals would have been removed forming a cumulate and depleting the magma of compatible trace elements.

In order to explain the petrogensis of Corbetti rhyolites and the relationship with the only basalt sample from the post –caldera activity , so far two opposite hypothesis can be considered : i) the rhyolites are not from daughter magma of a basalt magma of COR3 composition, but they are from a partial melting of upper or lower crust as already hypothesized by Gibson and Macdonald (1969); ii) the rhyolites would have been formed by protracted fractional crystallization process starting from a magma of composition as that of the primitive basalt of Gedemsa and that during the crystallization the crystals have been removed depleting the magma of compatible trace elements. In both these two scenarios the Corbetti basalt COR3 would not be related to the rhyolites.

However, the complexity of the structure and the composition of the crust beneath the Main Ethiopian Rift and the different magmatic segment that have been recognized along the rift (Mackenzie et al. 2005, Corti 2008), suggest further investigations for better constrain these two different hypothesis for the petrogenesis of Corbetti rhyolites.

3.5 Concluding remarks

Corbetti caldera geochemistry shows, as observed elsewhere along the Main Ethiopian Rift, a bimodal volcanism characterized by the typical compositional gap along the geochemical sequence from basalt to rhyolites. However, in contrast to other Quaternary calderas, such as Alutu, Gedemsa, Boseti and Fantale, that have intermediate (trachy-andesite, trachyte) rocks along their volcanic history, Corbetti caldera emplaced only peralkaline rhyolites products with the exception of one rare basalt deposit, for both the eruptive epochs.

Trace element concentrations in rhyolites confirm the stratigraphic reconstruction (chapter 2), showing an enrichment in the whole rocks from the pre to the post caldera activity deposits ,but the lack of any other intermediate rocks did not allow a clear analysis of a possible magmatic evolution from the basalt to the rhyolite. The comparison with data from Alutu, Gedemsa, Boseti, Fantale and Boina centre (Afar) allowed therefore, a better understanding of Corbetti geochemistry and allowed the interpretation of the petrogenesis of Corbetti rhyolites and basalt as formed from two different magma sources.

The main outcomes are summarized as follow:

- Corbetti rocks show a large range of silica content (SiO_2 46.2 - 75.4 wt%) if the basalt deposit, COR3, (*Corbetti Composite Lithosome)* is included. They show a wide silica content gap of about 28 wt %.
- The rhyolitic products of Corbetti caldera can be classified as peralkaline on the basis of the value of agpaitic index, AI= 1.5 and as pantellerite on the basis of Al_2O_3 and FeO^T wt% content (Fig. 3.5 MacDonald (1974)).
- The Corbetti rhyolites belong to a high-K calc-alkaline series, whereas the basalt sample falls in a medium-K calc-alkaline series (Fig. 3.8)
- When considering the rhyolites for pairs of incompatible element contents as LILE vs HFSE and HFSE vs HFSE, they clearly show two distinct groups between the deposits of the pre-syn caldera epoch (*Corbetti Caldera Lithosome*) and the deposits of the post-caldera epoch (*Urji, Danshe and Chabbi Composite Lithosome*) (Fig. 3.9, 3.10). This agrees with the stratigraphic reconstruction of Corbetti activity, as proposed in this work.
- Comparing trace elements concentration of Corbetti products with those from Quaternary calderas along the MER (Alutu, Gedemsa, Boseti , Fantale), that emplaced intermediate rocks, and with the Boina-Centre (Afar), that shows all the geochemical sequence from basalt to rhyolite, is evident as

Corbetti rocks match with the end-members, basalt and rhyolites, of the deposits from the other calderas along the Main Ethiopian Rift.

- When plotteing on a Ni , Cr, MgO diagrams, (Fig. 3.16) the basalts from the other calderas show three different groups from the higher to the lower content of Ni and MgO, and two groups from the higher to the lower content of Cr and MgO respectively. Corbetti basalt sample (COR3) falls in the group of higher Ni , Cr and MgO concentration, and a peridotite mantle source could be also hypothesized for Corbetti basalt, as it has been interpreted, for the group of basalts from Gedemsa volcano (Giordano et al. (2013)) also on the basis of constant isotopic ratios (Sr, Nd, Pb),
- The concentration of incompatible elements, such as the ratio of Rb/Nb, vs Rb (Fig. 3.14), for Corbetti rhyolites, match with those rhyolites from Alutu, Gedemsa, Fantale that record signs of crustal contamination, (Peccirillo et al. (2003), Giordano (2006), Hutchison (2015)).
- In the primordial mantle-normalized trace element diagram (Fig.3.15), Corbetti rhyolites match with the most evolved products from all the other calderas and they show a strong depletion in Ba and Sr content. In particular the Sr concentration shows an extremely low value that would be explained by the extreme crystallization (~ 90 %), necessary to reach the rhyolite melt starting from a mildly alkali basalt, and by the fact that most of the Sr had already entered in the crystal lattice of the alkali feldspar already crystallized.
- Corbetti peralkaline silicic rocks and the basalt might be formed from two different melts, which are genetically_independent. The basalt might be from a deeper reservoir in the upper mantle (between 40-70 km) whereas the silicic liquids might be generated in the crust.
- Two different hypothesis could explain the petrogenesis of Corbetti rhyolites: i) the rhyolites are not from daughter magma of a basalt composition as the COR3 Corbetti basalt, but they are from a partial melting of upper or lower crust as already hypothesized by Gibson and Macdonald (1969); ii) the rhyolites would have been formed by protracted fractional crystallization process starting from a magma of composition as that of the primitive basalt of Gedemsa and that during the crystallization the crystals have been removed depleting the magma of compatible trace elements. In both these two scenarios the Corbetti basalt COR3 would not be related to the rhyolites.

Table 1 : Major (wt%) and trace element (ppm) composition of whole rock from pyroclastic deposits of Corbetti Caldera Lithosomes

sample	COR1	COR2	COR3	DA	UR1	UR2P	CH1	CH5P	CH6P
SiO_2	73.98	73.66	46.22	74.63	75.40	73.71	74.23	74.47	74.61
TiO_2	0.32	0.32	3.09	0.24	0.21	0.32	0.41	0.25	0.24
Al_2O_3	8.73	8.96	13.99	8.96	9.09	9.41	9.27	9.11	8.97
FeO_T	5.97	5.32	12.95	4.74	4.67	4.88	4.86	4.70	4.74
MnO	0.27	0.27	0.19	0.22	0.21	0.22	0.19	0.21	0.21
MgO	0.09	0.09	7.5	0.05	0.04	0.06	0.24	0.04	0.06
CaO	0.40	0.32	11.16	0.31	0.40	0.33	1.15	0.21	0.21
Na_2O	4.47	5.23	2.45	5.33	4.55	5.53	4.37	5.54	5.37
K_2O	4.97	5.21	0.50	4.98	4.87	4.98	4.64	4.92	5.04
P_2O_5	0.14	0.02	0.54	0.02	0.02	0.02	0.09	0.01	0.01
LOI	1.26	3.17	4.57	4.32	4.74	4.03	3.99	2.96	3.16
SUM	100	100	100	100	100	100	100	100	100
Sc	2.515	2.71	31.73	0.75	0.42	0.41	1.70	0.45	0.60

Table 1 (continued)

sample	COR1	COR2	COR3	DA	UR1	UR2P	CH1	CH5P	CH6P
V	1.50	2.29	324.18	1.42	1.02	4.29	12.77	1.06	2.59
Cr	8.35	18.29	199.15	1.66	4.24	25.65	11.25	1.49	8.36
Ni	17.32	98.25	194.06	3.23	25.43	64.49	48.09	9.63	13.17
Cu	32.93	61.03	272.75	20.64	34.36	53.58	97.21	26.63	49.52
Rb	131.50	115.60	5.56	145.42	139.59	198.49	124.88	143.62	139.79
Sr	9.32	6.22	429.77	3.99	3.81	12.16	31.22	2.98	4.11
Ba	16.89	30.98	220.79	49.95	46.50	68.63	83.60	69.54	80.41
Cs	0.99	1.31	0.29	1.61	1.62	1.46	1.51	1.60	1.61
Pb	17.92	17.50	2.89	23.98	23.15	21.62	23.65	24.79	20.85
Th	13.50	13.38	1.05	17.19	17.17	15.32	15.83	16.63	16.69
La	84.53	108.15	14.83	163.36	162.05	148.18	136.85	164.48	163.38
Ce	178.61	232.12	35.09	350.51	372.21	327.08	303.50	343.25	380.19

Table 1 (continued)

sample	COR1	COR2	COR3	DA	UR1	UR2P	CH1	CH5P	CH6P
Nd	91.68	114.74	168.47	178.88	176.32	160.22	147.65	179.98	151.40
Pr	25.20	31.81	5.20	48.81	48.35	44.02	40.52	49.02	46.95
Sm	16.89	21.26	5.56	31.39	31.89	29.56	26.48	32.07	30.26
Eu	2.41	3.11	1.99	4.82	4.84	4.46	3.99	4.92	4.99
Tb	2.82	3.66	0.82	5.47	5.43	4.92	4.48	5.45	5.60
Gd	16.82	22.00	5.54	33.79	33.32	30.16	27.26	33.41	33.99
Yb	9.60	11.93	1.99	16.94	16.83	15.09	14.13	16.58	17.01
Lu	1.34	1.85	0.29	2.55	2.56	2.34	2.14	2.51	2.58
Y	106.95	137.36	27.954	190.47	187.67	204.57	159.26	193.85	180.50
Zr	1042.76	882.88	136.88	1214.85	1184.05	1476.09	1023.68	1220.60	1611.67
Er	9.43	12.43	2.25	18.29	17.91	15.95	14.84	17.61	17.97
Tm	1.32	1.89	0.33	2.66	2.67	2.40	2.23	2.63	2.67
Hf	21.93	20.46	3.04	28.63	28.67	23.49	23.99	28.42	32.85

Table 1 (continued)									
Ta	9.68	8.59	1.21	12.31	11.01	10.73	10.24	11.85	12.13
Nb	125.33	115.06	22.34	131.35	129.09	150.72	128.22	140.68	167.71
U	3.47	4.28	0.23	5.33	5.59	4.73	5.57	5.19	4.69

Table 2 : Major element (wt%) content of the analyzed standards JB1a,RGM1, BR, SY-3

sample	JB1a	JB1a certified value	RGM1	RGM1 certified value	BR	BR certified value	SY-3	SY3 certified value
SiO_2	52.61	52.16	73.50	74.08	39.53	39.52	60.79	60.76
TiO_2	1.29	1.30	0.25	0.26	2.72	2.69	0.15	0.15
Al_2O_3	14.29	14.51	13.74	13.83	10.44	10.55	11.88	11.97
FeO_T	9.16	9.10	1.94	41.88	13.29	13.32	6.68	6.61
MnO	0.15	0.15	0.04	0.03	0.20	0.21	0.33	0.33
MgO	7.80	7.75	0.27	0.28	13.80	13.74	2.64	2.72
CaO	9.37	9.23	1.23	1.15	14.33	14.27	8.52	8.4
Na_2O	2.79	2.74	4.26	4.08	3.15	3.16	4.17	4.2
K_2O	1.43	1.42	4.39	4.33	1.47	1.45	4.28	4.31
P_2O_5	0.27	0.25	0.06	0.05	1.05	1.08	0.56	0.55
SUM	99.94	99.39	99.98	100	100	100	100	100

Table 3: trace element content (ppm) of the analyzed standard JB1a

sample	JB1a	JB1a certified value
V	206.0	206.0
Cr	427.3	415.0
Ni	153.0	134.0
Cu	57.0	55.0
Rb	40.1	42.0
Sr	435.4	443.0
Ba	507.4	497.0
Cs	1.12	1.20
Pb	7.00	7.40
Th	8.78	8.80
La	37.90	38.10
Nd	24.90	25.50
Pr	7.53	7.30
Sm	4.99	5.02
Eu	1.49	1.47
Tb	0.68	0.69
Gd	4.97	4.54
Yb	2.04	2.10
Lu	0.31	0.32
Y	23.1	24.0
Zr	141.7	146.0

Table 3 (continued)		
Er	2.11	2.18
Tm	0.31	0.31
Hf	3.41	3.48
Ta	1.63	1.60
Nb	27.88	27.00
U	1.53	1.60

Tables 1- 2 3 : Comparison of the analysed standards JB1a,RGM1, BR, SY-3 with the USGS certified values provides an indication of the accuracy and precision of the analyses of the samples.

References

Albarede, F. (1992). How deep do common basaltic magmas form and differentiate?. Journal of Geophysical Research 97 (B7), 10997-11009.

Altaye, E., 1984. Geology and Surface Alteration of the Corbetti Caldera Area, Ethioia. Geothermal Institute, University of Auckland. (Project for Diploma in Energy Technology).

Baker, M. B. and Stolper E. M. (1994). Determining the composition of high-pressure mantle melts using diamond aggregates. Geochimica et Cosomochimica Acta 58, 2811-2827.

Barberi, F., Ferrara, G., Santacroce, R., Treuil, M. & Varet, J. 1975. A transitional basalt-pantellerite sequence of fractional crystallisation, the Boina centre (Afar Rift, Ethiopia). Journal of Petrology 16, 22-56.

Barberio, M.R., Donati, C., Danato, P., Yirgu, G., Peccerillo, A., Wu, T.W., 1999. Petrology and geochemistry of Quaternary magmatism in the northern sector of the Ethiopian Rift between Debre Zeit and Awash Park. In: Boccaletti, M., Peccerillo, (Eds.), The Ethiopian Rift System. Acta Vulcanologica, 11, pp. 69–81.

Black S, Macdonald R, Kelly MR (1997) Crustal origin for peralka- line rhyolites from Kenya: evidence from U-series disequilibria and Th isotopes. J Petrol 38:277–297.

Boccaletti, M., Getaneh, A., Mazzuoli, R., Tortorici, L., Trua, T., 1995. Chemical variations in a bimodal magma system: the Plio-Quaternary volcanism in the Dera Nazret area (main Ethiopian Rift, Ethiopia). Africa Geoscience Review 2, 37–60.

Boccaletti, M., Mazzuoli, R., Bonini, M., Trua, T., Abebe, B., 1999. Plio-Quaternary volcanotectonic activity in the northern sector of the Main Ethiopian Rift: relation- ships with oblique rifting. Journal of African Earth Science 29, 679–698.

Bohrson, W. A. & Reid, M. R. (1997). Genesis of peralkaline volcanic rocks in an ocean island setting by crustal melting and open-system processes: Socorro Island, Mexico. Journal of Petrology 38, 1137-1166.

Brotzu, P., Morbidelli, L., Piccirillo, E.M., Traversa, G., 1974. Petrology features of Boseti mountains, a complex volcanic system in the axial portion of the Main Ethiopian Rift. Bulletin Volcanologique 38, 206–234.

Brotzu P, Morbidelli L, Piccirillo EM, Traversa G (1980) Volcano- logical and magmatological evidence of the Boseti volcanic complex (Main Ethiopian Rift). Acc Naz Lincei (Roma) 47:317–362

Cameron, K.L. and Cameron, M. (1986) Whole-rock/groundmass differentiation trends of rare earth elements in high-silica rhyolites. Geochemica et Cosmochemica Acta, 50, 759–769.

Caroff, M., Maury, R. C., Leterrier, J., Joron, J. L. & Cotten, J. (1993). Trace element behavior in the alkalic basalt comenditic trachyte series from Mururoa atoll, French Polynesia. Lithos 30, 1-22.

Chernet, T., Hart, W.K., 1999. Petrology and geochemistry of volcanism in the northern Main Ethiopian Rift-southern Afar transition region. In: Boccaletti, M., Peccerillo, A. (Eds.), The Ethiopian Rift System. Acta Vulcanologica, 11, pp. 21–41.

Cioni, R., Cristiani, C., De Rosa, R., Marianelli, P., Mazzuoli, R., Ayalew, D., Yirgu, G. & Bompressi, E. (2001). Trachyte- pantellerite syn-eruptive magma mixing: evidence from the caldera-forming ignimbrite at Gedemsa (Main Ethiopian Rift). In: GEOITALIA 2001, 3rd Earth Science Forum, Abstract Volume. Chieti: Federazione Italiana Scienze della Terra, pp. 711-712.

Civetta L, D'Antonio M, Orsi G, Tilton GR (1998) The geochemistry of volcanic rocks from Pantelleria island, Sicily Channel: petrogenesis and characteristics of the mantle source region. J. Petrol 39:1453–1491

Cole, J. W. : Gariboldi volcanic complex, Ethiopia. 12th Ann. l~ep. Res. Inst. African Geol. Univ. Leeds, 30--32 1968.

Corti, G., 2008. Control of rift obliquity on the evolution and segmentation of the main Ethiopian rift. Nature Geoscience 1, 258–262.

Davies, J. R. & Macdonald, R. (1987). Crustal influence in the petrogenesis of the Naivasha basalt-comendite complex: com- bined trace element and Sr-Nd-Pb isotope constraints. Journal of Petrology 28, 1009-1031

Druitt TH, Costa F, Deloule E, Dungan M, Scaillet B (2012) Decadal to monthly timescales of magma transfer and reservoir growth at a caldera volcano. Nature 482(7383):77–80

Ewart, A. and Griffin, W.L. (1994) Application of proton-microprobe data to trace element partitioning in volcanic rocks. Chemical Geology, 117, 251–284.

Fedele F., Lustrino M., Melluso L., Morra V., Zanett A., Vannucci R., (2015) Trace-element partitioning between plagioclase, alkali feldspar, Ti-magnetite, biotite, apatite, and evolved potassic liquids from Campi Flegrei (Southern Italy). American Mineralogist, 100, 233-249.

Ferrara, G., and Treuil, M., 1974, Petrological implications of trace element and Sr isotope distributions in basalt-pantellerite series: Bulletin of Volcanology, v. 38, p. 548-574.

Furman, T., Bryce, J., Rooney, T., Hanan, B., Yirgu, G., Ayalew, D., 2006a. Heads and tails: 30million years of the Afar plume. In: Yirgu, G., Ebinger, C.J., Maguire, P.K.H. (Eds.), The Afar Volcanic Province within the East African Rift System. Geological Society, London, Special Publications, 259, pp. 95–119.

Gasparon, M., Innocenti, F., Manetti, P., Peccerillo, A., Tsegaye, A., 1993. Genesis of the Pliocene to recent bimodal mafic–felsic volcanism in the Debre Zeyt area, Central Ethiopia: volcanological and geochemical constraints. Journal of African Earth Sciences 17, 145–165.

Geist D, Howard KA, Larson P (1995) The generation of oceanic rhyolites by crystal fractionation: the basalt-rhyolite association at Volcàn Alcedo, Galapagos Archipelago. J Petrol 36:965–982

Gibson, I. L. : Preliminary account of the volcanic geology of Fantale, Shoa. Bull. Geophys. Obs. Addis Ababa 10, 59--67 ,1967

Gibson, I.L., 1972. The chemistry and petrogenesis of a suite of pantellerites from the Ethiopian rift. Journal of Petrology 13, 31–44.

Giordano F., 2006. Genesi ed evoluzione del magmatismo del settore settentrionale del Main Ethiopian Rift, attraverso uno studio geologico, geochimico ed isotopico delle aree vulcaniche di Gademsa e Fantale. PhD thesis, Universita' degli Studi di Napoli, Federico II, Facolta di Scienze Matematiche, Fisiche e Naturali.

Giordano F. ,D'Antonio M. ,Civetta L., Tonarini S., Orsi G., Ayalew D. ,Yirgu G. Dell'Erba F., Di Vito M.A., Isaia R. 2013. Genesis and evolution of mafic and felsic magmas at Quaternary volcanoes within the Main Ethiopian Rift: Insights from Gedemsa and Fanta 'Ale complexes. Lithos 188, 130-144.

Harris, C., 1986. A Quantitative Study of Magmatic Inclusions in the Plutonic Ejecta of Ascension Island. Journal of Petrology 27, 251-276.

Holt, G.S. (1998) Trace element partitioning of alkali feldspar in Burro Mesa Rhyolite and other units of the Trans-Pecos Magmatic Province. Unpublished M.S.thesis, 190 p. Baylor University, Waco, Texas.

Hutchison, W., Pyle,D., M., Mather, T., A., Yirgu, G., Biggs,J., Cohen, B., E., Barford, D., N., Lewi, E. 2016. The eruptive history and magmatic evolution of Aluto volcano: new insights into silicic peralkaline volcanism in the Ethiopian rift. Journal of Volcanology and Geothermal Research, doi: 10.1016/j.jvolgeores.2016.09.010

Icenhower, J. and London, D. (1996) Experimental partitioning of Rb, Cs, Sr, and Ba between alkali feldspar and peraluminous melt. American Mineralogist, 81, 719–734.

Korringa, M.K. and Noble, D.C. (1971) Distribution of Sr and Ba between natural feldspar and igneous melt. Earth and Planetary Science Letters, 11, 147–151.

Kushiro, I. (1996). Partial melting of a fertile mantle peridotites at high pressure: an experimental study using aggregates of diamond. In Earth Processes: Reading the isotope code (eds. A. Basu and Hart S.), pp. 109-122. Geophysical Monography 95, AGU.

Lacroix, A.: Les rhyolites et les trachytes hyperalcalins quartzifres, a propos de ceux de la Coree. 1927.Compt. Rend. 185, 1410--1415

Larsen, L.M. (1979) Distribution of REE and other trace elements between phenoc- rysts and peralkaline undersaturated magmas, exemplified by rocks from the Gardar igneous province, south Greenland. Lithos, 12, 303–315.

Le Bas MJ, Le Maitre RW, Streckeisen A, Zanettin B 1986. A chemical classification of volcanic rocks based on the total alkali- silica diagram. J Petrol 27:745–750

Lightfoot, P. C., Hawkesworth, C. J. & Setnha, S. F. (1987). Petrogenesis of rhyolites and trachytes from the Deccan Trap: Sr, Nd and Pb isotope and trace element evidence. Contributions to Mineralogy and Petrology 95, 44-54.

Lowenstern, J.B., and Mahood, G.A., 1991, New data on magmatic H2O contents of pantellerite, with applications for petrogenesis and eruptive dynamics at Pantelleria: Bulletin of Volcanology, v. 54, p. 78-83.

Macdonald, R., Gibson, I. L., 1969. Pantelleritic Obsidians from the volcano Chabbi (Ethiopia). Contributions to Mineralogy and Petrology 24, 239-244.

Macdonald, R., Davies, G. R., Bliss, C. M., Leat, P. T., Bailey, D. K. & Smith, R. L. (1987). Geochemistry of high-silica rhyolites, Naivasha, Kenya rift valley. Journal of Petrology 28, 979-1088.

Mahood, G. A. & Stimac, J. A. (1990). Trace-element partitioning in pantellerites and trachytes. Geochimica et Cosmochimica Acta 54, 2257-2276.

Mahood, G.A., and Hildreth, W. (1983) Large partition coefficients for trace elements in high-silica rhyolites. Geochimica et Cosmochimica Acta, 47, 11–30.
Mineralogy and Petrology 100, 183-191.

Mackenzie, G.D., Thybo, H., Maguire, P.K.H., 2005. Crustal velocity structure across the Main Ethiopian Rift: results from two-dimensional wide-angle seismic modelling. Geophysical Journal International 162, 994–1006. http://dx.doi.org/10.1111/j.1365-246X.2005.02710.x.

McDonald I and K.S. Viljoen, 2006. Platinum-group element geochemistry of mantle eclogites: a reconnaissance study of xenoliths from the Orapa kimberlite, Botswana. Applied Earth Science IMM transactions sections B. Doi: 10, 1179/174327506X138904

Melekhova E., Annen C., Blundy J., 2013. Compositional gaps in igneous rock suites controlled by magma stsem heat and water content. Nature Geoscience 6, 385-390

Mungall JE, Martin RF (1995) Petrogenesis of basalt-comendite and basalt-pantellerite suites, Terceira, Azores, and some implications for the origin of oceanic rhyolites. Contrib Mineral Petrol 119:43–55.

Nash, W.P. and Crecraft, H.R. (1985) Partition coefficients for trace elements in silicic magmas. Geochemica et Cosmochemica Acta, 49, 2309–2322.

Nelson, S. A. & Hegre, J. A. (1990). Volca`nLas Navajas, a Pliocene– Pleistocene trachyte/peralkaline rhyolite volcano in the northwestern Mexican volcanic belt. Bulletin of Volcanology 52, 186–204.

Nicholls, J. and Carmichael, I.S.E. (1969) Peralkaline liquids: A petrological study. Contributions to Mineralogy and Petrology, 20, 268–294.

Peccerillo, A., Mandefro, B., Solomon, G., Hambisa, G., Beru, H. & Tesfaye, K. (1998). The Precambrian rocks from Southern Ethiopia: petrology, geochemistry and their interaction with the recent volcanism from the Ethiopian Rift Valley. Neues Jahrbuch fu□r Minereralogie, Abhandlungen 173, 237-262.

Peccerillo, A., Barberio, M.R., Yirgu, G., Ayalew, D., Barbieri, M., Wu, T.W., 2003. Relationships between mafic and peralkaline acid magmatism in continental rift settings: a petrological, geochemical and isotopic study of the Gedemsa volcano, central Ethiopian rift. Journal of Petrology 44, 2003–2032.

Peccerillo, A., Donati, C., Santo, A.P., Orlando, A., Yirgu, G., Ayalew, D., 2007. Petrogenesis of silicic peralkaline rocks in the Ethiopian Rift: geochemical evidence and volcanological implications. Journal of African Earth Sciences 48, 161–173.

Petrelli M., Poli G., Perugini D. & Peccerillo A. (2005) Petrograph: a New Software to Visualize, Model, and Present Geochemical Data in Igneous Petrology, Geochem. Geophys. Geosyst., Vol. 6, Q07011, DOI 10.1029/2005GC000932, 26 July 2005

Rapprich, V., ÊáÊek,V. Verner, K., Erban V., T. Goslar, Y.Bekele , Legesa F., Hroch T., Hejtmánková P. 2015. Wendo Koshe Pumice: The latest Holocene silicic explosive eruption product of the Corbetti Volcanic System (Southern Ethiopia). Journal of Volcanology and Geothermal Research 310 (2016) 159–171.

Ren M., 2004. Partitioning of Sr, Ba, Rb, Y, and LREE between alkali feldspar and peraluminous silicic magma. American Mineralogist, Volume 89, pages 1290–1303

Ronga, F., Lustrino, M., Marzoli, A., Melluso, L., 2010. Petrogenesis of a basalt–comendite– pantellerite rock suite: the Boseti Volcanic Complex (Main Ethiopian Rift). Mineralo- gy and Petrology 98, 227–243.

Roux, J. and Varet, J. (1975) Alkali feldspar liquid equilibrium relationships in peralkaline oversaturated systems and volcanic rocks. Contributions to Miner- alogy and Petrology, 49, 67–81.

Scaillet, B., Macdonald, R., 2001. Phase relations of peralkaline silicic magmas and petrogenetic implications. Journal of Petrology 42, 825–845.

Treuil, M., 1973. Criteres petrologiques, geochimiques et structuraux de la genese et de la differentia-tion des magmas basaltiques: example de l'Afar. 2eme partie: Geochimie. *Unpub. Thise de Doctoral d'Etat. Orleans, Orsay*

Trua, T., Deniel, C., Mazzuoli, R., 1999. Crustal control in the genesis of Plio-Quaternary bi-modal magmatism of the Main Ethiopian rift: geochemical and isotopic evidence.Chemical Geology 155, 201–231.

White, J.C., Parker, D.F., and Ren, M. (2000) Systematic control of crystal and melt chemistry on feldspar trace element partitioning for Rb, Sr, and Ba, part I: peralkalic trachyte and rhyolite. Geological Society of America Abstracts with Programs, 32 (7), 148.

White, J.C., Holt, G.S., Parker, D.F., and Ren, M. (2003) Trace-element partitioning between alkali feldspar and peralkalic quartz trachyte to rhyolite magma. Part I: Systematics of trace-element partitioning. American Mineralogist, 88, 316–329.

White, J.C. (2003) Trace-element partitioning between alkali feldspar and peralkalic quartz trachyte to rhyolite magma. Part II: Empirical equations for calculating trace-element partition coefficients of large-ion lithophile, high field-strength and rare-earth elements. American Mineralogist, 88, 330–337.

Wilson, M. (1989). Igneous Petrogenesis. Kluwer, Dordrecht.

Wood, B.J. and Fraser, D.G. (1976) Elementary thermodynamics for geologists, 303 p. Oxford University Press, London

4. Conclusions : The volcanic history of Corbetti caldera (Main Ethiopian Rift)

In this chapter the results from the stratigraphic, geochemical investigations and dating analyses, are discussed together in a wider scenario with the aim to provide a whole understanding of the volcanic history of Corbetti caldera, based on the results of this research. However, this study highlights that further investigations are needed to better constrain our understanding of the eruptive history of Corbetti caldera.

4.1 The volcanic history of Corbetti caldera

Corbetti caldera volcanic complex shows a stratigraphic setting similar to those of Alutu, Gedemsa, Boseti and Fantale. All these Quaternary calderas are characterized by a lava dome and flows, developed during the pre-caldera activity, and by a clear caldera depression and the related PDC deposits. They also show a post- caldera activity, mainly developed within the caldera depression, related to different eruptive vents. However, the stratigraphic reconstruction here proposed (chapter 2), reveals that all Corbetti eruptive history (pre-syn – post caldera activity) was characterized by monogentic vents. In particular the post-caldera activity occurred in three different eruptive centers, active closely in the time. This information, that is inferred from the stratigraphy , can be related to the features of the sub-volcanic system.

Indeed a monogenetic volcanic center is characterized by an eruptive activity , that can also lasts several years, but that once ended the center is not active any more. This results in deposits that do not show signs of quiescence as paleosoils or layers of reworked deposits. This may suggest that there was not recharge of primitive magma, magma mixing or fractionation in Corbetti sub-volcanic system during the two eruptive epochs of the pre and post-caldera activity.

This is confirmed by the $^{40}Ar/^{39}Ar$ dating, that show as the Corbetti magmatic plumbing system produced a constant composition (rhyolite-pantellerite) for about 158ka. The stratigraphic features are strongly related with the geochemical feature of the deposits, and one important finding reveals that the Corbetti basalt (COR3) might not be the parental basalt of the rhyolites.

In this aspect Corbetti shows a different eruptive history from Alutu, Gedemsa, Boseti and Fantale volcanoes, that produced also intermediate and more primitive products.
It has been seen that the basalts emplaced by these calderas were the parent basalt of the rhyolites, and that a fractional crystallization genesis for the most evolved deposits has been hypothesized for these volcanic systems. On the contrary, the fact that the basalt of the *Corbetti Composite Lithosome* might not be related to the rhyolites, imposes alternative hypothesis for the petrogenesis of the Corbetti rhyolites.

It could be argued from the comparison of Corbetti rhyolites with those from Alutu, Gedemsa, Boseti and Fantale, (chapter 3), that the rhyolites are from fractional crystallization of a magma with the same composition as that of the parental basalt of the Alutu, Gedemsa, Boseti, Fantale, rhyolites.

Although further investigation are required for further constrain the understanding of Corbetti volcanic system, in light of the data collected so far, the most likely scenario for the activation of volcanic eruptions along the history of Corbetti caldera, might be the amount of volatile entrapped in the melt, and the rate of the extensive tectonic inducing a decrease of lithostatic pression and a consequent volatile exsolution.

4.2 Conclusions and future work

The aim of this project is a better knowledge of the Corbetti volcanic history and behavior in order to reduce the uncertainty related to the volcanic hazard of the area, and to provide new data on this volcanic complex, that should be considered in the wider scenario of the magmatism and volcanism of the Main Ethiopian Rift.
The new stratigraphic reconstruction and mapping based on the UBSU method, the full (major and trace elements) geochemical characterization of the all of the deposits from both pre-syn and post caldera epochs , the new $^{40}Ar/^{39}Ar$ dating, that date the caldera forming eruption, and especially, the study for the first time of the basalt deposit (COR3) and its relationship with the rhyolites, bring important and fundamental findings on the history of this volcanic complex. This work is a pioneering study on one of the less known volcanoes in the Main Ethiopian Rift.

However to further constrain our knowledge and understanding of Corbetti caldera, more investigations should be done. In particular, analyses of volatile (F,S, Cl, H_2O, CO_2) composition and concentration in MIs in quartz or sanidine crystals from all of the deposits of both syn and post caldera activity. These analyses can provide more information about the pre-eruptive condition as also depth of equilibration and pressure of crystallization. Analyses of isotopic ratios as $^{87}Sr/^{86}Sr$ and $^{143}Nd/^{144}Nd$, for each deposit of all of the four lithosomes (*Corebtti Composite Lithosome, Danshe Lithosome, Urji Lithososme and Chabbi Composite Lithosome*) of Corbetti caldera, along with further analyses of isotopic ratio of $^{206}Pb/^{204}Pb$, $^{207}Pb/^{204}Pb$ and $^{208}Pb/^{204}Pb$, and U series disequilibria and Th isotopes, could better constrain the petrogenesis and evolution of the Corbetti rhyolites and their possible relationship with the crust, or different mantle sources starting from a magma of basalt composition.